

Variable Star Section of Czech Astronomical Society and Valašské Meziříčí Observatory

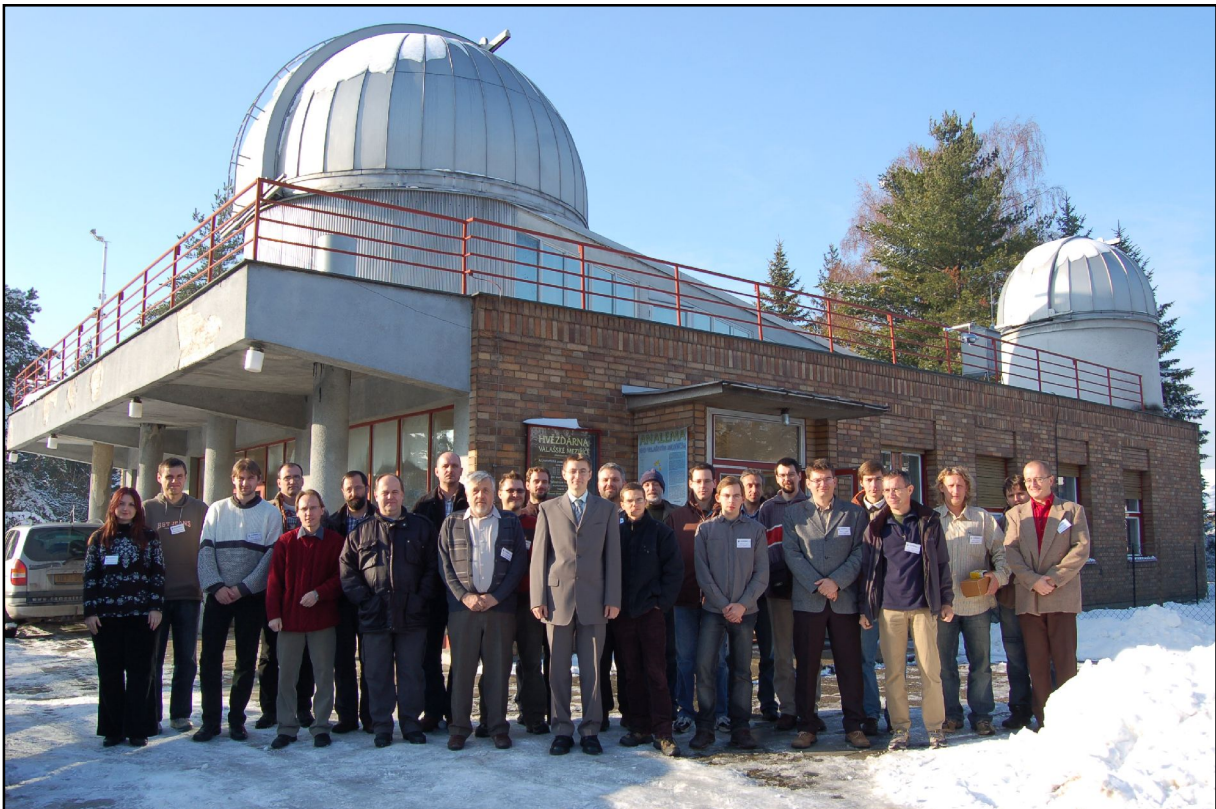
# Proceedings of the 39<sup>th</sup> Conference on Variable Stars Research

---

Valašské Meziříčí Observatory, Czech Republic, EU

16<sup>th</sup> – 18<sup>th</sup> November 2007,

Chief editor **Luboš Brát**



Participants of the conference in front of the observatory

## TABLE OF CONTENT

Alternative Solution for an Low-Cost Optical All-Sky Monitor .....	<b>3</b>
<i>M. SPURNY, M. KRIZEK, R. HUDEC, J. ZICHA, M. NEKOLA</i>	
The beginning of asteroseismological observations at Kolonica Saddle .....	<b>7</b>
<i>T. DOROKHOVA, P. A. DUBOVSKY, I. KUDZEJ, N. DOROKHOV, A. RYABOV</i>	
The Binary Stars With Pulsating Component .....	<b>17</b>
<i>P. ŠVAŘÍČEK</i>	
CCD Photometry: Measurement uncertainty .....	<b>21</b>
<i>M. CHRASTINA, F. HROCH</i>	
ESA Gaia and Variable Objects .....	<b>29</b>
<i>R. HUDEC, V. ŠIMON, L. HUDEC</i>	
Identification and Analyses in Optical Light of Gamma-ray Sources with Astronomical Archival Plates .....	<b>32</b>
<i>R. HUDEC, F. MUNZ</i>	
Superhumps in Kolonica .....	<b>36</b>
<i>P. A. DUBOVSKÝ, S. PARIMUCHA, I. KUDZEJ</i>	
New Variables In Archival CCD Fields .....	<b>42</b>
<i>L. HAMBÁLEK</i>	
Objects of High Energy Astrophysics as Optically Variable Objects .....	<b>49</b>
<i>R. HUDEC</i>	
On the light curves of symbiotic stars .....	<b>59</b>
<i>A. SKOPAL</i>	
On the Possibility of the Amateur Detection of GRBs by Ionospheric Response .....	<b>67</b>
<i>R. SLOŠIAR, R. HUDEC</i>	
Optical Photometry of Be/X-ray Binary V 615 Cas = LS I +61°303 .....	<b>70</b>
<i>L. BRÁT</i>	
Recommended tips for variable stars observers .....	<b>79</b>
<i>P. ZASCHE</i>	
Transiting Exoplanet Light Curve Solution by Phoebe Code .....	<b>81</b>
<i>S. PODDANÝ</i>	

## INTRODUCTION

*The 39th Conference on Variable Stars Research was hold at Valašské Meziříčí Observatory (Czech republic) from 16<sup>th</sup> till 18<sup>th</sup> November 2007. The conference was organized by Variable Star Section of Czech astronomical society and Valašské Meziříčí Observatory. Czech conferences on variable star research are unique meetings of professional and amateur astronomers and took place for almost 40 years each november's full moon.*

*Papers in this proceedings are sorted in alphabetical order of papers title.*

*Let me thanks to all of authors for their talks and posters and to all participants for their contribution to discussion!*

*in Pec pod Sněžkou, 1<sup>st</sup> November 2008*

*Luboš Brát  
- proceedings editor and chief of SOC*

# Alternative Solution for an Low-Cost Optical All-Sky Monitor

M. SPURNÝ<sup>1</sup>, M. KRIZEK<sup>1</sup>, R. HUDEC<sup>2,4</sup>, J. ZICHA<sup>3</sup> AND M. NEKOLA<sup>2</sup>

1) Observatory, Karlovy Vary, Czech Republic

2) Astronomical Institute, Academy of Sciences of the Czech Republic, CZ-251 65 Ondřejov, Czech Republic

3) Czech Technical University, Faculty of Mechanical Engineering, Prague

4) Czech Technical University, Faculty of Electrical Engineering, Prague

## Abstract

We report on the development and tests of an alternative optical all-sky monitor recently tested at the Karlovy Vary Observatory. The monitor is based on a Peleng 8 mm fish-eye lens (1:3,5-1:16) and CANON EOS 350D digital CCD camera. This type of monitor represents a low-cost device suitable for easy replication and still able to detect brighter optical transients simultaneously to GRB triggers. Such OTs have been observed in the past for some of the GRBs such as GRB990123 or GRB060117 indicating that some fraction of GRBs can generate optical transient emission accessible by simple small aperture instrumentation as described here.

## CZ Abstrakt

Je popsán vývoj a testy alternativního celoblohového monitoru spočívajícím na objektivu Peleng 8 mm fish-eye a digitálním CCD fotoaparátu CANON EOS 350D. Jde o nízkonákladové zařízení vhodné pro snadnou duplikaci. Přitom tento systém by mohl detekovat jasné optické transienty doprovázející některé gama záblesky (GRB).

---

## Introduction

Even the fastest optical follow-up telescopes cannot access the times close or identical to times of GRBs, and the time domain before GRB remains completely hidden.

These time domains can be accessed only by optical wide-field monitors (as the position of the GRB is unpredictable). The all-sky monitors offer the best sky coverage. An alternative approach is to monitor the FOVs of recent GRB satellites with optical WF cameras. Some of the all-sky monitors operated on daily basis are based on the use of photographic emulsion (allowing long exposures and fine spatial resolution). However, the photographic emulsion is not very sensitive to short optical flares and has some additional disadvantages.

The alternative digital all-sky monitoring is provided by the CONCAM system. However, the limiting magnitudes are not very deep, so one can hardly expect such system will be able to detect optical transients (OTs) of GRBs.

The brightest OTs related to GRBs observed so far were observed at magnitudes 9 ... 10 (GRB990123, GRB060117). For GRB060117, the optical transient was followed due to technical reasons from 2 min after the GRB trigger and already declining, so one can deduce that the peak brightness probably exceeded mag 8. We hence need monitors able to detect short OTs with duration of about 1 min and fainter than magnitude 8.

## The instrumentation

The used instrumentation is simple and low-cost. The camera has two parts, namely the Peleng 8 mm fish-eye lens (1:3,5-1:16) that provides a 24 mm circular 180° field of view, and a CANON EOS 350D digital CCD camera. The total cost of the hardware is around 1500 USD, ie. one order less than the CONCAM system. One can hence expect the system to be easily and cheaply replicated to numerous sites.

One can consider the alternative type of the digital camera, such as Canon EOS 5D with a larger CCD chip (but somewhat larger pixel size) hence covering the whole FOV of the fish-eye lens.

We plan to improve the performance of the system by designing, in collaboration with the Czech Technical University in Prague, specially dedicated mount and miniature dome for the camera.

## Conclusions

An alternative low-cost (~ 1.5 k\$) optical digital all-sky monitoring system has been assembled and it is tested recently. The preliminary results indicate the limiting magnitude even for non-guided system and for one image with exposure of 30 sec amounts to mag 8. Deeper magnitudes are expected for guided system and longer or cumulated exposures, then the expected limiting magnitude can reach the mag 10 – 11 range. This makes the system suitable for wide-field monitoring in the sky for brighter optical transients. The system can be very easily

duplicated to numerous sites. Future improvements are planned such as desing of a miniature camera mount and dome to allow guided images.

### Acknowledgements

The project described in this contribution is in some parts (providing simultaneous optical data for satellite experiments) related to the ESA PECS Project 98023 and grant GA CR 205/08/1207.



*Fig 1: The Peleng fish-eye lens*



*Fig. 2: The complete camera system*

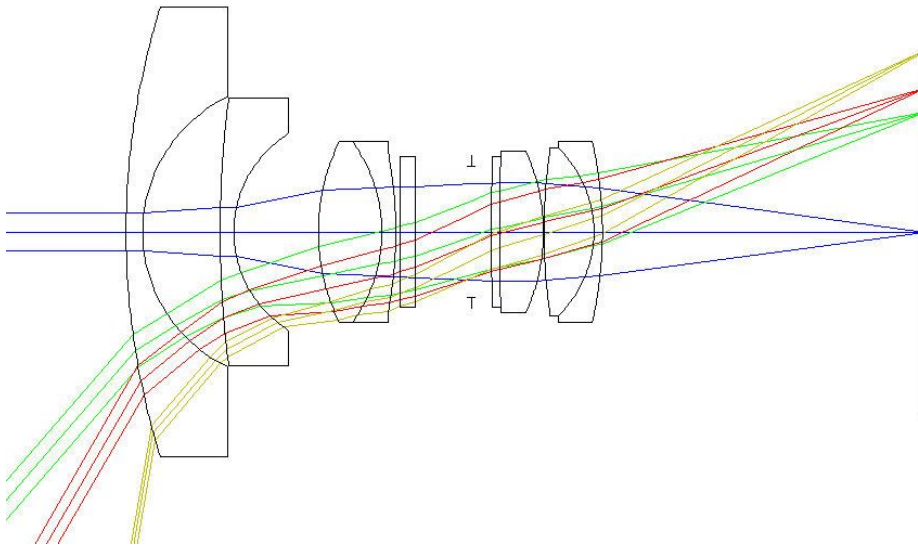


**Fig 3** The schema of the used fish-eye lens. It should be noted that the lens consist of 10 glass elements. Although no detailed measurements about spectral efficiency of the lens, by analogy with similar lenses one can expect that there will be no or very little response below 400 nm.

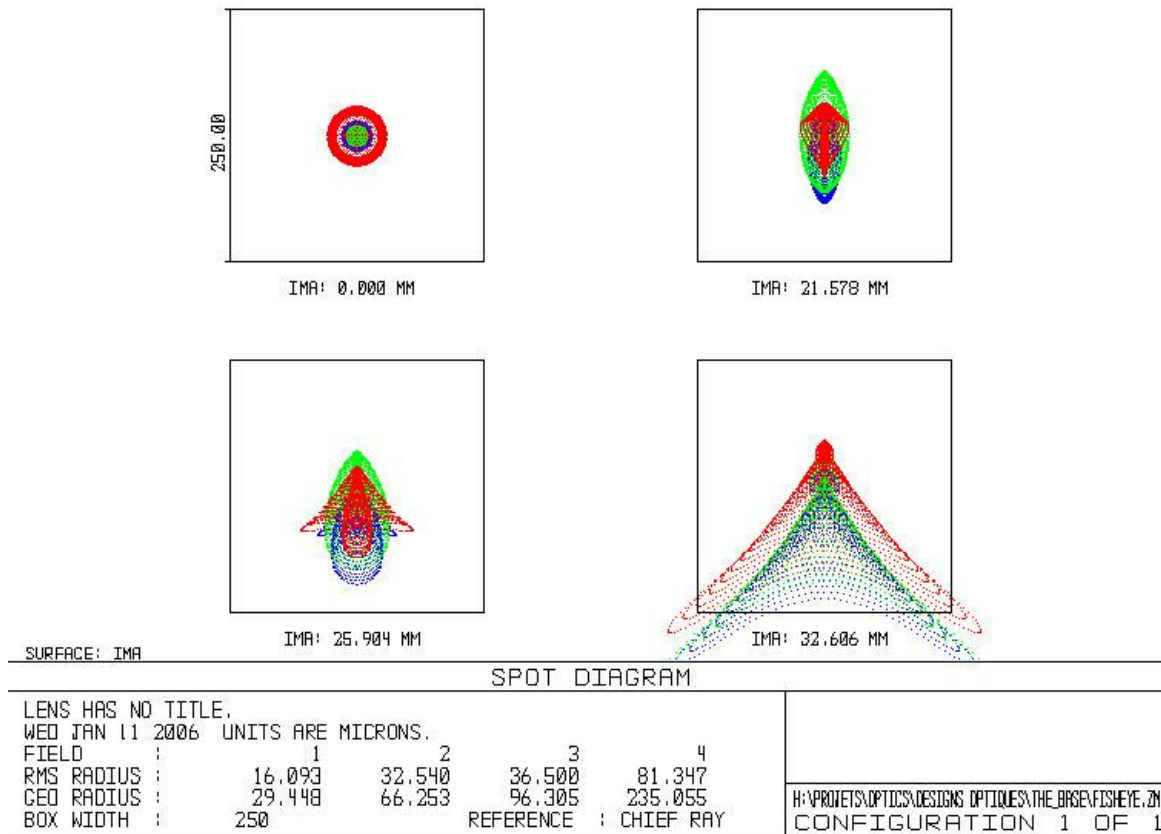


**Figure 4:** The huge front lens plays a peculiar role : it gathers all the light from all angles from +90° down to -90°, leading to a 180° field of view. The figure shows the spot diagram of a lens : this would be the image of a star located at different fields from the centre (IMA : 0.000 mm). As the field increases from the centre (optical axis), the star image gets degraded, at 85° the star shape is clearly extended



*Figure 5: An example of non-guided image, exposure time 30 seconds*



*Figure 6: Example of the guided image, exposure 240 sec. Only a fraction of the image is shown.*

# The beginning of asteroseismological observations at Kolonica Saddle

TATIANA DOROKHOVA<sup>1</sup>, PAVOL A. DUBOVSKY<sup>2</sup>, IGOR KUDZEJ<sup>3</sup>, NIKOLAY DOROKHOV<sup>1</sup>, ANDREY RYABOV<sup>1</sup>

- 1) Astronomical Observatory of Odessa National University, Ukraine, [tnd@te.net.ua](mailto:tnd@te.net.ua)
- 2) Astronomical Observatory at Kolonica Saddle, [var@kozmos.sk](mailto:var@kozmos.sk)
- 3) Vihorlat Astronomical Observatory, [vihorlatobs1@stonline.sk](mailto:vihorlatobs1@stonline.sk)

**Abstract:** There are presented the results of the low amplitudes Delta Scuti variables V2314 Oph and VW Ari photometry obtained with the two-star photometer installed at the Vihorlat National Telescope (VNT) during June-July and Sept-Oct 2007. The target selection, observational and reducing techniques were performed in the program context and standards of the well known asteroseismological networks WET, DSN and STEPHI. V2314 Oph was observed in the frame of mini-multisite campaign.

**CZ Abstrakt:** Predstavujeme výsledky fotometrických pozorovaní nízkoamplitúdových premenných hviezd V2314 Oph a VW Ari získaných dvojkanálovým fotoelektrickým fotometrom inštalovanom na Vihorlatskom národnom teleskope (VNT) počas mesiacov jún – júl a september – október 2007. Výber objektov, pozorovacích a redukčných metódik bol robený v súlade so známymi asteroseizmologickými sieťami WET, DSN a STEPHI. V2314 Oph bola pozorovaná v rámci minikampane viacerých observatórií.

## 1. Introduction

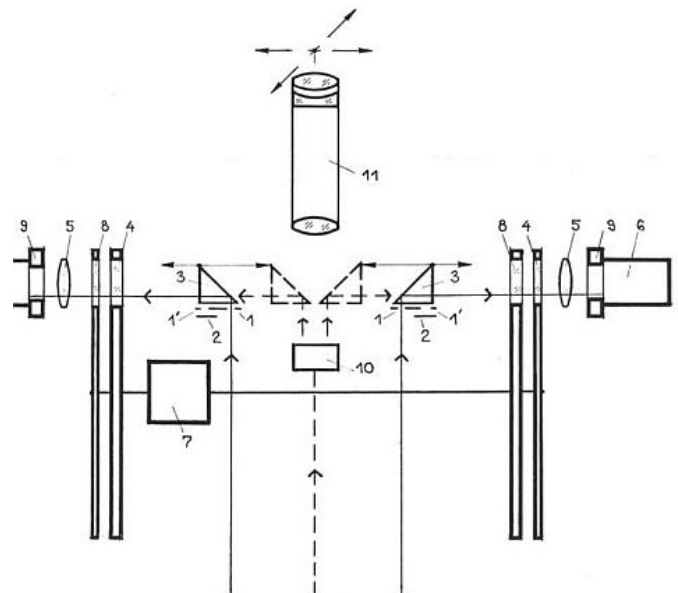
Asteroseismology studies stellar oscillations and pulsations. The accurate measurements of the oscillations' frequencies are helping for the stellar interior investigations and carry the information on physical conditions in regions of the star that are not accessible through ordinary observing techniques (see, e.g., the review of Brown & Gilliland 1994). The asteroseismic observations require the special accuracy and, apparently, the special techniques. From early 1980s the lengthen multi-site campaigns were arranged to avoid the days aliases in the ground-based photometric observations. Further, the well known asteroseismologic networks commenced the regular observations: Whole Earth Telescope (WET, <http://wet.physics.iastate.edu/>), Delta Scuti Network (DSN, <http://www.univie.ac.at/tops/>) and STELLAR Photometer International (STEPHI, <http://www.lesia.obspm.fr/~stephi/>). The techniques, problems and advantages of these networks' photometry are described, specially for  $\delta$  Scuti stars, in Breger & Handler (1993), Breger (1998), Handler (1998). Last years many collaborative efforts were spent for developing of the new Vihorlat Astronomical Observatory at the Kolonica Saddle (VAO KS, Kudzej et al. 2007a) in according to these standards: asteroseismology require data of as long as possible continuous series (see, e.g., Breger 1998). In this paper we concentrated on 2 targets related recently to the group of  $\lambda$  Bootis stars, which is important for asteroseismology, see for definition review (Paunzen 1999). The study of these low amplitudes stars gave us an opportunity to tune and improve the instrumentation (Kudzej et al. 2007b) and to accomplish and debug the techniques.

## 2. Instrumentation and techniques.

The main telescope of the observatory is Vihorlat National Telescope (VNT) (Kudzej et al. 2007a). The diameter of the main mirror is 1 meter and the effective focal length of Argunov – Fashevskiy optical system is 9 meters. The Cassegrain focus of the telescope is equipped by the high speed two-star photometer, which was constructed in Astronomical Observatory of Odessa National University. The optical scheme of the photometer is shown in Figure 1.

**Figure 1.** The optical scheme of two-star photometer

- 1 - diaphragm (5 different diameters)
- 1' - diaphragm for sky measurement
- 2 - cover automatically uncover diaphragm 1 or 1'
- 3 - mirrors reflecting the light to the photomultiplier
- 4 - filter wheel
- 5 - Fabry lens
- 6 - photomultiplier
- 7 - simultaneous turning of filter wheels
- 8 - neutral filter
- 9 - photomultiplier cooling
- 10 - mechanical displacement of mirrors
- 11 - microscope



The observing method was differential photometry typically with 10 sec. integration time. Target star in the channel 1, comparison star in the channel 2. The sky background is measured automatically through diaphragms for sky measurement (30 arcsec diameter) every 100 – 200 exposures. The corresponding calibration to the different star diaphragm's diameter was performed exposing bright sky during twilight. The calibration for different response of two channels was performed as well. We observed well known constant stars in good atmospheric conditions. During the observation of target star we made another calibration between channels based on measurement of artificial light source – photodiode implemented inside the photometer (Dorokhov, 1999).. This measurement was done few times during the night. The typical observing series looks as follows:

5K,[5Vsky, 100-200Vstar, 5Vsky].....[5Vsky, 100-200Vstar, 5Vsky], 5K.

The data were corrected for coincidence counting losses, a sky background contribution and reduced to the uniform sensitivity by the channels calibrations' multiplying. The extra-atmospheric magnitudes were obtained by using the simple Bouguer method. Then the measurements were binned to 2 min integrations and differential magnitudes *var-comp* were calculated.

For the frequency analysis there was used the well-known package of programs PERIOD04 (Lenz & Breger M. 2005).

### 3. V2314 Oph

V2314 Oph (HD 161223), ( $\alpha = 17^{\text{h}} 44^{\text{m}} 04^{\text{s}}$ ,  $\delta = +06^{\circ} 03' 07''$  (2000),  $V = 7.43$  mag, Sp A2) was discovered as a  $\delta$  Scuti variable during the observations in the field of the open cluster IC 4665 by Martin & Rodriguez (1995). They determined the main period of 0.144 d and suspected the multiperiodical pulsations due to varying from night to night amplitude. In addition MR95 obtained  $[\text{Fe}/\text{H}] = -0.53$  by analyzing their uvby $\beta$  photometry and classified the star as a field SX Phe pulsator with the longest period known to date. V2314 Oph is in the field of IC 4665 but is not a member of the cluster (Crawford & Barnes 1972).

From 2002 the star was observed in a frame of South Korean program of SX Phe variables' investigations by Chulhee Kim et al. (2007). There were originally planned obtaining precise photometric data of V2314 Oph for resolving its frequency pattern and have undertaken differential CCD and PMT observations in some observatories with a good sky seeing and instrumentations.

At the same time Gray & Corbally (2002) suspected that V2314 Oph is not an SX Phe type but a mild  $\lambda$  Boo type star. For the more accurate star's spectrum definition 7 spectra were obtained during 3 nights of 2002 using a coude-echelle spectrometer (Musaev et al. 1999) mounted to the 2-m "Zeiss" telescope at the Peak Terskol Observatory (Northern Caucasus, Russia). Kim Chulhee et al. (2007) determined the abundances of 19 chemical elements with a high accuracy using the spectral synthesis.. The abundance pattern of V2314 Oph was found to be similar to that of  $\lambda$  Bootis-type stars.

From the differential time-series CCD photometry Chulhee Kim et al. (2007) derived also the frequency pattern of V2314 Oph:  $f_1 5.9450\text{c/d}$ ,  $f_2 11.195\text{c/d}$ ,  $f_3 5.128\text{c/d}$ ,  $f_4 7.411\text{c/d}$ . However, the frequency solutions for the data obtained in 2003 and 2004 have some discrepancies due to the short heterogeneous series of the data.

Telescope	Date	Observer(s)	Comment
VNT 1m PMT 2-st	9 nights 7 Jun -26Jul	Dubovsky Dorokhov Dorokhova Kudzej	Observatory at the Kolonica Sedlo, Slovakia
Majdanak Zeiss600 CCD FLI IMG1001E	7 nights 13-19 Jun	Ibrahimov	
Terskol 28 cm CCD	7 nights after June 24	Andreev	
OSN 0.9 m six-channel uvbybeta photometer	6 nights 19Jun -24Jul	Martin Ruiz Aceituno Casanova	Sierra-Nevada Observatory Spain

Table 1. The Journal of V2314 Oph multi-site campaign.

Thus in 2007 there was undertaken the multi-site campaign for definition of the V2314 Oph frequency solution. The Journal of the campaign is listed in the Table 2. The mixed detectors were applied: 2 PMT and 2 CCD photometers. All observatories used new instrumentations and new techniques except the well known Sierra-Nevada 6 channel photometer (Nielsen, 1983).

**Our observations:**

Totally at the VAO KS there were obtained 29.8 hr of 2-star photometry during 9 nights of June–July 2007. The Johnson V filter was mainly used except 3 nights where B filter was applied. In the Table 2 the observational log of only VAO KS observations is presented.

Date	Start (UT)	Length(hr)	Filr	$\sigma$ (mag)
Jun 07	22:00	4	V	0.0022
Jun 08	20:00	4.3	V	0.0022
Jun 09	21:00	3	V	0.0170
Jun 12	20:41	4	V	0.0018
Jun 17	22:40	2	V	0.0017
Jul 18	21:50	3	B	0.0278
Jul 19	20:44	2	B	0.0261
Jul 25	20:00	3	B	0.0053
Jul 26	20:00	4.5	V	0.0049
<b>Total</b>		<b>29.8</b>		

Table 2. Journal of the VAO KS observations of V2314 Oph.

In the last column there are presented the standard error of 12-point integrations. For the analysis were used only 6 nights, other observations were removed because of large scattering and/or low instrumental sensitivity, or bad guiding (see Kudzej et al. 2007b).

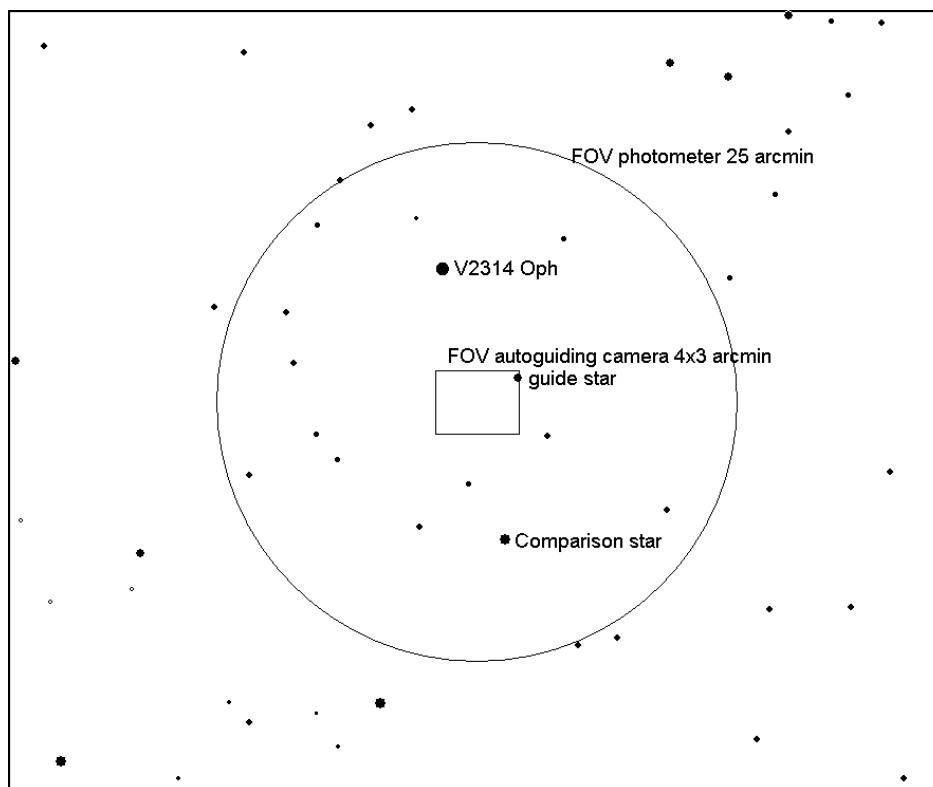


Figure 2. Field of view of V2314 Oph

The preliminary analysis of the VNT data revealed 3-frequencies' solution shown in Table 3: a frequency with an according amplitude and signal-to-noise ratio.  $F_2$  is apparently the one-day alias of the main frequency revealed by Chulhee Kim et al. (2007). In Figure 3 the light curve of V2314 Oph for these 6 nights and the synthetic curve of revealed 3 frequencies are presented.  $F_1$  was distorted possibly due to including the B-filter data of 25 July (HJD 2454307) which do not coincide in phase with the rest data. The comparing with the synthetic light curve extrapolated from 4 frequencies fit of OSN y-photometry shown that all data except of 25 July (HJD 2454307) are coincident well in a phase (Figure 3). As a whole this result looks not bad, considering that nights at the latitude of VAO KS are very short in June, atmospheric humidity is high and extinction is unstable. Besides we revealed that the photomultiplier and the amplifier of second channel of the photometer have a lower sensitivity than these of the first channel. Then the photomultiplier has been replaced by the better one and the amplifier has been improved.

	frequency [c/d]	amplitude [mag]	S/N
F <sub>1</sub>	9.670±0.0004	0.016±0.0007	9.14
F <sub>2</sub>	7.955±0.0007	0.011±0.0007	6.25
F <sub>3</sub>	12.783±0.0012	0.007±0.0007	3.7
Residuals		0.009	

Table 3. Frequency solution of VNT data for V2314 Oph

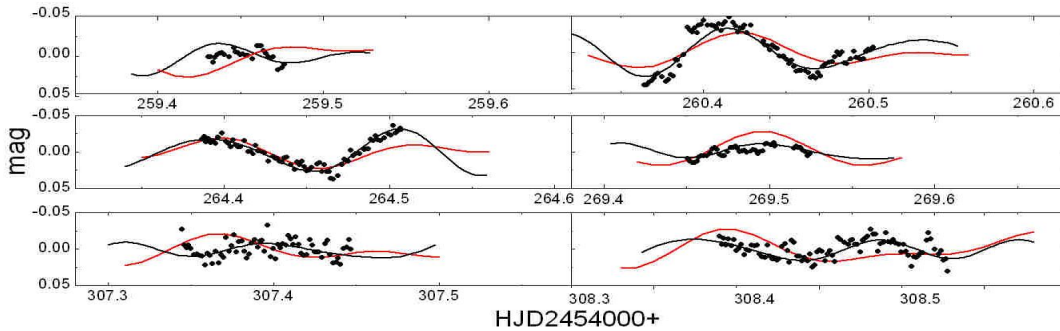


Figure 3. VNT data - 6 nights (07.06.07-26.07.07) with the fit of 3 own frequencies (black line) and extrapolated artificial curve of OSN data (red line).

#### 4. VW Ari

VW Ari was “an autumn object” for the asteroseismologic test in the VAO KS. VW Ari (BDS 1269A, HD15165, V=6.7 mag, A3) is a primary component of the visual binary system having the strong metal-deficient chemical composition. The secondary component BDS 1269B (HD15164, V=8.3 mag, F0) is a normal F type star. The stars are separated at an angular distance of 74 arcsec. VW Ari was a target of the fifth campaign of STEPHI network where 4-channel photometry of Xinglong Observatory (China) and Observatorio del Teide (Tenerife, Spain) was used for the detail frequency resolution (Liu et al. 1996). Further the dual-channel photometry from the Mt. Dushak-Erekdag was united with the STEPHI5 network’s data and the very interesting 5-frequency solution was revealed by Dorokhova (1999). The star was related to the  $\lambda$  Boo class that was supported also by the spectral features (Chernyshova et al. 1998). This have explained the nature of binary system BDS 1269: both stars belong to the Population I. The development of ideas concerning the pulsations’ behavior of VW Ari is presented in the Table 4.

Time	Frequency solution	Authors
1976 Oct	6.71, 11.1	Percy, 1980
1976 Nov	6.35, 10.74	Rucinsky, 1978
1976 Oct-Nov	6.35, 10.72, 6.07, 6.56	Kurtz, 1980
1987 Oct	6.23, 6.51, 11.77, 9.71, 11.34	Li&Jiang, 1993
1976 Oct-Nov	6.21, 6.52, 11.83, 9.71, 11.38	
1982.09- 1983.02	3.51, 6.23, 7.52, 9.34, 10.28, 11.00, 11.18	McNamara&Horan, 1984
1993 Oct	6.23, 6.52, 9.35, 10.82, 9.51, 10.73, 12.84	Liu et al., 1996 (STEPHI V)
1993 Oct	6.23, 6.52, 9.34, 10.81, 12.85	Dorokhova, 1999

Table 4. History of VW Ari variability investigations.

**Our observations:**

Figure 4 showed the field of view of VW Ari with vicinities. After initial observations we should change *comp*=HD15095 ( $V=7.5$ , Sp G0) to HD15042 ( $V=7.7$ , Sp B9). HD15042 was a check star in the STEPHI5 photometry (Liu et al. 1996) and did not show any variability. Although new comparison star is on the larger distance from the variable but we could use the former comparison as a guide star for automatic guiding of the telescope by using Mintron CCD camera.

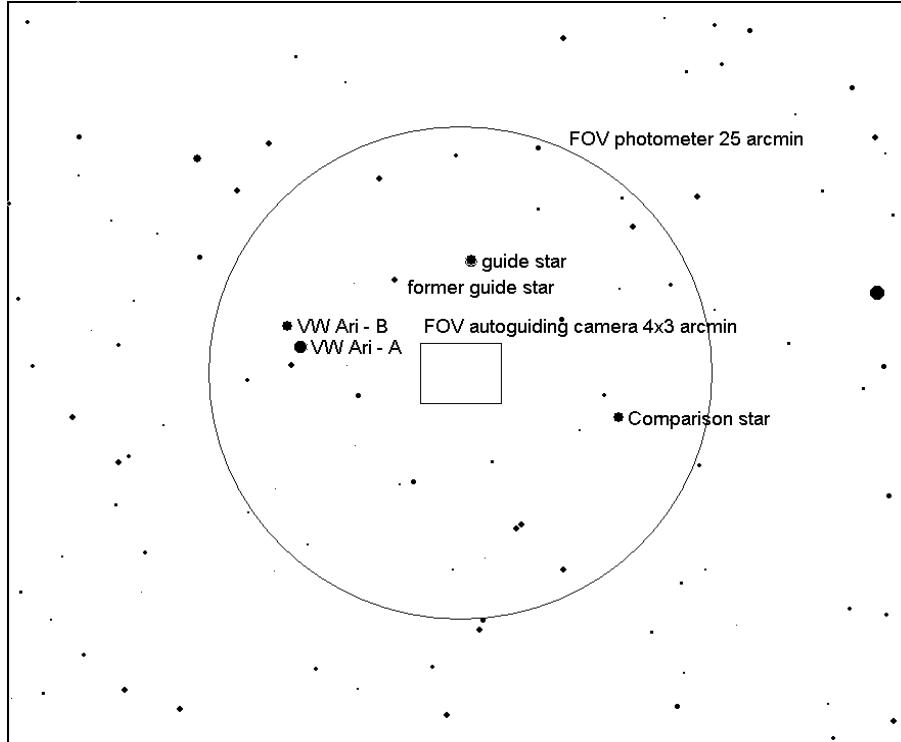


Figure 4. The field of view of VW Ari

We have obtained 12 continuous 2-channel observing runs from 2007-08-23 to 2007-11-19 which are listed in the Table 5.

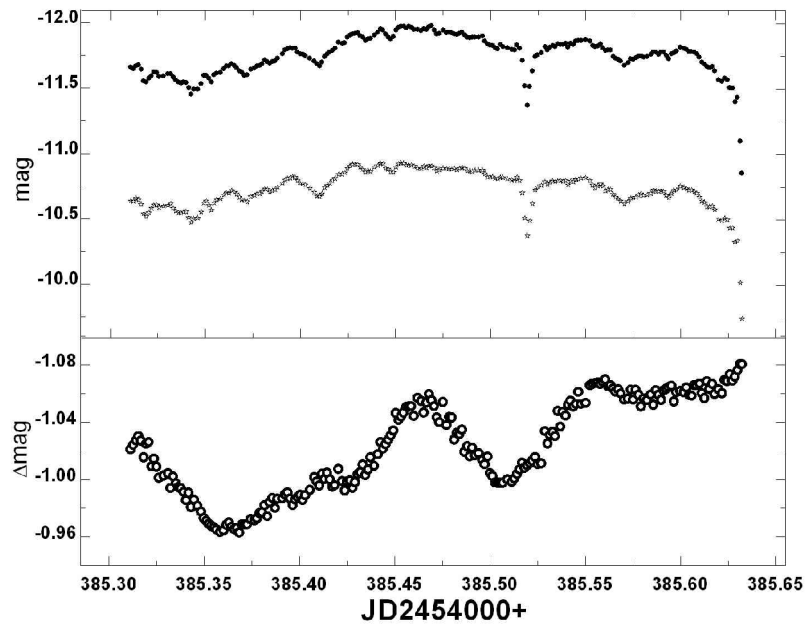


Figure 5. The two-star photometry of VW Ari within 11.10.2007. On the top panel the light curves of *var* and *comp* stars in each channel in instrumental magnitudes with gaps from clouds are shown, on the bottom panel the differential light curve is presented.

In Figure 5 there are shown the example of the dual-channel observations in the imperfect night with an unstable atmospheric transparency and clouds. As a result of normalization by the channel2 data many defects of the light curve were removed.

Then the data were reduced with the techniques described in the section 2. However, it is necessary to recognize, that the problem of channels' verification has not been solved completely. It should be also noted, that the simple Bouguer method of atmospheric extinction estimations is obviously insufficient since the observations were performed frequently in nonideal, cloudy and foggy, nights. For accounting an atmospheric influence we focused on the factors described in the paper of Pakstiene & Solheim (2003): the Rayleigh scattering and aerosol extinction. It is possible also the effect Forbes influence and that the refraction effect moved the comparison star in diaphragm on the large air masses ( $\geq 1.5$ ). That all could be the reasons that light curves were bent up on the larger than 1.5 air masses (see bottom panel in Figure 5).

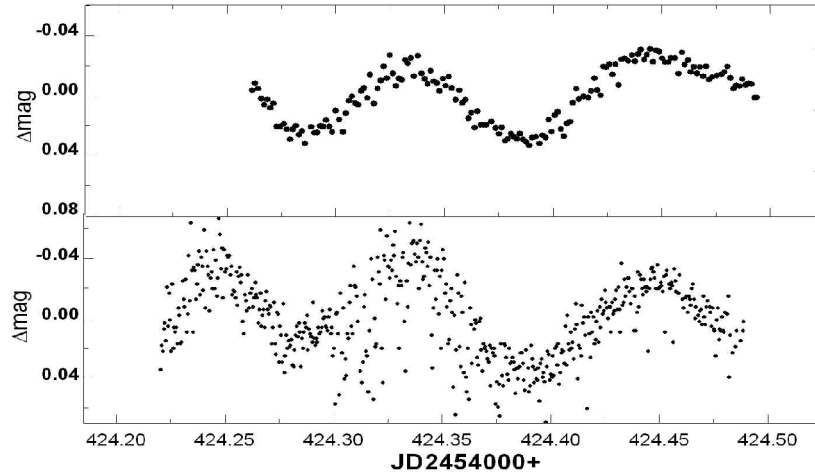


Figure 6. Simultaneous observations of VW Ari using the VNT + photometer (filter V) and the 30 cm guide + SBIG ST9 (filter B) in differential magnitudes relative to average for the night. The scattering on the bottom panel is due to a stray lighting of the pixels.

We have examined the reasons of light curves' distortion with the simultaneous observations of VW Ari using the VNT + photometer and the 30 cm guide + SBIG ST9 (Figure 6). Actually, in many cases the CCD photometry was crucial for an examination of new telescope and new two-star photometer (Kudzej et al. 2007b). As it is seen from the Figure 6 the extinction effects, probably, have no practical importance because these have not distorted the CCD light curve.

On this stage we have removed curves' distortions by polynomial fit of 2 order, however it could affect the result frequency solution (see Pakstiene & Solheim 2003).

Date (2007)	Start (JD 2454000 +)	Length(hr)	Filr	$\sigma$ (mag)
Aug 25	338.455	3.6	V	0.018
Aug 26	339.501	3.4	V	0.002
Sep 13	357.417	5.1	V	0.0019
Sep 15	359.412	3.1	V	0.003
Sep 16	360.390	4.7	V	0.002
Sep 23	367.385	6.1	V	0.0018
Sep 24	368.370	6.6	V	0.002
Oct 09	383.323	7.7	V	0.0049
Oct 10	384.322	7.9	V	0.002
Oct 11	385.312	7.9	V	0.0049
Oct 14	388.314	8.2	V	0.0019
Nov 19	424.220	6.6	V	0.0018
<b>Total</b>		<b>70.9</b>		

Table 5. VW Ari observational log

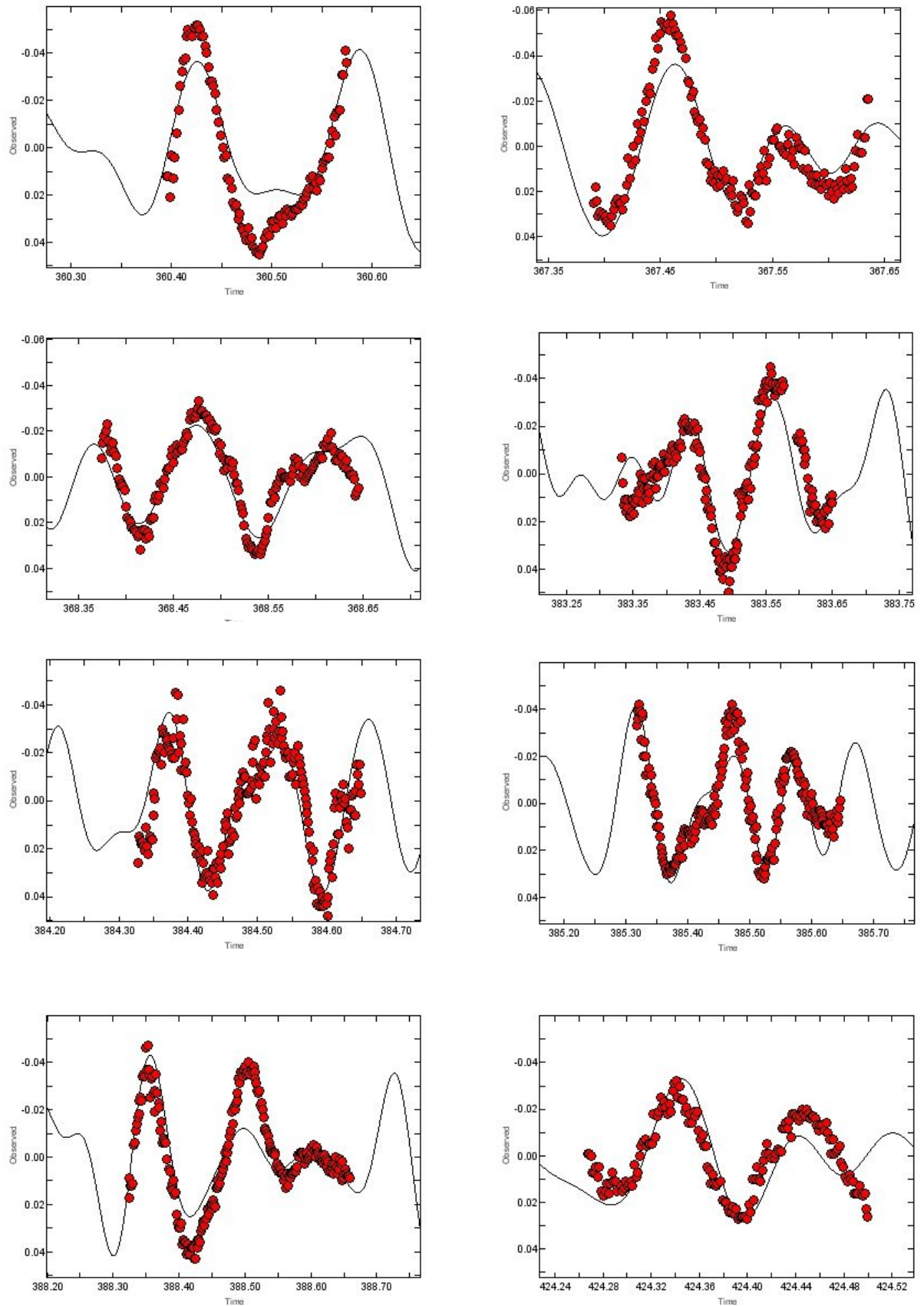


Figure 7. The light curves of VW Ari for 8 from 9 observed nights with the fit of 5 frequencies: Time is in HJD 2454000+, Observed is in mag.

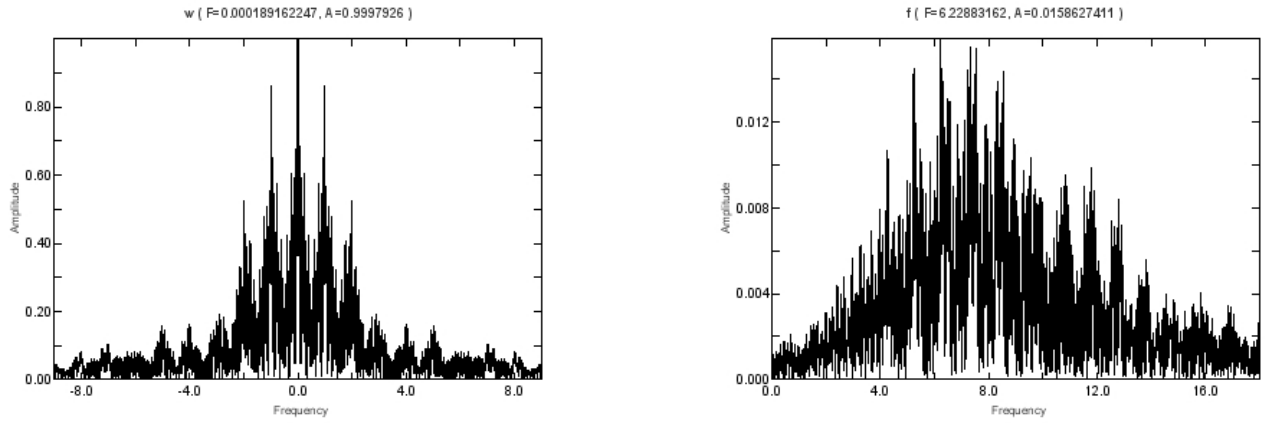


Figure 8. The spectral window (left) and the amplitudes Fourier spectrum (right) of VW Ari data, frequency is in c/d.

	frequency [c/d]	amplitude [mag]	S/N
F <sub>1</sub>	6.224 ± 0.00018	0.017 ± 0.00037	8.47
F <sub>2</sub>	7.562 ± 0.00019	0.016 ± 0.00037	8.33
F <sub>3</sub>	10.811 ± 0.00032	0.0098 ± 0.00037	6.67
F <sub>4</sub>	8.892 ± 0.00041	0.0077 ± 0.00037	4.51
F <sub>5</sub>	12.606 ± 0.00054	0.0058 ± 0.00037	4.44
Residuals		0.010	

Table 6. Frequency solution of VNT data for VW Ari

57.8 hrs of time-resolved photometry spanning 65 nights were applied for the periodogram analysis. The first 2 nights from the Table 5 were not used due to a problem with a telescope guiding, there was also a problem with the time reference in Sep 13 (JD 2454357). In Figure 7 the light curve of VW Ari for 8 from 9 observed nights with the 5 frequency synthetic light curve of solution presented in Table 6.

The very good spectral window and amplitudes Fourier spectrum of VW Ari observations are shown in Figure 8. Comparing with the Table 4, 3 main frequencies have been detected correctly. 2 other frequencies are close to detected by previous authors. The residuals in the Table 6 are sufficient for one-site observations.

### 5. Conclusions:

For inspection of the new Observatory and new instrumentations we selected two of low amplitudes  $\lambda$  Bootis type stars which are still of a concern of asteroseismology although their pulsation behaviour already was examined.

2 star - techniques have got an opportunity obtaining of sufficient amount of the high quality observations during a season in the atmospheric conditions of Central Europe.

V2314 Oph was observed in the frames of multi-site campaign. For the preliminary analysis there were used 19.5 hr of 2-star photometry during 6 nights of June–July 2007. The VNT data have yielded 3-frequencies' solution. F<sub>2</sub> is apparently the one-day alias of the main frequency revealed by Chulhee Kim et al. (2007). Two other frequencies were distorted though the very short nights, unstable atmospheric humidity and extinction in June at the latitude of the VAO KS. The comparing with the synthetic light curve of Sierra-Nevada photometry shown good coincidence in a phase. Some problems with the equipment were obviated.

The autumn observations of another asteroseismic object VW Ari shown much better result. We could use for the periodogram analysis 57.8 hr of time-resolved photometry spanning 65 nights. A comparison of the obtained 5-frequency solution with the patterns of previous authors shown a coincidence of 3 main frequencies. The residuary problems of channel calibration and extra-atmospheric reduction will be solved in the next researches.

Besides, we intend to apply new CCD detectors with the VNT that will allow to observe fainter objects, to have some comparison stars and to preserve the important equipment stability from night to night (see Breger 1998). Asteroseismology of objects in open clusters and associations is now in initial promising stage.

One of effective networks using small or medium size telescopes is STACC (Small Telescope Array with CCD Cameras, <http://www.phys.au.dk/~srf/STACC/>).

### ***Acknowledgements:***

Grant of the Slovak Research and Development Agency LPP-0049-06.

Bilatelar APVV grant SK-UK-01006.

Ukrainian MON grant No M/153-2006

The National Scholarship Programme of the Slovak Republic.

### ***References:***

- Breger M., 1998, XCOV13 and Asteroseismology of Delta Scuti Stars, [1998BaltA...7..211](#)
- Breger M., Handler G., 1993, Extending the WET technique to lower frequencies, [1993BaltA...2..468B](#)
- Brown T. M., Gilliland R. L., 1994, Asteroseismology, [1994ARA&A..32...37B](#)
- Dorokhov N. I., 1999, Calibration system in a two-channel photometer, [1999KNFT...15..189D](#)
- Dorokhova T., 1999, Unification of VW ARIETIS observations obtained in multisite campaign, [1999KFNT...15b.160D](#)
- Chernyshova I. et al., 1998, The unusual A-star VW Ari: chemical composition revisited, [1998CoSka..27..332C](#)
- Crauford D., Barnes J., 1972, Four-color and H $\beta$  photometry for open clusters. VIII. IC 4665, [1972AJ.....77..862C](#)
- Gray R., Corbally C., 2002, A Spectroscopic Search for  $\lambda$  Bootis and Other Peculiar A-Type Stars in Intermediate-Age Open Clusters, [2002AJ...124..989G](#)
- Handler G., 1998, Methodological Aspects of Delta Scuti Star Seismology, [1998BaltA...7..227H](#)
- Farraggiana R., Bonifacio P., 1999, How many lambda Bootis stars are binaries?, [1999A&A...349..521F](#)
- Kim Chulhee et al., 2007, Chemical Composition and Differential Time-Series CCD Photometry of V2314 Ophiuchi: A New  $\lambda$  Bootis-Type Star, [2007AJ...134..926K](#)
- Kudzej I., Dubovsky P. A., Dorokhova T., Dorokhov N., Koshkin N., Parimucha S., Ryabov A., Vadila M., 2007a, First Results of CCD and Photoelectric Photometry on Astronomical Observatory at Kolonica Saddle, [2007OEJV...75...10K](#)
- Kudzej I., et al., 2007b, Odessa Astronomical Publications, vol. 20, in press
- Lenz P., Breger M., 2005, Period04 User Guide, [2005CoAst.146...53L](#)
- Li Z.; Jiang S., 1993, Multiple Frequencies Pulsation of the Delta-Scuti Variable BDS:1269A, [1993AcApS..13..233L](#)
- Liu Y. et al., 1996, On the multiperiodicity of the  $\delta$  Scuti star BDS 1269A (VW Arietis). The fifth campaign of STEPFI network in 1993, [1996A&AS..120..179L](#)
- Martin S., Rodriguez E., 1995, HD 161223 - a New Variable in the Field of IC 4665, [1995IBVS.4273....1M](#)
- Martin Ruiz S., 2007, private communications
- McNamara B.; Horan S., 1984, The remarkable multiple mode Delta Scuti star BDS 1269A, [1984ApJ...282..741M](#)
- Musaev F. et al., 1999, Coudé echelle spectrometer for the Terskol 2-meter telescope, [1999KPCB...15..216M](#)
- Nielsen R.F., 1983, A new generation uvby, H $\beta$  photometer, [1983ITABO..59..141N](#)
- Paunzen E., 1999, The Group Of  $\lambda$  Bootis Stars, [1999Ap&SS.266..379P](#)
- Percy J., 1980, The periods of BDS 1269 A, [1980AcA....30...91P](#)
- Rucinski S., 1978, The unique visual binary BDS 1269, [1978AcA....28..545R](#)

# The Binary Stars With Pulsating Component

PETR ŠVARÍČEK

Astronomical Institute of the Charles University, Prague, Czech Republic

**Abstract:** A method, which uses stellar oscillations to indirect stellar interior analysis – asteroseismology – is presented in this paper. Oscillations are closely related to the state parameters inside a star and a knowledge in the frequencies of stable stationary waves is the matter of seismic analysis. The methods of detection are also mentioned. We presented overview of types of close binary stars with pulsating component or both components and forced oscillations as well as free oscillations in short-period and long-period binaries. The influence of eccentricity resp. variable tidal forces on triggering and modifying stellar oscillations are discussed. The importance of close eclipsing binaries study for determination of internal stellar structure is pointed out.

**Abstrakt:** V tomto článku je prezentována metoda, která hvězdné oscilací využívá pro nepřímou analýzu hvězdného nitra – asteroseismologii. Oscilace jsou úzce svázány se stavovými veličinami uvnitř hvězdy a znalost frekvencí stabilních stojatých vln je základem pro seismickou analýzu. Metody detekce jsou rovněž zmíněny. Představujeme přehled typů těsných dvojhvězd s pulzující složkou či složkami a stručně zmiňujeme vynucené a volné oscilace v dlouho a krátko periodických binárních systémech. Vliv orbitalní excentricity resp. proměnných slapových sil na spouštění a modifikaci oscilací je rovněž diskutován. Poukazujeme na význam studia těsných zákrytových dvojhvězd pro určování hvězdných parametrů.

---

## 1. Introduction To The Asteroseismology

If we want to talk about star oscillations, it is necessary to mention a method, which uses this oscillations to indirect stellar interior analysis - asteroseismology. It allows us to „obtain“ the information of stellar regions, from where we are not able to detect any electromagnetic radiation.

The basic technique of asteroseismology is to observe periodic perturbances revealing in some measurable quantities. These perturbances – oscillations – are closely related to the state parameters inside a star. A knowledge in this parameters allows us to determine the behaviour of plazma element in some position. Thus, if the respective element will be fused with surrounding matters and will cause destruction of perturbation or will oscillate round the equilibrium point or will move to another position in star.

The random thermal motions induces the oscillations with continuous spectrum of frequencies inside the star, but only the stationary waves are long lasting. Frequencies of these waves are discrete and are called eigenvalue frequencies. The identification of these frequencies is the matter of seismic analyse of all kind.

According to the character of forces inducing the oscillation, we define three types of periodic perturbances. Gravitational oscillations (g), acoustic or pressure (p), and fundamental „sea-like“ surface waves (f).

Another type of oscillation is related to the existence of two ionization form of one chemical element ( in most cases H or He) which have different opacities. Such mechanism is called opacity mechanism and leads to pure radial oscillations ( classic Cep stars). The existence of convective zones leads to non-radial oscillation with  $l > 0$ .

## 2. Methods Of Measurement

Among the most used methods is the method based on measurement of doppler shifts for suitable spectral lines reflecting local motions caused by oscillations. High-resolution spectrographs are used to the measuments. Unfortunately, the amplitudes of oscillations are very small in most cases and short period of observation should be cover by high density data.

The photometric measurement of the total radiant flux is very native Metod of detecting the stellat oscillations. This way has one big advantage – simple instruments can be used and it is also possible to measure more than one star at the same time. Unfortunately, the atmosphere of Earth affects this measurement.

The last method is based on studying of spectral line profile variations caused by thermal fluctuation as the wave goes throught the stellar interior. The lines of Balmer series are usually used.

### 3. Representation Of The Oscillation

The oscillation on the surface of the star can be mathematically represented by means of spherical harmonic function.

$$Y_l^m(\theta, \varphi) = \sqrt{\frac{(2l+1)(l-m)!}{4\pi(l+m)!}} \cdot e^{im\varphi} \cdot P_l^m(\cos\theta)$$

Each of oscillation mode is characterized by three number. Radial parameter „n“ denotes the number of radial nodal plane from center to the surface of the star, angular parameter „l“ denotes the number of nodal planes on the surface and azimuthal parameter „m“ denotes the number of surface nodal planes passing the pole.

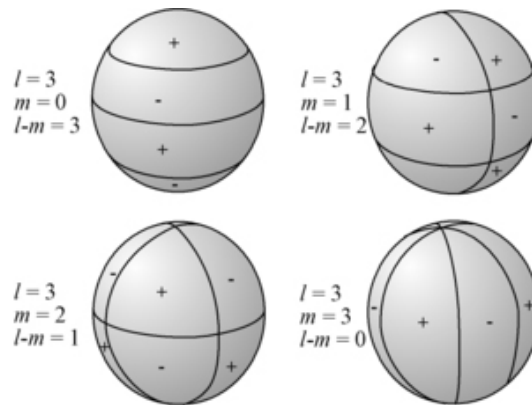


Fig 1: Schematic representation of spherical harmonic on the unit sphere.  $Y_{lm}$  is equal to 0 along  $m$  great circles passing through the poles, and along  $l-m$  circles of equal latitude (internet source – wikipedia.org).

### 4. Inverse And Other Problems

Only the knowledge of the frequencies of eigenvalue oscillations does not allow us to determine the stellar interior parameters. Here comes the method of mathematical physics called “Inversion”, which is about computing of model of star with similar mass and of similar spectral type, from which the theoretical frequencies are in best agreement with the observed values. We can claim about such model with high probability, that it describes the real stellar physical parameters.

Unfortunately, sometimes it’s a very difficult or even impossible to identify the modes of oscillation uniquely. For instance  $\delta$  Scuti type star XX Pyx can be mentioned. Thirteen oscillation frequencies were used and number of models, which produced spectra in good agreement with the observation, was about 40000.

There are a few factors by which the identification of frequencies and oscillation modes is affected. We should mention e.g. precision of available data, circumstellar shell or mass flow. It is also necessary to point out that not all of detectable variations are caused by pulsation. The false variation in data sets can be also produced by LTTE, irregular shape of star or corotating structures.

### 5. Pulsating Stars

If we want to find a pulsating star, it’s not necessary to go far away. Our mother star Sun reveals about 1800 oscillation periods so far.

Radial pulsating „classic“ Cepheids belong to the most widely known pulsating stars. These stars provide us reliable way, how to measure distances in universe, because of the period-luminosity relationship.

$\beta$  Cephei belongs to the evolved B type stars revealing periodic changes of brightness and radial velocities with periods below 0.3 days. Their pulsations – often multiperiodic – can be explained by means of opacity mechanism. The period-luminosity relationship cannot be well defined for this stars contrary to „classic“ Cepheids stars.

Among the other star pulsators we should mention following types of stars:  $\delta$  Scuti, roAp, SX Phe,  $\gamma$  Dor, WD, NS etc.

## 6. What Are The Binary Stars With Pulsating Component Useful For?

Considering that a significant fraction of oscillating stars are members of multiple systems, it seems legitimate to ask how much duplicity and atmospheric oscillations affect each other.

A more general motivation for studying stellar oscillations in binaries is at least threefold:

1. To understand what role duplicity plays in triggering or modifying stellar oscillations. This requires systematic studies of a large sample of oscillators in binaries.
2. The study of rapid variations and their occasions. Whether they arise from stellar oscillation or e.g. corotating structures or not.
3. To apply asteroseismology in all details and derive internal rotation behaviour, accurate stellar age, metallicities and of course to derive one of the most important parameters in current stellar models – convective overshooting parameter.

## 7. Forced Oscillations

Numerous theoretical studies predict the occurrence of forced oscillations in close binaries due to resonance between dynamical tides and free gravity-mode oscillations of spherical degree  $l = 2$ . Willems & Aerts (2002) found in their studies of RV curves in pulsating systems, that amplitudes of RV curves increased with increasing eccentricity. They obtained sinusoidal RV curves whenever the orbital period was an exact multiple of oscillation period of degree  $l = 2$ . Irregular RV curves are expected, if the orbital period slightly differs from an exact multiple of the free oscillation period.

It is obvious that the shape of the star in the eccentric system is changing during the orbiting due to variable tidal force. It leads to the complex variability and cyclic variations of the oscillation period. The rotation of the star is another complication. This fact has a negative effect on the analysis of RV curves variations and line profiles. At the same time it is also impossible to obtain the values of the frequencies separately at periastron or apastron, because there is no reason to consider them being in the phase during different periastron passages. Thus, the long observational time brings no gain. Standard Fourier analysis of such data could lead to the false claim of the multiperiodicity – proper model of oscillations for the right frequency analysis is required.

Good example of the system with forced oscillations seems to be slowly rotating B star designated as HD 177863 with eccentricity  $e = 0.60$  and orbital period  $P_{\text{orb}} = 11.9^{\text{d}}$  (De Cat et al. 2000). The dominant intrinsic period in RV residuals and in the multicolor photometric variations is  $1.19^{\text{d}}$ , which is exactly 10 times shorter than the orbital period. Willems & Aerts (2002) showed, that this frequency is corresponding to the forced oscillation of  $l = 2, m = -2$  for radial orders  $n$  between 27 and 53.

Another candidate revealing forced oscillations is HD 209295 with eccentricity  $e = 0.35$  and orbital period  $P_{\text{orb}} = 3.1^{\text{d}}$  ( $f_p = 0.33$  c/d), according to Handler, Balona & Shobbrook (2002). Among numerous frequencies derived by authors, there are low frequencies  $f_p = 1.13$  c/d,  $2.3$  c/d, the acoustic mode frequency  $25.96$  c/d, and their combinations. Handler et al. (2002) identified this low frequencies with the pulsating mode of  $l = 2, m = -2$ .

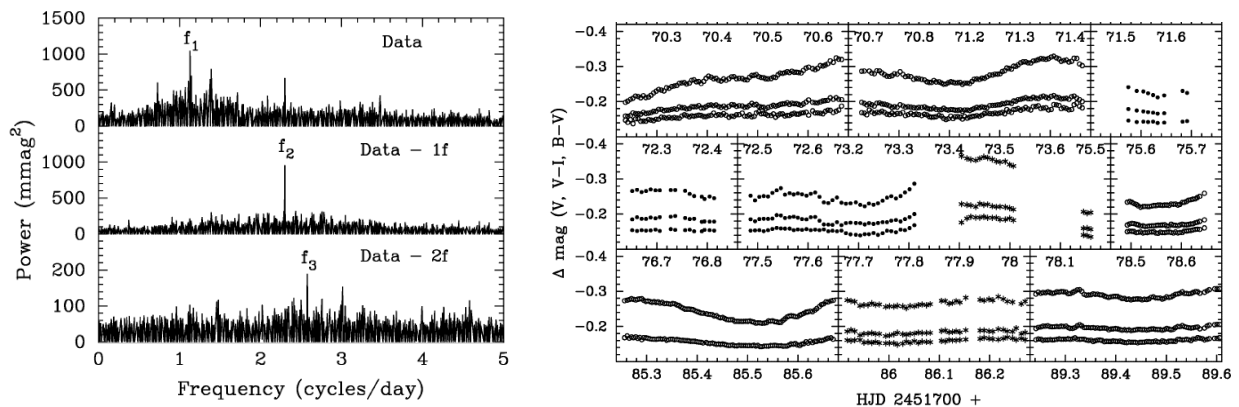


Fig 2: The power spectrum and the light curves of HD 209295 with variations (Handler et al. 2002)

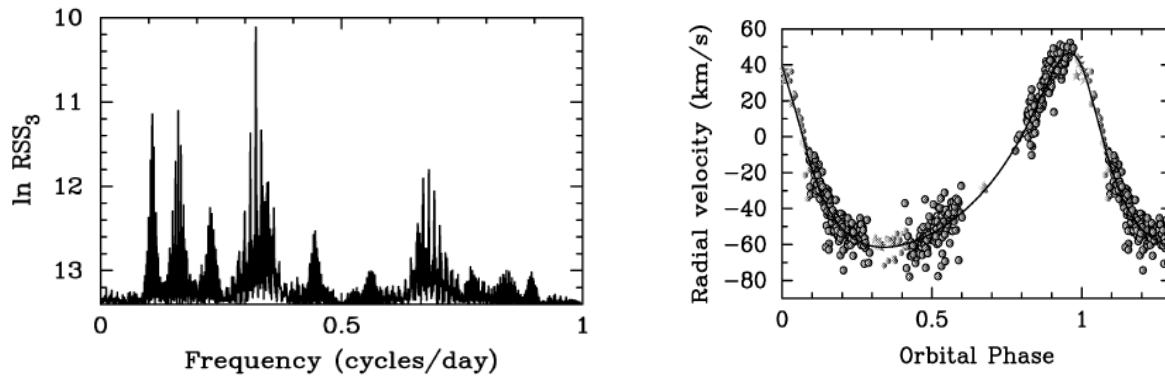


Fig 3: The power spectrum and the RV curve of HD 209295 (Handler et al. 2002)

### 8. Free Oscillations In Short-Period Binaries

Smith (1985) proposed, that free acoustic oscillations in the binary system  $\alpha$  Vir (Spica,  $P = 4.01$  d,  $e = 0.15$ ) are modified by tidal effects, but the idea was not developed since then.

Multiple acoustic high-degree modes were found for the massive close binary systems  $\psi^2$  Ori (B1III + B2V,  $P_{\text{orb}} = 2.5^{\text{d}}$ ,  $e = 0.05$ , Telting, Abbott & Schrijvers 2001) and  $\nu$  Cen (B2IV + ?,  $P_{\text{orb}} = 2.6^{\text{d}}$ ,  $e = 0.0$ , Schrijvers & Telting 2002). There were no detectable changes found in the oscillations by tides.

Early type B star,  $\epsilon$  Per (B0.5IV,  $P_{\text{orb}} = 14.07^{\text{d}}$ ,  $e = 0.52$ , Tarasov et al. 1995), belongs to the classical variable systems revealing line-profile variations. However, there is no agreement, whether its short-periodic variations are caused by multiple oscillations (Gies et al. 1999) or another complex phenomena e.g. corotating structures (Harmanec 1999) or both.

EN Lac binary system reveals variations of RV curve amplitude near the periastron (Lehman et al. 2001).

All the stars mentioned above are situated in the  $\beta$  Cep instability strip and one can expect non-radial pulsations to be excited via the  $\kappa$  mechanism.

### 9. Free Oscillation in Short-Period Binaries, Especially The Eclipsing One

Eclipsing binary stars belong to the special group of binaries. The binaries are the best laboratories to test our stellar models. By means of analysis of RV curve and light curves we can derive such parameters as masses, radii, luminosities, effective temperatures, metallicities, and age. These parameters are sufficient starting point for advanced seismic modelling based on the identified frequencies. Convective overshooting parameter is a very important quantity, but its value is charge by relatively large uncertainty in current stellar evolution model.

Among eclipsing binary stars with pulsating component, we should mention e.g. EN Lac, V539 Ara, Y Cam, RZ Cas, AS Eri, RU Umi etc.

### 10. Oscillation In Long-Period Binaries

The reason, why we consider long-period binaries (orbital period is at least two orders of magnitude longer than their oscillation periods) separately, is that one does not expect any measurable influence of the tidal forces on the rapid variations.

$\alpha$  Cen A (G2V + K1V,  $P_{\text{orb}} = 79$  yrs,  $e = 0.52$ ) is an exemplary system of such binary. There were detected 28 solar-like oscillation modes in the frequency range 1.8 to 2.9 mHz in the primary (Bouchy & Carrier 2001) and 12 such modes in the frequency range 3 to 4.6 mHz in the secondary (Carrier & Bourban 2003) two years later. The excitation mechanism and nature of these modes are the same as for the Sun, thus it is possible direct helioseismic analysis.

Another interesting binary system is  $\beta$  Cen ( $P_{\text{orb}} = 357.02^{\text{d}}$ ,  $e = 0.814$ , Auserloos et al. 2002). Both of the stars reveal line-profile variations, however no photometric variations were detected. We are likely dealing here with high-degree non-radial oscillation modes, which tend to cancel out mutually in photometric data.

Pigulski & Boratyn (1992) showed in the case of  $\beta$  Cep ( $P_{\text{orb}} \sim 90$  yrs), that the secular variations of the main pulsational period are direct caused by LTTE. If we did not consider this fact, the Fourier analysis would lead to false claim of multiperiodicity.

A remarkable object with extreme eccentricity  $e = 0.92$  and orbital period  $P_{\text{orb}} \sim 10$  let is  $\delta$  Sco. A strong Balmer emission and large optical brightening with cyclic variations on a time scale of a few months were detected during the last periastron passage in 2000. However, the question arises what extent a steep gradient in the tidal forces is responsible for this phenomena (see Miroshnichenko et al. 2003 for discussion).

## 11. Little Conclusion

Asteroseismology have experienced blustering progress during few past decades, mainly in connection with increasing of instrumental accuracy and past or present observational project gathering a huge amount of high density data e.g. MOST or COROT. Study of binary stars is the best way for astronomers and astrophysicists to obtain and constrain basic stellar properties in current stellar evolutional models. Research of eclipsing binaries with pulsating component is the proper way to obtain more accurate values of basic stellar properties, especially convective overshooting parameter, one of the most uncertain parameter in current models.

## References

- Aerts, C., Harmanec, P. 2004, ASPC, 318, 325
- Ausseloos, M., Aerts, C., Uytterhoeven, K., et al. 2002, A&A, 384, 209
- Bouchy, F., Carrier, F., 2001, A&A, 374, L5
- Carrier, F., Bourban, G. 2003, A&A, 406, L23
- De Cat, P., Aerts, C., De Ridder, J., et al. 2000, A&A, 355, 1015
- Gies, D., Kambe, E., Josephs, T. S., et al. 1999, ApJ, 525, 420
- Handler, G., Balona, L. A., Shobbrook, R. R. 2002, MNRAS, 333, 262
- Harmanec, P. 1999, A&A, 341, 867
- Lehmann, H., Harmanec, P., Aerts, C., et al. 2001, A&A, 367, 236
- Miroshnichenko, A. S., et al. 2003, A&A, 408, 305
- Pigulski, A., Boratyn, D. A. 1992, A&A, 253, 178
- Schrijvers, C., Telting, J. H. 2002, A&A, 394, 603
- Smith, M. A. 1985, ApJ, 297, 224
- Tarasov, A. E., Harmanec, P., Horn, J., et al. 1995, A&AS, 110, 59
- Telting, J. H., Abbott, J. B., Schrijvers, C. 2001, A&A, 377, 104
- Willems, B., Aerts, C. 2002, A&A, 384, 441

# CCD Photometry: Measurement uncertainty

MAREK CHRSTINA, FILIP HROCH

Department of Theoretical Physics and Astrophysics, Faculty of Science, Masaryk University,  
Kotlářská 2, 611 37 Brno, Czech Republic  
Email: [chrastina@kozmos.sk](mailto:chrastina@kozmos.sk), [hroch@physics.muni.cz](mailto:hroch@physics.muni.cz)

## Abstract:

Aperture photometry is one of the methods which allows to measure intensity of a star on a CCD frame. There exist several programs which can be used for this, such as DAOPHOT, MuniPack, C-MuniPack. If we use any method for data processing, it is very important to know how the method works. In this paper we discuss how it measures the brightness of a star. However, the knowledge of stellar brightness is insufficient because each measurement has an error. We discuss also in this paper the simply method how can be estimate the measurement uncertainty. Above mentioned codes use this method. It is based on aperture photometry used to stellar brightness estimation and on the using of statistics. It does not require complicate calculations or additional measurements. Brightness and its uncertainty are determinate only from the CCD frame.

## CZ Abstrakt:

Apertúrna fotometria je jedna z metód, pomocou ktorej môžeme zmerať intenzitu hviezdy na CCD snímke. Existuje niekoľko programov, ako napr. DAOPHOT, MuniPack, C-MuniPack, ktoré s touto metódou pracujú. Nech už na spracovanie dát používame akúkoľvek metódu, je nesmierne dôležité vedieť ako metóda funguje. V našom článku rozoberáme metódu, ktorú vyššie zmienené programy používajú na meranie jasnosti hviezdy. Avšak znalosť jasnosti hviezdy sama o sebe nestačí, pretože každé meranie je zaťažené chybou. V článku tiež rozoberáme jednoduchú metódu ako môžeme odhadnúť neistotu merania. Túto metódu používajú vyššie zmienené programy. Je založená na apertúrnej fotometrii použitej na odhad jasnosti hviezdy a na štatistike. Nevyžaduje komplikované výpočty ani dodatočné merania. Jasnosť a jej neistota sú určené iba z príslušnej CCD snímky.

---

## 1. Observed Brightness

A basic observable quantity for a star is its brightness. For any given telescope, filter and detector system, the observed brightness of an object expressed in magnitudes, is given by

$$m = -2.5 \cdot \log_{10} f + m_0 \quad (1)$$

This is a form of Pogson equation, where  $f$  is a stellar flux. We collect the flux for certain (so-called exposure or integration) time. Thus, CCD frame includes information about the stellar intensity, i.e. the flux multiplied by the exposure time. Our measurement scale is calibrated by the constant  $m_0$  (so-called "the zeropoint"). It is determined by measuring the flux for "standard" stars that serve as reference calibrators. This zeropoint in magnitudes is the single scaling factor for an astronomical imaging system such as CCD photometry. However, CCD camera provides the intensity measurements in ADUs (Analog-to-Digital Units). If we plug those values into the formula (1), we can sweep all the calibration factors into the system's zeropoint. If done this way, the zeropoint represents the magnitude of an object that would produce a detected signal accumulation of 1 ADU (Larson 2007).

Astronomers often refer to "instrumental magnitudes", where the value of  $m_0$  is not tied to a well-defined set of standards, but to certain predetermined value. This is perfectly fine as long as one is only interested in differences their magnitudes, i.e. in relative fluxes between measured objects, if one make so-called differential photometry. If we compare the fluxes, constant  $m_0$  drops out so its value is not so important. Instrumental magnitudes provide only qualitative information. Without calibrating the measurement scale to the real standards, in this way determined instrumental magnitudes can be used only for relative analysis. Value of the constant is usually  $\sim 23.5$ - $26.0$  mag for most earthly observing sites. *So we decided to choose 25.0 mag as the default value for C-Munipack package. By this definition, an instrumental magnitude of 25.0 will be assigned to the stellar intensity of 1 ADU.*

## 2. CCD Aperture Stellar Photometry

Aperture photometry is one of the methods which allows to measure intensity of a star on a CCD frame. Consequention of the method is as follows. A virtual aperture around the star on the frame is made. From several reasons circular aperture is used most often, although in principle it can have other shape too, for example elliptical or polygonal. *For now, C-Munipack package use only circular apertures with user-specific radius.*

For each aperture the stellar intensity is taken to be the total intensity in an aperture minus the background intensity which mostly contains the sky intensity. Total intensity is determined simply as a sum of all pixel values inside the aperture. We point out that aperture photometry takes into account partially including pixels, too. It may happen that aperture boarder does not go among the pixels but go through them. The same part of the pixel value as the part of the pixel area inside the aperture is taken to total intensity.

The background intensity is estimated statistically as a mean value of a background nearby the measured star. Clearly it be made from an image region devoid of obvious stars, but representative of the expected background below the star's image. Thus, this background sample must be taken close enough to the star but at the same time far enough away the star in order to be not contaminated by its light. *For this purpose C-Munipack package uses an annulus (typically of outside and inside 20 and 30 pixels respectively, can be changed by user) around the object (aperture center).*

The background sample represents statistical data set of individual pixel values. By determinating its mean value we obtain the mean background intensity related to one pixel. *C-Munipack package determines this value by using robust statistics that markedly suppress the influence of outliers caused by e.g. the presence of the very faint stars in the background sample.* The background intensity in an aperture is then calculated as the number of pixels in the aperture multiplied by the mean background per pixel.

*Instrumental magnitude is calculated by C-Munipack package according to that above mentioned, mathematically expressed as (Hroch 1998):*

$$N_{\text{aperture}} = \sum_{n=0}^{n_{\text{aperture}}} p(n) \text{ [ADU]} \quad (2)$$

$$m = 25.0 - 2.5 \cdot \log_{10} \frac{N_{\text{star}}}{1 \text{ ADU}} \quad (3)$$

$$m = 25.0 - 2.5 \cdot \log_{10} \frac{N_{\text{aperture}} - n_{\text{aperture}} N_{\text{sky}}}{1 \text{ ADU}} \quad (4)$$

where  $N_{\text{aperture}}$  is total signal (intensity) in chosen aperture in ADU,  $n_{\text{aperture}}$  is number of pixels in this aperture,  $p(n)$  are the values of these pixels in ADU and  $N_{\text{sky}}$  is mean intensity of nearby sky background per pixel in ADU/px. Thus, in ideal case  $N_{\text{star}}$  is the intensity related only to the star.

### 3. Statistics. Poisson distribution

The variance  $D$  of a random variable  $X_i$  is a measure of its statistical dispersion, indicating how its possible values are spread around the expected value. Is defined as follows:

$$D(X) = \frac{1}{n} \sum_{i=1}^n (X_i - \bar{X})^2 \quad (5)$$

where  $n$  is number of values  $X_i$  of random variable  $X$ ,  $\bar{X}$  is mean value found as e.g. arithmetic average of values  $X_i$ . Thus, unit of  $D$  is squared unit of  $X$ . It can be simply shown that:

$$D(X) = \overline{X^2} - \bar{X}^2 \quad (6)$$

Of course, it is possible to define the other measures of the dispersion. One reason for the use of the variance in preference to other measures of dispersion is that the variance of the sum (or the difference) of uncorrelated (independent) random variables is the sum of their variances:

$$D\left(\sum_{i=1}^n X_i\right) = \sum_{i=1}^n D(X_i) \quad (7)$$

This fact can be simply shown. Formula used to be designated as "standard law" of uncertainty propagation. We notice that the opposite implication, i.e. if formula (7) is true that random variables are independent each other, is not true.

For obtaining the measure of dispersion which has the same unit as the variable, we define the standard deviation  $\sigma$  as square root of the variance. It represents "natural" measure of the data dispersion around the mean value.

$$\sigma = \sqrt{D(X)} \quad (8)$$

Let's see what the "propagation of errors" calculation gives us for CCD photometry. Let's say that the uncertainty for the number of electrons collected in one pixel is independent of the uncertainty for any other pixel in the image. This means that if a set of  $n$  pixels each has the same uncertainty  $\sigma$ , the sum of the electrons in those  $n$  pixels will have an uncertainty larger than uncertainty for one pixel by a factor of  $\sqrt{n}$ ; the average over  $n$  pixels will have an uncertainty equal to that of one pixel divided by  $\sqrt{n}$  (Kundracik 1997).

$$D(\bar{X}) = D\left(\frac{1}{n} \sum_{i=1}^n X_i\right) = \frac{1}{n^2} \sum_{i=1}^n D(X_i) = \frac{1}{n^2} \sum_{i=1}^n \sigma^2 = \frac{\sigma^2}{n} \quad (9)$$

$$\sigma(\bar{X}) = \frac{\sigma}{\sqrt{n}} \quad (10)$$

Formula (10) mathematically expresses naturally expected result that the uncertainty of arithmetic average decreases as the number of measurements increases. However, increasing of this precision by increasing of the number of measurement  $n$  is a little bit slow. Thus, it is better to decrease the single measurement uncertainty  $\sigma$ . Notice that generally we do not know this  $\sigma$ , so it must be estimated. It can be shown that in this case the better estimation of  $\sigma^2$  than eq. (5) is this one:

$$\sigma^2 = \frac{1}{n-1} \sum_{i=1}^n (X_i - \bar{X})^2 \quad (11)$$

### 3.1 Poisson distribution

Consider a time interval during which  $N$  photons have arrived, at random moments. The probability that  $n$  photons arrived in the time sub-interval follows from the binomial distribution. This reduces to a Poisson process in the regime where individual photons are counted. Poisson distribution of probability has a random variable, which expresses the number of appearances of events with little probability in given time or volume interval. Spectrum of Poisson noise is frequency independent (that kind of noise is so-called white noise).

For sources of noise that behave under the auspices of Poisson statistics (which includes photon noise from the source itself), we know that 1 sigma uncertainty ( $1 \sigma$ ) for a signal level of  $N$  is given by:

$$\sigma_{\text{Poisson}} = \sqrt{N} \quad (12)$$

This means that if an amount of arrived photons is large enough, the variation would be equal to the square root of the typical (the mean) number of arrived photons. Therefore, the uncertainty assigned to any contribution to the photon count is set equal to the square root of that contribution to the count.

If the signal mean value is high enough, Poisson distribution will become almost undistinguishable from Gauss distribution although technically remains Poissonic. It allows using both of them. Associated error to this will be much smaller than instrumental errors and compared with them may be neglected.

There occurs the term of shot noise, mostly in electronics. It is only the other name for a Poisson process which describes the random fluctuations in a measurement signal due to the random arrival time of the signal carriers (electron, photon, etc.). It is a type of electronic noise that occurs when the finite number of particles that carry energy, such as electrons in an electronic circuit or photons in an optical device, is small enough to give rise to detectable statistical fluctuations in a measurement.

Shot noise results from the fact that the current is not a continuous flow but the sum of discrete pulses in time, each corresponding to the transfer of an electron through the conductor. Its spectral density is proportional to the average intensity and is characterized by a white noise spectrum up to a certain cut-off frequency, which is related to the characteristic time. It is a quantum noise effect, related to the discreteness of photons and electrons. It represents a fundamental limit to the optical intensity noise, under which it is impossible to go. In devices such as tunnel junctions the electrons are transmitted randomly and independently of each other. Thus the transfer of electrons can be described by Poisson statistics, which are used to analyze events that are uncorrelated in time.

### 3.2 Notes on terms

There occurs the terms as the measurement error and the uncertainty or the estimate error in the statistical measurement processing. Since the terms are often interchanged and do not mean the same thing, we explain what we mean.

Term of error is used to designate the fact that the quantity value obtained from experiment is different from real one. Real measurement error is unknown as well as real quantity value. In principle they cannot be measured absolute precisely. For this reason experimentators try to estimate the possible measurement error via experiment analysis, i.e. try to obtain the estimation of error. This estimation is designated as uncertainty or estimate error, which is in ideal case a little bit larger than real error. It is clear that the uncertainty depends on the way how it is estimated. It gives possible error values, so it has probabilistic (statistical) character. The uncertainty is always associated with the probability distribution. It determines values which are the most and the least probable.

Each measurement has an error. We can trace individual error or noise sources via experiment analysis. Term of noise simply represents something what unwanted influences our measurement and results in measurement error.

## 4. Uncertainty of single photometric measurement

### 4.1 Uncertainty and S/N ratio

In section 1 we describe how the brightness of a star is determined. Now, we will concern about uncertainty of this determination. Finally, we express the brightness in magnitudes, so it is suitable to express its uncertainty in the same unit as well. The Pogson equation (1) thereon offers the solution. As a result of finite S/N (signal/noise) ratio the uncertainty can be estimated in magnitudes as the difference of the total intensity (including the stellar intensity as well as the noise intensity) and the stellar intensity (Simonetti 2004):

$$\Delta m = 2.5 \cdot \log_{10} \frac{S+N}{S} = 2.5 \cdot \log_{10} e \cdot \ln \frac{S+N}{N} \approx 2.5 \cdot 0.43429 \cdot \frac{N}{S} \approx 1.0857 \frac{N}{S} \quad (13)$$

where we used the conversion of decadic logarithm to natural logarithm and Taylor series for function  $\ln(1+x)$  that gives the first-order approximation  $\ln(1+x) \approx x$ . The final result is appropriate for  $S/N \gg 1$ , so for the case of small noise in compare with the signal (stellar intensity).

We can see from this that S/N ratio is the inverse of the standard deviation in magnitudes:

$$\sigma \approx \Delta m \propto \frac{N}{S} \quad (14)$$

This approximation is fine as long as S/N is at least 5 or so, what is caused by the logarithmic character approximation. This represents the simply way how to estimate the standard deviation of stellar brightness, i.e. uncertainty, in magnitude units.

In the case of CCD photometry the number of electrons is suitable unit for the signal as well as the noise, but due to the astronomical tradition they are evaluated in the magnitude units. Fortunately, the derivation (13) provides also the correction factor between an uncertainty in electrons (=photons, at 100% CCD chip quantum efficiency) and that same uncertainty in magnitudes, the value of 1.0857.

### 4.2 S/N ratio. Unit conversion

Now, we know how to estimate uncertainty from S/N ratio, so it remains to calculate the ratio. If we have an ideal case, where it is no additional noise source one still remains, Poisson statistics of the stellar photons for which (s. eq. 12) is given:

$$\frac{S}{N} = \frac{S}{\sqrt{S}} = \sqrt{S} \quad (15)$$

where values are in the number of electrons. The statistics of counting depends on the number of photons that hit the chip and that are converted to electrons by the CCD and not the ADUs present in the CCD image. The statistics in ADUs would be a little bit different, e.g. due to the fact that gain of CCD is not a real constant but it also has its uncertainty, statistics. Unfortunately, information about the gain uncertainty is usually not available. Of course, it is possible to measure it, but it requires well-equipped laboratory and many experimental experiences as well. It cannot be expected from common observers, so we assume that the gain is true constant although it is not in fact.

A pixel value in ADUs is equal to the number of electrons detected in that pixel, divided by the gain of the CCD, where gain  $G$  is in units of  $e^-/ADU$ . In this way, the signal or the noise can be converted from ADUs to electrons and vice versa.

$$\frac{S}{1e^-} = \frac{G}{1e^-/ADU} \frac{S}{1ADU} \quad (16)$$

Let  $C$  is the sum over all the pixels containing signal due to incident photons from a star in ADUs, so S/N could also be rewritten in number of electrons:

$$\frac{S}{N} = \frac{GC}{\sqrt{GC}} = \sqrt{GC} \quad (17)$$

or

$$\frac{S}{N} = \frac{C}{\sqrt{C/G}} \quad (18)$$

implying that S/N can be measured at some location in the image using the pixel values to compute the signal, but then the Poisson noise deduced from these pixel values must be scaled down by  $\sqrt{G}$  in calculating the signal-to-noise ratio.

### 4.3 Noise

By the time that the magnitude of an object is estimated from its image in a CCD frame, a number of different random errors will have contributed to this measurement. Here arises the question how to figure other noises in the total measurement uncertainty. Equation (18) is an approximate upper bound which can serve as a rough ballpark estimation of S/N when the star is bright enough, because of the number of electrons produced by its photons is very large compared to the number of electrons produced by any other process. Thus for  $S/N \gg 1$  which is the same assumption as for the derivation (13) of the standard deviation.

The uncertainty for the number of electrons collected in one pixel is independent of the uncertainty for any other pixel in the image or rather we suppose it. For example dark current originates from the lattice defects of silicon detector, which generate extra electrons. Each released electron is statistically independent event, so the dark current follows the Poisson distribution just as stellar photons (Berry & Burnell 2005). Considering that the dark current electrons are independent inside one pixel, they are independent of the electrons inside the other pixels. But there still remains a spatial dependence of the uncertainty associated with dark current due to each pixel generates a slightly different level of dark current, so the noise level as well as the dark current's inherent Poissonian contribution is different for each pixel (Budding & Demircan 2007).

Another unwanted signal is the bias. However, it is not a random process but a constant output signal offset. It is caused by electronics which detect and amplify the signal from detector. However, bias is linked with readout noise, i.e. with random fluctuations in amplifier circuits which are added to the each output from detector. Readout noise is constantly regardless of the bias amplitude and the signal level (Budding & Demircan 2007).

We can say that all electrons released by incident photons (from the object of interest, or from the "sky" along the line of sight) or by other processes (e.g. "dark current") in the CCD chip are independent each other and obey Poisson statistic (Simonetti 2004).

As we see from the law of uncertainty propagation (eq. 7) the total uncertainty which is influenced by many errors is given by the square root of the sum of the squared individual error uncertainties.  $s_i$  are the individual variances and  $\sigma_i$  are the individual standard deviations.

$$N = \sqrt{\sum_i s_i} = \sqrt{\sum_i \sigma_i^2} \quad (19)$$

There are many noise sources in the CCD photometry. Anybody who wants to determine the uncertainty of photometric measurement must to consider which noise sources takes into account. Generally, it is supposed a few most important noise sources independent each other (Berry & Burnell 2005). Usually, it is taken photon statistics as the most important noise source and a few others such as sky, dark, readout and digitization noise etc. Digitization noise is simply said the rounding error related to the digitization process. The range as well as the resolution of A/D converter are finite, so one digital value corresponds to values of analogue signal from any interval. Therefore, it arises an error which is larger as the resolution of A/D converter is smaller. It is also clear that S/N ratio is important only for the lower signal levels.

Aside from the charge transfer efficiency, which has to be very high, another potential component to image noise comes from the various high frequency oscillators involved in the gating circuitry. This clocking noise rises with signal load and clocking frequency, but it can normally be controlled by manufacturers to a negligible level for astronomical applications (Budding & Demircan 2007).

#### 4.4 CCD equation

In the papers it is supposed to be a formula for the estimation of the total noise  $N$  from the individual partial noises (Howell 1989, Howell et al. 1996, Howell et al. 2001). For instance this one:

$$N = \sqrt{N_{\text{star}} + n_{\text{pix}} \left(1 + \frac{n_{\text{pix}}}{n_B}\right) (GN_S + GN_D + N_R^2 + G^2 \sigma_f^2)} \quad (20)$$

where  $N_{\text{star}}$  is signal from a star,  $n_{\text{pix}}$  is number of pixels in an aperture,  $n_B$  is number of pixels used for the mean background (sky) intensity calculation,  $N_S$  is background (sky) noise,  $N_D$  is dark noise,  $N_R$  is readout noise,  $G$  is gain and  $\sigma_f$  is estimation of 1 sigma A/D converter uncertainty.

This formula is occurred in several different forms due to which noise sources are taken into account and in what mathematical form. Notice that this "liberty" is not given only by creative abilities of the equation author but first by physics. Noises in each instrumental system and at each observing site can be important in different way, so they must be accounted in different way.

Advantage of this method consists in that at the same time it points out the importance of individual noises. If we want to more precise measurements, we immediately know which noise sources have to be reduced. Its disadvantage inheres in requirement of quantitative knowledge of individual noises. For this the many additional measurements and often well-equipped laboratory are needed.

#### 4.5 Noise estimation from CCD frame

If we leave the requirement of quantitative knowledge of individual noises, i.e. we reduce only on the knowledge of the total measurement uncertainty; we can go the other way. We can use our CCD frame, in which in principle is hidden all what we want to know, but we are not able to obtain it. This is the reason of requirement for additional measurements in previous section 4.4.

We interest in determination of the star brightness and its uncertainty. However, image of the star in CCD frame is made not only by incident stellar photons but also by sky photons and other noises. Therefore, it is not possible to measure the stellar brightness directly. We can only estimate it, for instance due to eq. (4). This is only the estimation because we do not know the real background value under the star image but only its estimation. For the same reason if we interest in stellar brightness uncertainty we cannot find it directly. Again, we can only estimate it.

Our estimation will come out from the estimation of the individual quantities which are present in the stellar brightness calculation (eq. 4) and from the usage of the uncertainty propagation law (eq. 7). For the estimation of individual quantities we will come out from what is available, so from CCD frame.

A background sample used to find the mean sky intensity (s. sec. 2) of course includes not only the sky noise but all remains noises contributing to the total uncertainty except for noise due to the stellar photons. Beside others it namely includes dark noise, readout noise, level of contamination by neighboring stars, even noise due to numerous, but individually unrecognizable faint stars in the background and uncertainties caused by the dark frame correction and flat field correction.

If we estimate the mean value of the sky intensity we should say more precisely that we estimate the mean value of the background intensity, because the other noises cannot be separated in this way. Then we may determinate the uncertainty of this estimation with regard to the number of pixels used to it and estimate the stellar photon noise and use the law of uncertainty propagation and we would have the total uncertainty of the stellar brightness which includes all noises influencing the CCD frame origin. This method introduces very simply way how to estimate the measurement uncertainty which includes many noise sources without requirement of complicated calculations or additional measurements.

### Stellar photon noise

In the most cases the dominant noise source is the Poisson statistics of stellar photons because of its number is very large compared to others. The uncertainty of the number of captured photons is given by eq. (12), so we have:

$$\sigma_{\text{star}}^2 = G \frac{N_{\text{star}}}{n_{\text{frames}}} \quad (21)$$

where  $N_{\text{star}}$  is determined from CCD frame in ADUs due to eq. (4) and if multiplied by  $G$  constant of A/D converter's gain in e<sup>-</sup>/ADU it is converted into e<sup>-</sup>, exactly due to eq. (16). The averaging of the raw data frames yields to the statistical improvement as the number of the averaged frames is increased (eq. 10). Thus, the squared uncertainty for averaged  $n_{\text{frames}}$ -raw data frames will be  $n_{\text{frames}}$ -times lower (Stetson 1992).

### Background noise

For calculating the stellar brightness  $N_{\text{star}}$  we subtract the background intensity from the total intensity in an aperture (s. eq. 4). It is determined as the mean intensity in a background sample taken close to the aperture. Thus in fact we suppose that in small annulus around the object is small enough, so the level of the sky brightness is constant, which is good assumption. But in fact, values in each pixel of this background sample are more or less different from values of others. It supposed to be due to influence of various noises, calibration uncertainties and contamination by other stars. The measure of dispersion of the values around the determined mean value can serve as an estimation of the mean background intensity uncertainty related to one pixel  $\sigma_{\text{sky}}$ .

The mean background intensity  $N_{\text{sky}}$  is found only as an estimation. Therefore, its precision influences the precision of the stellar brightness estimation and it must be account to the total measurement uncertainty. The background mean is determined as the mean value of nearby pixel values, which are not necessary the same. Thus, there exist the pixel-to-pixel scatter and  $\sigma_{\text{sky}}$  as the standard deviation of  $N_{\text{sky}}$  in ADU/px, represents the pixel-to-pixel scatter of the calculated nearby mean background brightness. *Thus we calculate the variance of the background noise in  $n_{\text{aperture}}$ -pixels converted from ADUs into electrons as follows:*

$$\sigma_{\text{random}}^2 = G^2 \cdot n_{\text{aperture}} \cdot s_{\text{sky}} = G^2 \cdot n_{\text{aperture}} \cdot \sigma_{\text{sky}}^2 \quad (22)$$

where  $\sigma_{\text{sky}}$  is uncertainty of the background mean intensity related to one pixel in ADU/px estimated from the dispersion of background pixel values, if multiplied by  $G$  constant of A/D converter's gain in e<sup>-</sup>/ADU it is converted into e<sup>-</sup>, exactly due to eq. (16) and  $n_{\text{aperture}}$  is number of pixels in the aperture.

It is clear that if more pixels will be available for the mean background intensity estimation  $N_{\text{sky}}$ , its precision will be much better. Again it is the implication of eq. (10).

$$\sigma_{\text{mean}}^2 = G^2 \cdot u_{\text{mean}} \cdot n_{\text{aperture}}^2 = G^2 \frac{s_{\text{sky}}}{n_{\text{annulus}}} n_{\text{aperture}}^2 = G^2 \frac{\sigma_{\text{sky}}^2}{n_{\text{annulus}}} n_{\text{aperture}}^2 \quad (23)$$

where  $u_{\text{mean}}$  is uncertainty of background intensity related to one pixel with regards to the number of pixels  $n_{\text{annulus}}$  used for this estimation.

It can be seen the sense of  $\sigma_{\text{mean}}$  from this formula. If we determinate the uncertainty  $\sigma_{\text{random}}$  from infinite number of pixels, so if  $n_{\text{annulus}}$  approaches to infinite,  $\sigma_{\text{mean}}$  would approach to zero and its contribution to the total measurement uncertainty would be zero. It can be simply interpreted that in this case the determination of the uncertainty  $\sigma_{\text{random}}$  would be the most precisely so  $\sigma_{\text{random}}$  would represents real measurement error.

**Notes on units**

Generally, we handle with numbers of "something" e.g. number of pixels, number of electrons and ADUs are numbers as well. The number is the quantity of dimension one. Therefore, if we have number of something and make its square we obtain the number again. Physical dimension will not change at all, it will be the quantity of dimension one again. For instance the squared number of electrons gives certain number of electrons. Dimension for both quantities is the same, the number of electrons. Dimension of the squared number of electrons is the physical non-sense. Units, such as ADU, e<sup>-</sup>/ADU, ADU/px, are all dimensionless and only formal. We used them to accent the sense of each quantity.

$\sigma_{\text{sky}}$  is a standard deviations of background noise per pixel, so formally in units of ADU/px.  $\sigma_{\text{sky}}^2$  is variance of background noise per pixel but its formal unit is ADU/px and not (ADU/px)<sup>2</sup> or something similar. The variance as well as the standard deviation represent the uncertainty related to one pixel, so they are both in unit "per pixel" and although the variance is the squared standard deviation it is expressed in ADU.

Why  $G$  is squared in the equations (22) and (23)? Origin quantity is  $\sigma_{\text{sky}}$  and this we want to convert from ADU to e<sup>-</sup> and thus we must to multiply it by  $G$ . Because  $\sigma_{\text{sky}}$  is squared in both equations  $G$  must be squared as well.

Why  $n_{\text{aperture}}$  is squared in eq. (23)?  $u_{\text{mean}}$  was obtained as  $\frac{\sigma_{\text{sky}}^2}{n_{\text{annulus}}}$ , i.e. by dividing  $\sigma_{\text{sky}}^2$  by the number of pixels  $n_{\text{annulus}}$ . So from formal reasons it is needed for  $\sigma_{\text{mean}}^2$  calculation to multiply  $u_{\text{mean}}$  by the number of pixels and because  $\sigma_{\text{mean}}^2$  is related to the aperture, it should be  $n_{\text{aperture}}$ . The next multiplication by  $n_{\text{aperture}}$  is needed because we want to know the uncertainty for  $n_{\text{aperture}}$ -pixels.

**Notes on individual uncertainty importance**

Our method is based on the assumption that  $S/N \gg 1$ , i.e. the number of stellar electrons is far superior to the number electrons originated from other processes. Therefore, it is clear that  $\sigma_{\text{star}}$  is the most dominant noise source. If we compare eq. (22) and eq. (23), we find that

$$\sigma_{\text{random}} = \sqrt{\frac{n_{\text{aperture}}}{n_{\text{annulus}}}} \sigma_{\text{mean}} \tag{24}$$

Thus, relation between  $\sigma_{\text{random}}$  and  $\sigma_{\text{mean}}$  depends on the factor  $\sqrt{\frac{n_{\text{aperture}}}{n_{\text{annulus}}}}$ . In typical situations  $n_{\text{annulus}}$  is greater in one or two orders of magnitude than  $n_{\text{aperture}}$ , so  $\sigma_{\text{random}}$  is larger than  $\sigma_{\text{mean}}$ , typically about one order of magnitude.

**Total measurement uncertainty**

Let's come out from eq. (13) with regards to the law of uncertainty propagation (eq. 19). Thus, the equation which determines the total uncertainty looks like this:

$$\Delta m = 1.0857 \cdot \frac{\sqrt{\sum_i \sigma_i^2}}{S} \tag{25}$$

Point out that all terms are supposed to be in number of electrons rather than in ADUs as we mentioned above. To the total uncertainty contribute photon noise and background noise with regards to the number of used pixels. Individual noises are represented by their squared standards deviations. *Total standard deviation of single photometric measurement is calculated as a square root of a sum of individual variances* (Davis 1994):

$$\Delta m = 1.0857 \cdot \frac{\sqrt{\sigma_{\text{star}}^2 + \sigma_{\text{random}}^2 + \sigma_{\text{mean}}^2}}{N_{\text{star}}} \tag{26}$$

where value of 1.0857 is the correction factor between an uncertainty in electrons and that same uncertainty in magnitudes. Because the uncertainties as well as the stellar intensity are provided by CCD camera in ADUs it is needed to convert them to e<sup>-</sup>.

$$\Delta m = 1.0857 \cdot \frac{\sqrt{G \frac{N_{star}}{n_{frames}} + G^2 \cdot n_{aperture} \cdot \sigma_{sky}^2 + G^2 \frac{\sigma_{sky}^2}{n_{annulus}} n_{aperture}^2}}{GN_{star}} \quad (27)$$

and after a little modification

$$\Delta m = 1.0857 \cdot \frac{\sqrt{G \cdot \frac{N_{star}}{n_{frames}} + n_{aperture} \cdot \sigma_{sky}^2 + \frac{\sigma_{sky}^2}{n_{annulus}} n_{aperture}^2}}{N_{star}} \quad (28)$$

Just the last eq. (28) is used in code of C-Munipack package.

### Notes on method applicability

To conclusion we look at applicability of this method usage. This method is based on the assumption that  $S/N \gg 1$  and for this assumption it works very well. The assumption is natural and in the most cases it is realized. We want to obtain so precise data as it is possible, so we want to obtain the signal much larger than noise level. Most observations are made in this way. But there are some cases in which the observation are made on the noise level, e.g. observations of the optical afterglows of the short gamma-ray bursts by small telescopes. In this case, i.e. when  $S \sim N$ , it is not possible to take advantage of dominance one noise source as it was in our case. Estimation of the measurement uncertainty as well as the stellar brightness in this way is at least disputative and may lead to miscellaneous results (Howell et al. 1996).

### ACKNOWLEDGE

We thank to RNDr. Miloš Zejda for supplying by recently released books. This work has been supported by the grants GA ČR 205/06/0217 and 205/08/H005.

### REFERENCES

- Berry, R. & Burnell, J. 2005, The handbook of astronomical image processing (The handbook of astronomical image processing, 2nd ed., by R. Berry and J. Burnell. xxviii, 684 p., 1 CD-ROM (incl. Astronomical Image Processing Software AIP4WIN, v.2.0). Richmond, VA: Willmann-Bell, 2005)
- Budding, E. & Demircan, O. 2007, Introduction to astronomical photometry (Introduction to astronomical photometry, by E. Budding and O. Demircan. 2nd edition. Cambridge: Cambridge University Press, 2007 xvi, 434 p. Cambridge observing handbooks for research astronomers, vol. 6. ISBN 0521847117.)
- Davis, L. E. 1994, A Reference Guide to the IRAF/DAOPHOT Package
- Howell, S. B. 1989, PASP, 101, 616
- Howell, S. B. & Everett, M. E. 2001, in Third Workshop on Photometry, p. 1, ed. W. J. Borucki & L. E. Lasher,
- Howell, S. B., Koehn, B., Howell, E., & Hoffman, M. 1996, AJ, 112, 1302
- Hroch, F. 1998, in 20th Stellar Conference of the Czech and Slovak Astronomical Institutes, ed. J. Dusek, 30–+
- Kundracik, F. 1997, Spracovanie experimentálnych dát (Matematicko-fyzikálna fakulta Univerzity Komenského v Bratislave)
- Larson, A. M. 2007, IRAF Tutorial and Exercise II (Quick-look Photometry with Imexamine)
- Simonetti, J. H. 2004, N/A, 1, 1
- Stetson, P. 1992, User's Manual for DAOPHOT II

## ESA Gaia and Variable Objects

RENÉ HUDEC<sup>1,3</sup>, VOJTĚCH ŠIMON<sup>1</sup> AND LUKÁŠ HUDEC<sup>2</sup>

1) *Astronomical Institute, Academy of Sciences of the Czech Republic, Ondřejov, Czech Republic*

2) *Faculty of Mathematics and Physics, Charles University, Prague, Czech Republic*

3) *Czech Technical University, Faculty of Electrical Engineering, Prague*

### Abstract

Albeit focusing on astrometry, the ESA Gaia space mission will also provide spectrophotometry for all objects down to mag 20 over 5 years operation period. Typically 50 to 200 measurements per object including variable stars, cataclysmic variables and optical counterparts of celestial high-energy sources can be expected during this time interval. Also optical counterparts of celestial high-energy sources, including afterglows and optical transients of GRBs can be detected and investigated this way.

### CZ Abstrakt

Astrometrická družice ESA Gaia poskytne kromě ultrapřesné astrometrie také spektrofotometrii objektů do 20 magnitudy, přičemž pokrytí dosáhne doby 5 let. MJ. Takto bude možno studovat i kataklyzmické proměnné a optické protějšky vysokoenergetických zdrojů.

---

### INTRODUCTION

Space experiments are playing more and more important role in modern astrophysics. Within few years, another spacecraft will provide important astronomical data. Gaia is a cornerstone astrophysical mission of the European Space Agency ESA (<http://astro.estec.esa.nl>). It is a global space astrometry mission. Its goal is to make the largest, most precise map of our Galaxy by surveying an unprecedented number of stars – more than a thousand million. It will monitor each of its target stars about 100 times over a five-year period, precisely charting their distances, movements, and changes in brightness. Gaia's resulting scientific harvest is of almost inconceivable extent and implication. It will provide detailed information on stellar evolution and star formation in our Galaxy. It will also clarify the origin and formation history of our Galaxy. It is also very important that Gaia will pinpoint exotic objects in colossal and almost unimaginable numbers. Among others, tens of thousands of extragalactic supernovae will be discovered.

For many years, the state of the art in celestial cartography has been the Schmidt surveys of Palomar and ESO, and their digitized counterparts. Gaia will provide the detailed 3-d distributions and space motions of all these stars, complete to mag 20. The measurement precision, reaching a few millionths of a second of arc, will be unprecedented. This will allow our Galaxy to be mapped, for the first time, in three dimensions.

### VARIABLE OBJECTS BY GAIA

Albeit focusing on very precise astrometry, it is obvious that, with the above briefly described performance, Gaia will provide valuable inputs to various research fields of recent astronomy and astrophysics including the field of variable stars. Most of the variable star research will be performed within the Gaia Variability Coordination Unit CU7.

For the variable star science, there will be several advantages provided by Gaia. First, this will be the deep limiting magnitude of 20, much deeper than most of previous studies and global surveys. For example, no detailed statistics of variable stars has been investigated for magnitudes fainter than 18. Secondly, the time period covered by the Gaia observations, i.e. 5 years, will also allow some studies requiring long-time monitoring, recently provided mostly by astronomical plate archives and mostly small or magnitude-limited sky CCD patrols. But perhaps the most important benefit of Gaia for the variable star studies will surely be the fine color resolution. This will allow some detailed studies involving analyzes of color and spectral changes not possible before. The details of variable star studies with Gaia have been recently evaluated and are described in more detail mostly by the dedicated sub-workpackages within the workpackage Specific objects studies within the Gaia CU7.

The participation of High Energy Astrophysics (HEA) group at the Astronomical Institute of the Academy of Sciences of the Czech Republic in Ondřejov focuses on Gaia CU7 Variability Processing Unit with R. Hudec being a member of Gaia CU7 team. Two sub-work packages within the specific object studies on cataclysmic

variables (CVs) and optical counterparts of high energy sources have been proposed, evaluated, accepted, and allocated to be managed by R. Hudec. Additional participation is expected in image processing – this includes the algorithms designed for scanned Schmidt spectral plates (simulation of Gaia data and variability studies based on spectro-photometry).

The further participation represents direct participation in Gaia CU7 Data Processing Center (DPC) as a natural continuation of participation in INTEGRAL ISDC. This includes participation in software development in a team, and Java and object oriented programming as a natural extension of participation in INTEGRAL ISDC (since 1997).

Another participation is represented by Robotic Telescopes run with the same RTS2 operating software: BART, BOOTES1, BOOTES2, BOOTES-IR, FRAM, WATCHER, D50 cm CCD telescope (since 2007). Also small and private observatories are expected to participate.

**OPTICAL COUNTERPARTS OF HIGH-ENERGY SOURCES BY GAIA**

**Motivation**

Most high energy sources have also optical emission, mostly variable and accessible by Gaia. The monitoring of this variable optical emission provides important input to understanding the physics of the source. The idea is to focus on the sources not included in other categories of variable sources (e.g. not on AGNs, CVs etc.) covered by other sub-workpackages. The investigations and analyzes of optical counterparts of high energy astrophysics sources based on Gaia data require also complex analyzes with additional data. Specifically, for selected targets, multispectral analyzes using Gaia and other databases (such as the satellite X-ray and gamma-ray data, optical ground-based data etc) may be feasible. They will deal with long-term light changes and their evolution, especially active states and flares. For selected sources, dedicated complex analyzes will be undertaken, including spectrophotometry and investigation of the relation between the brightness and spectrum/color. This will enable a study and understanding of related physical processes. Also statistics of the whole sample of objects will be made.

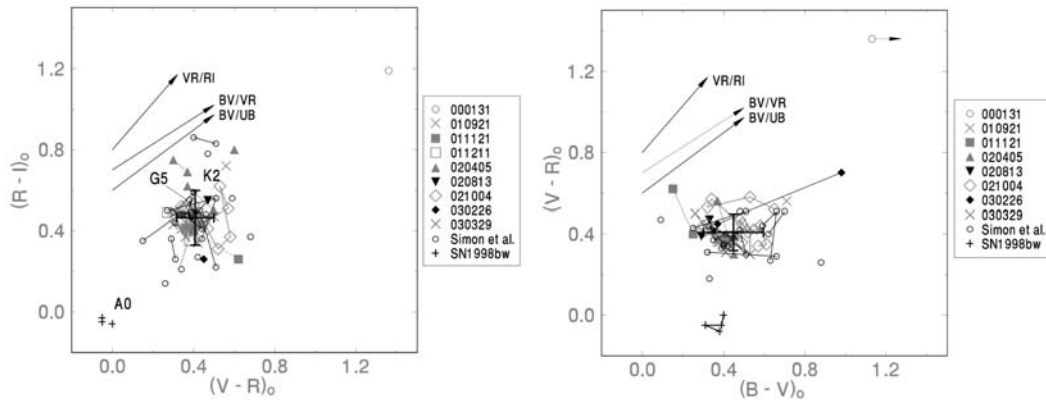


**FIGURE 1.** Examples of the color diagrams of OAs of GRBs. The data for  $t - T_0 < 10.2 d$  in the observer frame and corrected for the Galactic reddening are displayed. Multiple indices of the same OA are connected by lines for convenience. The mean colors (centroid) of the whole ensemble of OAs (except for GRB000131 and SN 1998bw) are marked by the large cross. The representative reddening paths for  $EB-V = 0.5$  and positions of the main-sequence stars are also shown. Adapted from [3, 4].

**Methods, and their results, proposed to achieve the objectives:**

1. Use of tools of standard time-series analysis (Fourier and wavelet analysis, methods of statistical time-series analysis (correlation, autocorrelation, noise and signal detection etc.), deterministic/chaotic behavior) to reveal the physical mechanisms of variations.
2. Study of the flaring behavior of objects including spectral changes (color-color diagrams, color evolution), study of correlation of brightness changes and spectral (color) changes, statistical analysis of the flaring behavior of the whole data sample.
3. Study of activity/inactivity modes incl. spectral changes, physical classification.

4. Complex analyzes with Gaia and supplementary data including data from dedicated ground-based robotic telescopes as well as from other sources (inc. satellite data).

### Ground-Based Support

Robotic Telescopes run with the same RTS2 operating software – BART, BOOTES1, BOOTES2, BOOTES-IR, FRAM, WATCHER, D50 cm CCD telescope (since 2007) – will provide additional photometric points for a better sampling, especially at activity states, and to verify flares and other specific types of variability.

### The spectral power of Gaia

The Gaia telescopes offer unique variability studies based on low dispersion spectra, i.e. the energy resolution of recorded star images. In this context, the application of algorithms developed for digitized astronomical archival plates may be important for Gaia. The novel algorithms for automated analyzes of digitized spectral plates have been recently developed by informatics students [1] and are suitable for

- Automated classification of spectral classes
- Searches for spectral variability (both continuum and lines)
- Searches for objects with specific spectra
- Correlation of spectral and light changes
- Searches for transients

The archival spectral plates taken with the objective prism offer the possibility to simulate the Gaia low dispersion spectra and related procedures such as searches for spectral variability and variability analyzes based on spectro-photometry. In the recent development, we focus on sets of spectral plates of the same sky region covering long time intervals with good sampling.

Fine division of the light signal into a number of filters in the Gaia instrument will provide us with information on the spectral energy distribution and color indices of very faint objects. Among others, observing the optical afterglows (OAs) of GRBs and the associated supernovae, which appear in the field of view during the Gaia scans, will be possible. The specific color indices of these objects (Fig.1) [3, 4, 5] and their time evolution will be very helpful in this regard. This method will enable also a searching for the so-called orphan afterglows, i.e. GRBs from which no gamma-ray emission is observed because of an unfavorable direction of the beam with respect to the observer. Since the optical emission is less beamed, it can be still observed, as predicted by theory [2]. The specific color indices of the optical afterglows of long GRBs (Fig.1) can be very helpful in resolving the orphan afterglows from other kinds of object.

### CONCLUSION

The Gaia mission of European Space Agency ESA will contribute essentially to scientific studies and physical understanding of variable stars in general, and of optical counterparts of high energy sources, CVs and related objects in particular. The variability studies based on low-energy spectra are expected to provide unique novel data and can use algorithms recently developed for automatic analyzes of digitized spectral Schmidt plates.

### ACKNOWLEDGMENTS

This research was supported by the ESA PECS project 98058. Some parts are related to ESA PECS 98023 and GA CR 205/08/1207.

### REFERENCES

- 1 Hudec, L., Algorithmes for automated spectral classification of stars, Bc. Thesis, Faculty of Mathematics and Physics, Charles University, Prague, 2007.
- 2 Rhoads, J.E., *ApJ*, **487**, L1 (1997).
- 3 Šimon, V., Hudec, R., Pizzichini, G., and Masetti, N., *A&A*, **377**, 450 (2001).
- 4 Šimon, V., Hudec, R., Pizzichini, G., and Masetti, N., “Colors of Optical Afterglows of GRBs and Their Time Evolution,” in **Gamma-Ray Bursts: 30 Years of Discovery: Gamma-Ray Burst Symposium**, edited by E. E. Fenimore and M. Galassi, AIP Conference Proceedings 727, American Institute of Physics, New York, 2004, pp. 487–490.
- 5 Šimon, V., Hudec, R., and Pizzichini, G., *A&A*, **427**, 901 (2004).

# Identification and Analyses in Optical Light of Gamma-ray Sources with Astronomical Archival Plates

RENÉ HUDEC<sup>(1,2,3)</sup> AND FILIP MUNZ<sup>(1,2)</sup>

1) *Astronomical Institute, Academy of Science of the Czech Republic, Ondřejov, Czech Republik,*

*E-mail: [rhudec@asu.cas.cz](mailto:rhudec@asu.cas.cz)*

2) *INTEGRAL ISDC, Versoix, Switzerland*

3) *Czech Technical University, Faculty of Electrical Engineering, Prague*

## ABSTRACT

The ESA INTEGRAL satellite (International Gamma Ray Laboratory) launched in October 2002 continues to deliver valuable data about the gamma-ray sky. Nearly 200 gamma-ray sources have been detected so far mainly by the IBIS onboard instrument, and others are expected in the future. The first 3.5 years of INTEGRAL public and Core Program data have revealed more than 400 sources and this number is expected to increase to more than 500 in the future (Bird et al. 2007). Alternative method to identify and to analyze INTEGRAL gamma-ray sources using optical light and astronomical archival plates is described.

## CZ ABSTRAKT

Popisujeme a diskutujeme alternativní metodu identifikace a studia kosmickým gama zdrojů v optickém oboru spektra s pomocí archivních astronomických desek. Ukázky studia gama zdrojů družice ESA INTEGRAL jsou diskutovány jako příklad.

---

## 1. IDENTIFICATION OF SOURCES

Only a fraction of these sources are either known sources or have been identified and classified already. From the 56 newly by INTEGRAL detected sources (IGR sources), only 20% have already firm classification, mostly with Cataclysmic variables (CVs), AGN, High Mass X-ray Binaries, Low Mass X-ray Binaries, Black Hole Candidates, and Anomalous X-ray Pulsars (Bird et al. 2007). One of the methods applied in the past is the identification by spectroscopy, which proved recently some new and interesting identification of INTEGRAL gamma-ray sources such as newly detected symbiotic and cataclysmic variables (e.g. Masetti et al., 2005).

## 2. LIMITATIONS OF RECENT METHOD

Although successful, this method has some limitations. First, it can be hardly applied for particular types of transients and recurrent transients. Secondly, it requires access to dedicated large aperture telescopes and spectrographs. Moreover, it can be laborious in the case of large error box and crowded field. And in some specific cases, only the spectral information alone is sometimes not enough for reliable classification of the objects.

## 3. THE PROPOSAL

In this paper, we propose an alternative method how to identify the still non-classified INTEGRAL gamma ray sources and newly detected INTEGRAL sources in the future (and of other high energy satellites). This method is based on the fact that (1) many of gamma-ray sources identified and classified so far do have optical counterparts, in many cases brighter than mag 18, and (2) a significant fraction of these sources is variable both in gamma-rays as well as in optical wavelengths.

## 4. MOTIVATION

The ESA INTEGRAL satellite focus on the Galactic Center region as well as on Galactic Plane Scans (GPS). Numerous new gamma-ray sources have been found in these regions by INTEGRAL, and only a fraction of these sources was successfully identified. The identification of INTEGRAL sources indicates that most of them have variable optical counterpart brighter than mag 18.

The recent progress in classification of newly detected INTEGRAL sources has indicated that the fraction of Cataclysmic Variables and Symbiotic Stars is larger than originally expected.

These sources are usually optically bright with magnitudes 10 ... 18 and can be easily and effectively studied at optical wavelengths by ground-based telescopes or, alternatively, by archival databases as described in this contribution.

## 5. SUITABLE DATABASES

The Sonneberg Field Patrol and Leiden/Johannesburg Franklin Adams Plates represent suitable database for identification and analysis of INTEGRAL sources. They both provide numerous data for regions along the Galactic Plane

## 6. SONNEBERG FIELD PATROL

Northern regions along the Galactic Plane (but also other fields) covered by numerous (typically 50...500) astrograph plates. Typical Field of View (FOV) is 10 x 10 deg and the typical limiting magnitude is B 17. In exceptional cases, also low-dispersion spectral plates are available

## 7. LEIDEN/JOHANNESBURG FRANKLIN ADAMS PLATES

These plates were taken in Johannesburg by the high quality Franklin Adams refractor (Taylor, 1904) in years 1923-1952 within the project originated by Prof. E. Hertzsprung and are located in Leiden. The plates cover selected fields along the southern Galactic plane as well as the Galactic centre. The typical number of plates per field is 300...400, FOV is 10 x 10 deg and limiting magnitude 17.

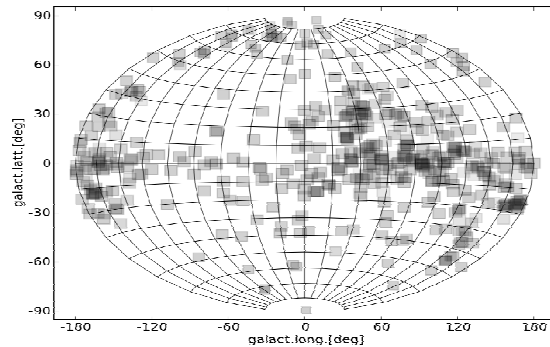


*Fig. 1. Distribution of Sonneberg Field Patrol Fields and Franklin Adams Fields (blue) in Galactic coordinates. The densely covered fields are darker.*

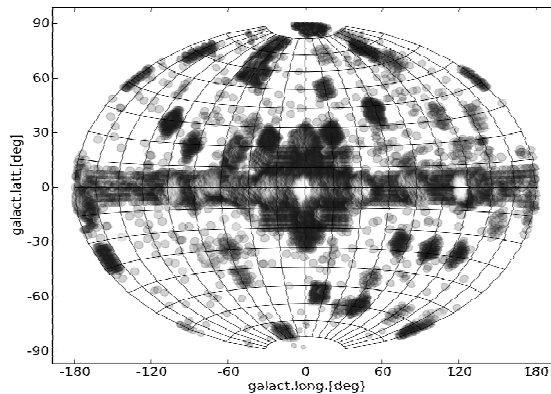


*Fig. 2. The coverage of INTEGRAL IBIS for revolutions 1 - 430.*

## 8. THE PROPOSED ANALYSIS

Using the data material mentioned here, the optically identified INTEGRAL sources with objects brighter than mag 17 can be investigated for long-term changes covering 10 ... 50 years. In addition, these data can be used to search for new optical identifications of non-classified INTEGRAL sources on hand of their optical variability.

## 9. ADDITIONAL PROSPECTS

Analyzing the light curves for flares and flaring activity, trying to fit the flare profiles, trying to look for possible periodicities and recurrences, study of colors and color changes with time, with consequent physical discussions and interpretations. Correlations with other objects, with related conclusions toward physical processes and physical models.

## 10. GALACTIC CENTRE

A particular interest will be devoted to region close to Galactic Centre where the INTEGRAL satellite coverage is large and where numerous HE sources are located a still new sources are discovered. This area is also covered by archival plates at particular observatories (e.g. Leiden, Franklin Adams plates taken in Johannesburg).

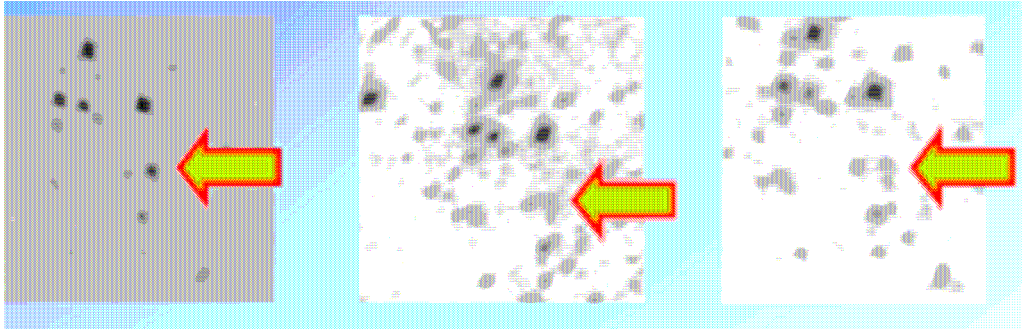


Fig. 3 IGR J12349-6434 = RT Cru hard X-ray symbiotic star on Leiden Franklin Adams Plates. INTEGRAL gamma-ray source visible on astronomical plates taken by 100 years old optical telescope. Violent (amplitude 3 magnitudes) optical brightness variations.

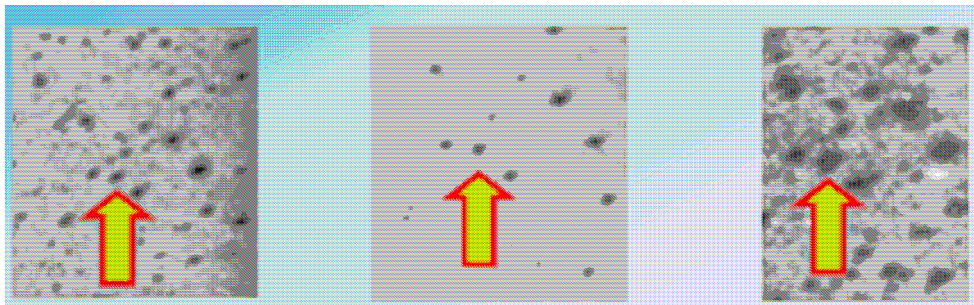


Fig. 4 IGR J10109-5746 hard X-ray symbiotic star. Optical variability on Franklin Adams plates, field 10, Leiden, year 1928

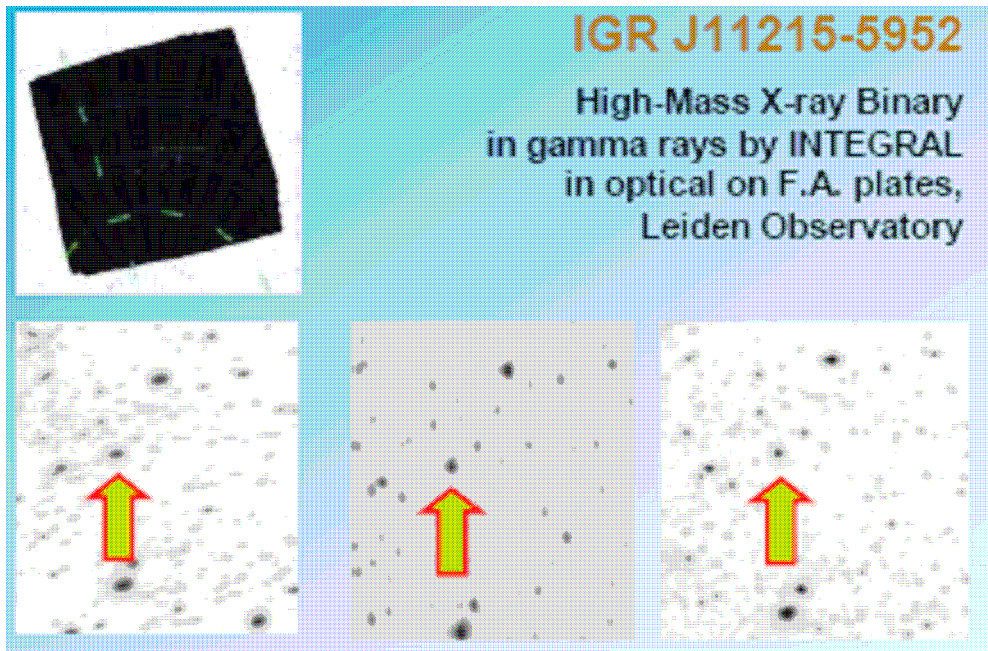


Fig. 5 IGR J11215-5952 High-Mass X-ray Binary in gamma rays by INTEGRAL and in optical on F.A. plates

**11. CONCLUSIONS**

A new cost-effective method for classification and optical identification of INTEGRAL sources has been proposed

This method can be applied both to detailed analyses of already identified sources as well as to identification of non-classified new sources. Dedicated software programs are in design and development.

**12. ACKNOWLEDGEMENTS**

We acknowledge the support provided by ESA PECS 90823 and 205/08/1207 by the GA CR A3003206.

**REFERENCES**

Bird A. et al. The Astrophysical Journal Supplement Series, Volume 170, Issue 1, pp. 175- 186,2007.

Masetti N. et al., Astronomy and Astrophysics, Volume 459, Issue 1, November III 2006, pp.21- 30, 2006.

## Superhumps in Kolonica

PAVOL A. DUBOVSKY<sup>1</sup>, STEFAN PARIMUCHA<sup>2</sup>, IGOR KUDZEJ<sup>3</sup>

- 4) Astronomical Observatory on Kolonica Saddle, [var@kozmos.sk](mailto:var@kozmos.sk)  
 5) Institute of Physics, Safarik University, Kosice, [parimuch@ta3.sk](mailto:parimuch@ta3.sk)  
 6) Vihorlat Astronomical Observatory Humenne, [vihorlatobs1@stonline.sk](mailto:vihorlatobs1@stonline.sk)

**Abstract:** We present a small sample of our observations of cataclysmic variable stars obtained at Kolonica Observatory, which is a part of the Vihorlat Observatory in Humenné (Kudzej et al., 2007). Kolonica Observatory is located on east-north part of Slovakia near borders with Ukraine. The largest telescope at observatory is an 1m Vihorlat National Telescope equipped with 2 channel photoelectric photometer in Cassegrain focus. SBIG ST9-XE from Hlohovec observatory is mounted in the Nasmyth focus. Another smaller telescopes HUGO and PÚPAVA are used for CCD photometric observations of cataclysmic variable stars and for minima times determinations of the selected eclipsing binaries. The presented data were obtained in 2006 and 2007. All our observations could be found at the web page of observatory <http://www.astrokolonica.sk>. Our observations demonstrate that also the small telescopes with low cost CCD camera could be used for a serious and useful observations.

**CZ Abstrakt:** Predstavujeme malú vzorku našich pozorovaní kataklizmatických premenných hviezd získaných na Kolonickom observatóriu, ktoré je súčasťou Vihorlatskej hviezdárne v Humennom (Kudzej et al., 2007). Kolonické observatórium sa nachádza v severovýchodnej časti Slovenska v blízkosti hraníc s Ukrajinou. Najväčší ďalekohľad na observatóriu je jednometrový Vihorlatský národný teleskop vybavený dvojkanálovým fotoelektrickým fotometrom v Cassegrainovom ohnisku. V Nasmythovom ohnisku ďalekohľadu je umiestnená kamera SBIG ST9-XE z hlohoveckej hviezdárne. Iné, malé ďalekohľady HUGO a PÚPAVA sa používajú na fotometrické pozorovania kataklizmatických premenných hviezd a na určovanie časov minimálnych zákrytových dvojhviezd. prezentované dáta boli získané v rokoch 2006 a 2007. Všetky naše pozorovania je možné nájsť na stránkach hviezdárne <http://www.astrokolonica.sk>. Naše pozorovania dokazujú, že aj malé ďalekohľady s lacnými CCD kamerami môžu prinášať hodnotné a užitočné pozorovania.

---

### Observed dwarf novae in outburst

We observed 7 SU UMa stars during superoutbursts. The basic reduction of the data was done with the program package C-Munipack (Mötl, 2006). The period for each of the stars was found with the period analysis software Peranso 2.2 (Vanmunster, 2006). The method used employs periodic orthogonal polynomials to fit observations, and the analysis of variance (ANOVA) statistic to evaluate the quality of the fit. This method was proposed by (Schwarzenberg-Czerny, 1996).

#### V844 Her

4 nights in april 2006  
 Lichtencknecker 150/2250 mm,  
 Meade DSI Pro  
 Filter: Clear  
 Exposure 30 sec  
 Superoutburst visually detected by Dubovsky  
 Published in Oizumi et al., 2007  
 Porb = 0.054643d  
 Observed superhumps period Psh=0.055885d.

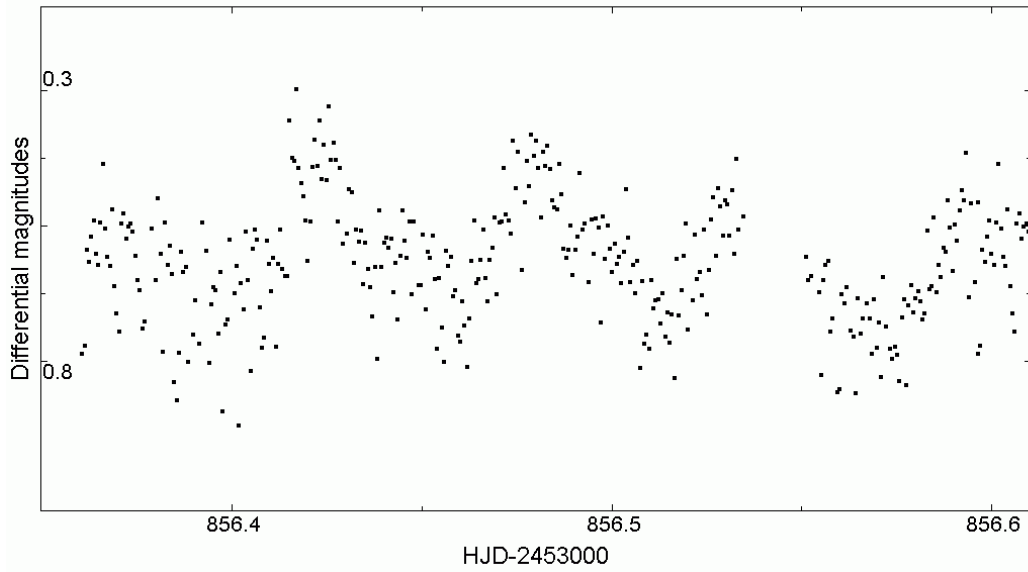


Fig. 1. Light curve of V844 Her 30-04-2006

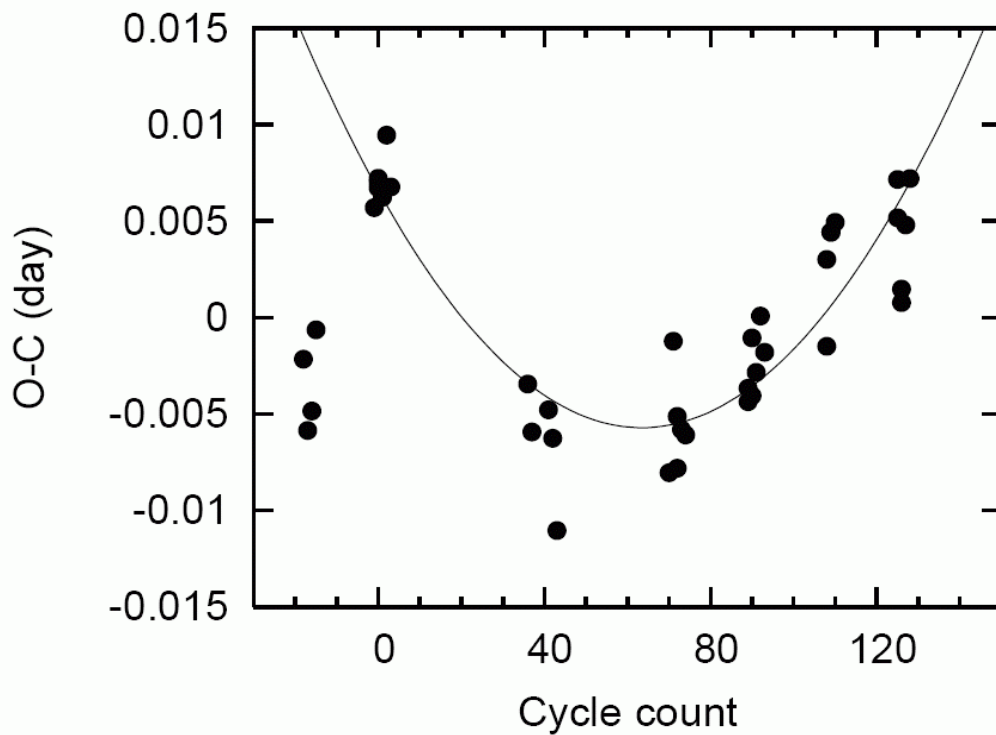


Fig. 2. - O-C diagram of the superhump maxima during 2006 superoutburst of V844 Her.

#### CI UMa

3 nights in July 2006

Hugo 265/1360 mm, Meade DSI Pro

Filter: Clear

Exposure 30 sec

Published in Parimucha, Dubovsky, 2006, OEJV, 50

Porb = 0.06041d

Observed superhumps period Psh = 0.0623d

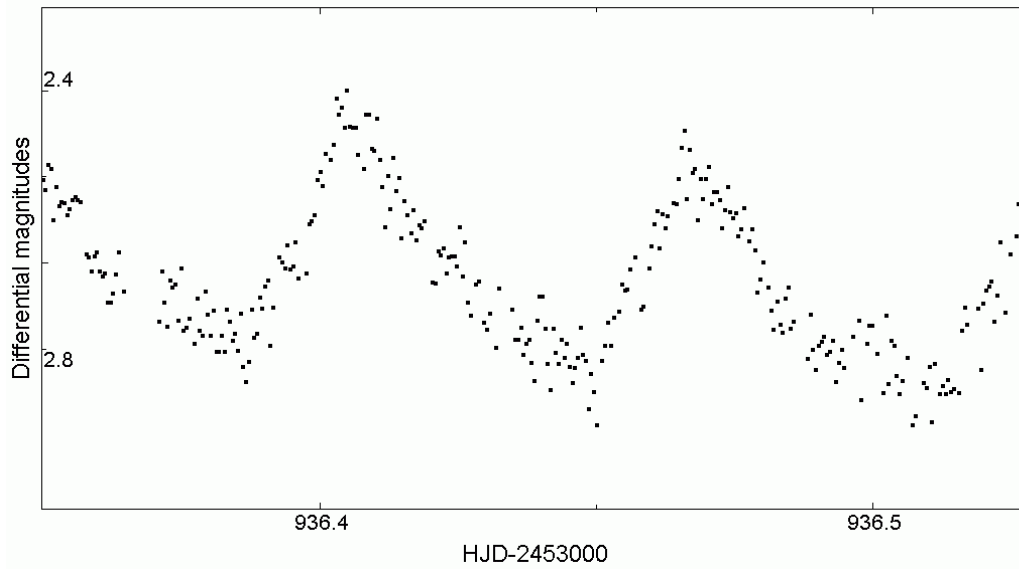


*Fig. 3. Light curve of CI UMa 19.07.2006*

### **RXS J053234.9+624755**

6 nights in July 2006

Hugo 265/1360 mm & Pointer 300/2400 mm

Meade DSI Pro

Filter: V & Clear

Exposure 30 sec

Published in Parimucha, Dubovsky, 2006, OEJV, 52

Porb = 0.0562d

Observed superhumps period Psh = 0.057d

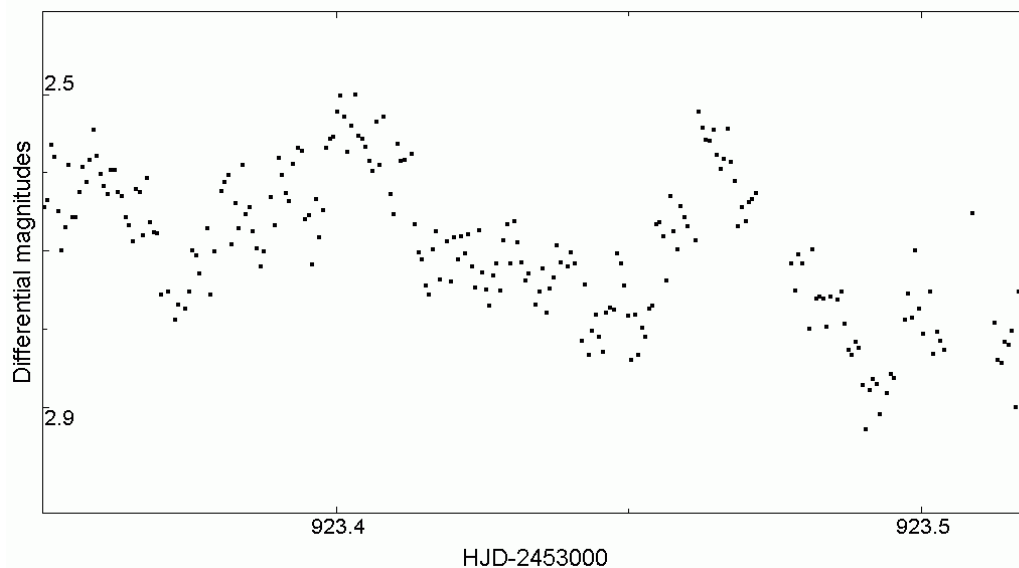


*Fig. 4. - Light curve of RXSJ053432 06.07.2006*

### **SW UMa**

3 nights in September 2006

Hugo 265/1360 mm

Meade DSI Pro

Filter: Clear

Exposure 30 sec

Porb = 0.056815d

Observed superhumps period Psh = 0.0580d

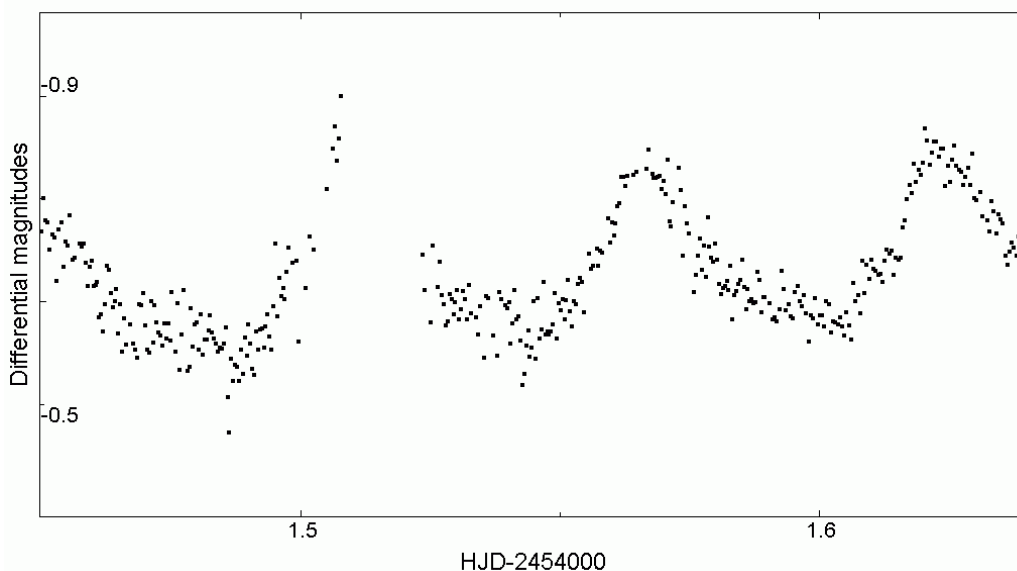


Fig. 5. - Light curve of SW UMa 22.09.2006

**MR UMa**

2 nights in April 2007

Hugo 265/1360 mm

Meade DSI Pro

Filter: V

Exposure 30 sec

Porb = 0.06375d

Observed superhumps period Psh = 0.0648d

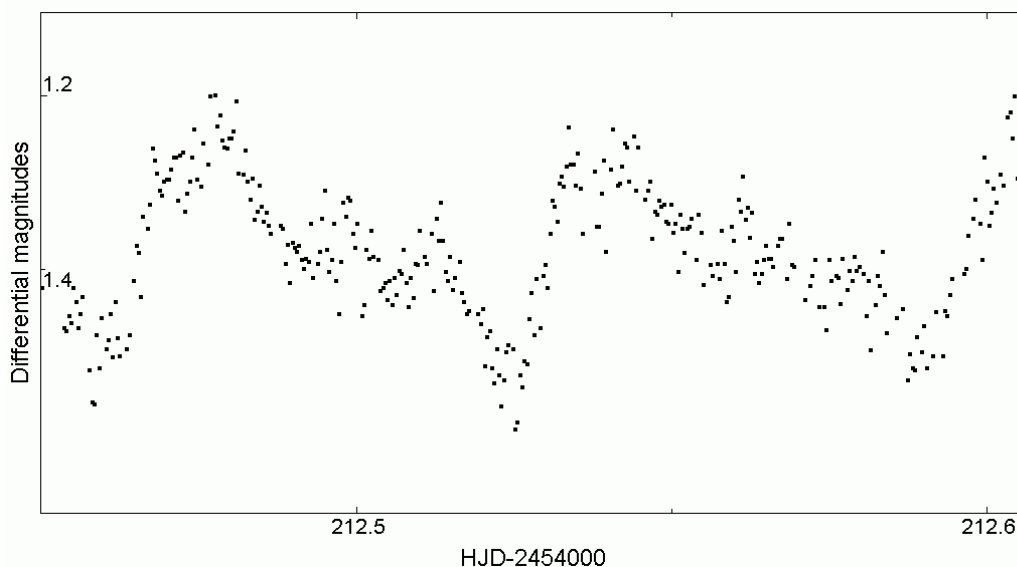


Fig. 6. - Light curve of MR UMa 21.04.2007

**NSV 1485**

5 nights in September 2007

Pupava 280/1500 mm

Meade DSI Pro

Filter: V

Exposure 30 sec

Porb = unknown

Observed superhumps period Psh = 0.0739d, T. Vanmuster from all CBA data Psh = 0.0742d

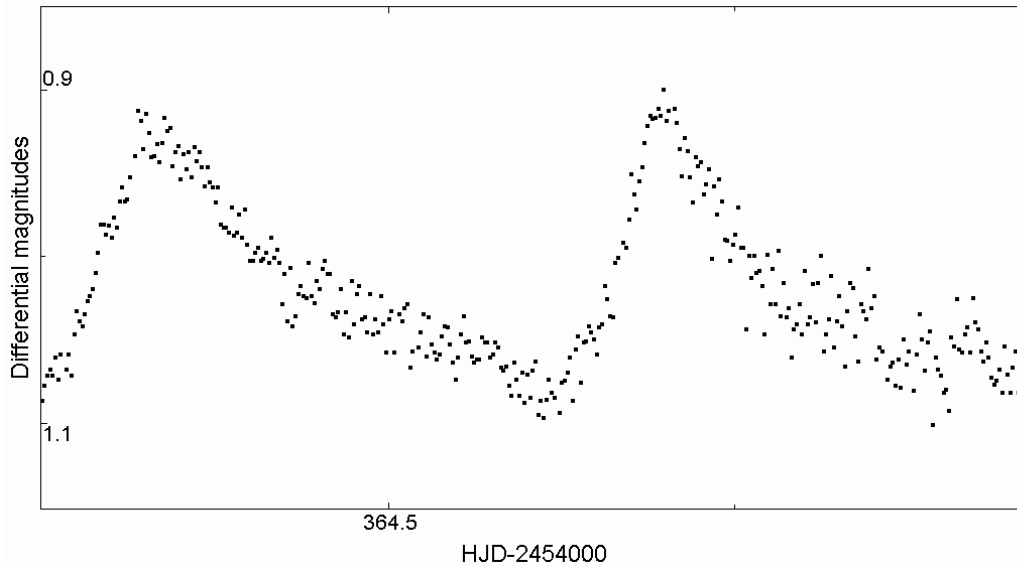


Fig. 7. - Light curve of NSV1485 20.09.2007

### UV Per

5 nights in October 2007

Pupava 280/1500 mm

Meade DSI Pro

Filter: V

Exposure 30 sec

Porb = 0.0649d

Observed superhumps period Psh = 0.0663d

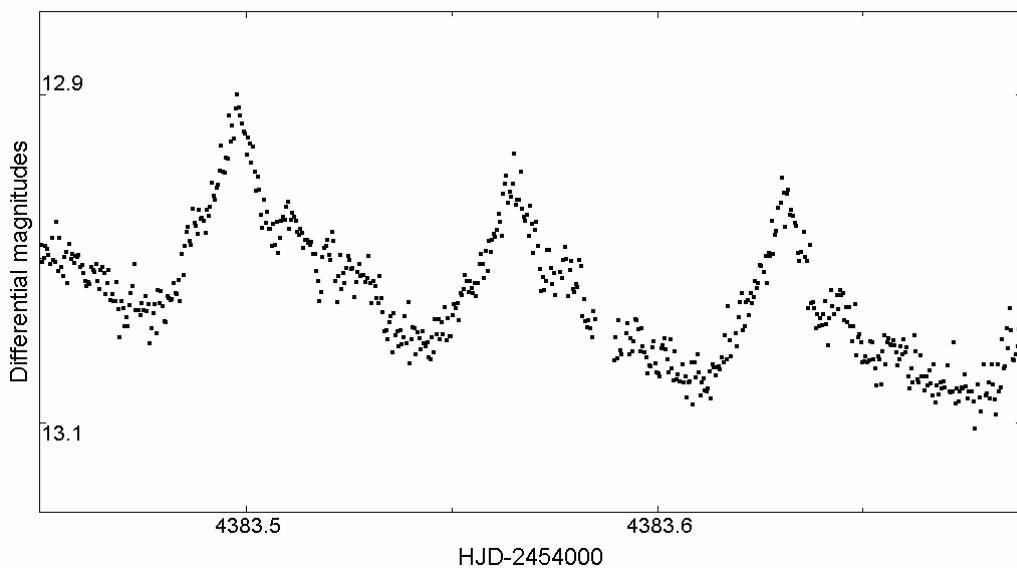


Fig. 8. - Light curve of UV Per 09.10.2007

### Another observing campaigns

**EM Cyg** – During the 2007 season we have obtained **67** time series observations with Pupava 280/1500mm Newton telescope and Meade DSI Pro CCD camera with V filter.

**Polars** – New observing program started in October 2007. Multicolor photometry of polars and intermediate polars on Vihorlat National Telescope equipped with SBIG ST9-XE CCD camera kindly provided by K. Petrik from Hlohovec observatory.

**TT Ari** – new campaign with different equipment including simultaneous observations.

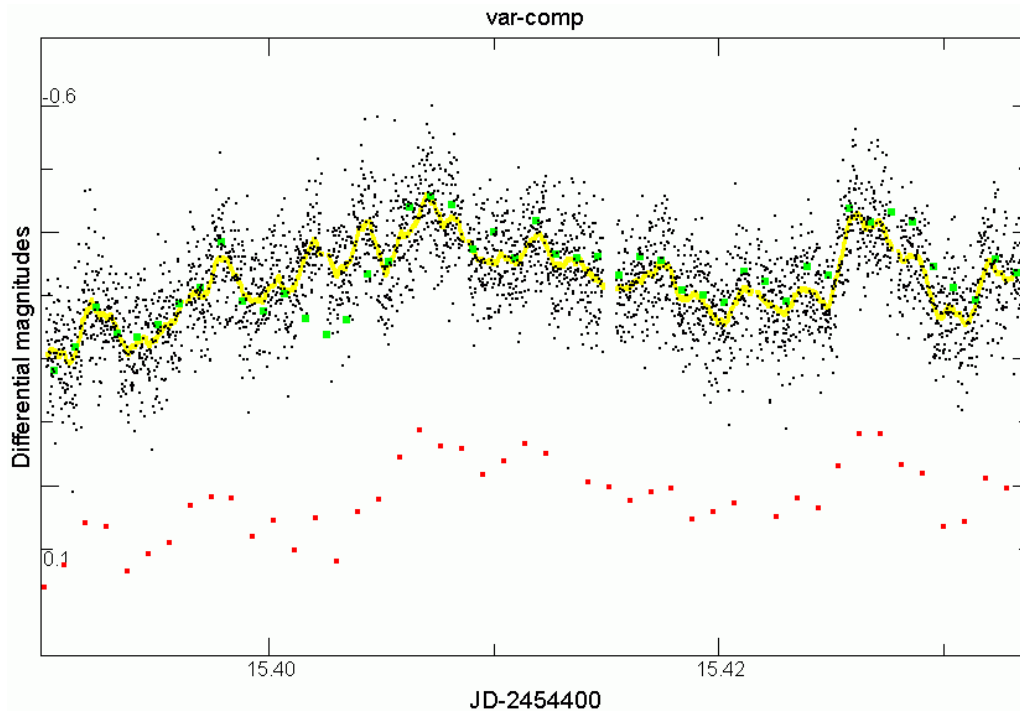


Fig. 9. - Observation 10-11-2007. CCD camera on 30 cm pointer and photometer on VNT observed the same target - TT Ari. Black dots represents original PEP data with exposure 1sec, yellow smoothed with rectangle filter 60 points, green CCD V data, red CCD R data with 30 sec exposures.

#### **Acknowledgements:**

Grant of the Slovak Research and Development Agency LPP-0049-06.  
 Bilateral APVV grant SK-UK-01006.  
 Ukrainian MON grant No M/153-2006  
 The National Scholarship Program of the Slovak Republic.  
 Grant VEGA 7011.  
 Grant VVGS 9/07-08.

#### **References:**

- Kudzej I., et al., 2007, Odessa Astronomical Publications, vol. 20 in press
- Motl D., 2006, C-Munipack Project V1.1,  
<http://integral.physics.muni.cz/cmunicipack/index.html>
- Oizumi S., et al., 2007, PASJ, 59, 643.
- Parimucha S., Dubovsky P., 2006, *Open Europ. J. Var. Stars*, 50
- Parimucha S., Dubovsky P., 2006, *Open Europ. J. Var. Stars*, 52
- Petrik K., Szasz G., Chrastina M.: 2004, *In: Perseus*, 6, 25-31.
- Schwarzenberg-Czerny, A., 1996, *ApJ*, 460, L107-110
- Vanmunster T., 2006, Peranso V2.xx, <http://www.peranso.com>

## New Variables In Archival CCD Fields

LUBOMÍR HAMBÁLEK ([lhambalek@ta3.sk](mailto:lhambalek@ta3.sk))

1) Astronomical Institute, Slovak Academy of Sciences, 059 60 Tatranská Lomnica, Slovakia

### Abstract

I present here some light curves of variable stars that were found during a survey of archival data obtained in previous four years at Astronomical Institute of Slovak Academy of Sciences. The process was to determine whether other variable stars can be detected among stars in a CCD field with centered interest on other projects' stars.

### CZ Abstrakt

Predkladám niekoľko svetelných kriviek premenných hviezd, ktoré boli objavené počas prehliadky archívnych dát získaných počas posledných štyroch rokov na Astronomickom ústave Slovenskej akadémie vied. Spracovanie bolo podmienené určením možnosti detekcie iných premenných hviezd medzi hviezdami v poli CCD zameranom na hviezdy skúmané inými projektmi.

**Keywords:** variable stars, eclipsing variable,  $\delta$  scuti variable, MuniWin

### Preparation

Data were obtained by using SBig ST-10MXE CCD camera with 500/2500 mm Newton telescope since February 2, 2003 until May 5, 2007. Data cover 582 nights of observations in more than 200 various fields. Only 66 of them were selected depending on the group of investigators. The multicolor data contained Johnson UBV and Cousins (RI)<sub>C</sub> passbands. However, many times only V(RI)<sub>C</sub> passbands were obtained.

Concurrently with the data acquisition a new database of all archived observations was prepared together with reduction frames. At last 17 fields were selected to perform a thorough investigation, see Table 1.

Constellation	Field objects	Constellation	Field objects
Aur	AH, V410	Leo	CE
Cas	CW, V723	Mon	V714
Cep	GW, WZ	Per	AX
Cyg	CG, GO, V401	Sge	CW
Her	AK, V857	Ori	V1387
Lac	V344	M67	n/a

Tab. 1

The main criterion was the length of individual observation nights as well as total number of satisfactorily long runs. Last, but not least one had to keep in mind to have a quite populated field. Some observers suggest that there shall be statistically at least one variable star for another one- or two hundred stars in the same field.

### Processing

The actual processing was performed with MuniWin (Motl, 2005) program. The built-in variable search procedure served well its purpose. However, a personal experience showed that it was necessary to neglect flat field correction prior to the actual search. The reason was to eliminate an unwanted effect in magnitude vs. delta magnitude (sigma plot) graph. With applied correction, almost all potential variable object candidates (as they showed later) were suppressed (Fig.1).

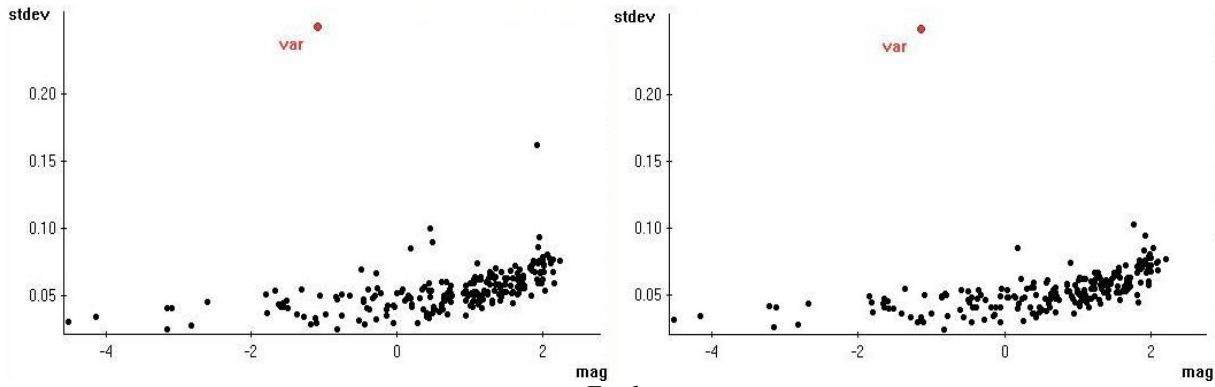


Fig.1

The effect of flat field correction: when reduced, stars show lesser standard deviations (left) and are hidden among other non-variables. Without flat field (right) the quality of individual frames drops slightly down, but differences are more prominent and easier to spot.

Later when all candidates were reliably identified and one wanted to proceed with multicolor photometry, the flat field correction was taken into account. The difficulty of this technique is that present-date version of MuniWin (1.1.12) uses only static aperture (various predefined) for all objects. One has to investigate fainter and brighter objects separately. This shows more important when data from more nights with variable seeing are processed at once. The constant problem is that objects in vicinity of frame borders may cause false identification during their partial eclipse along the edge of the CCD chip (Fig.2). This occurs when the autoguiding is not present and field stars may slightly translate their positions.

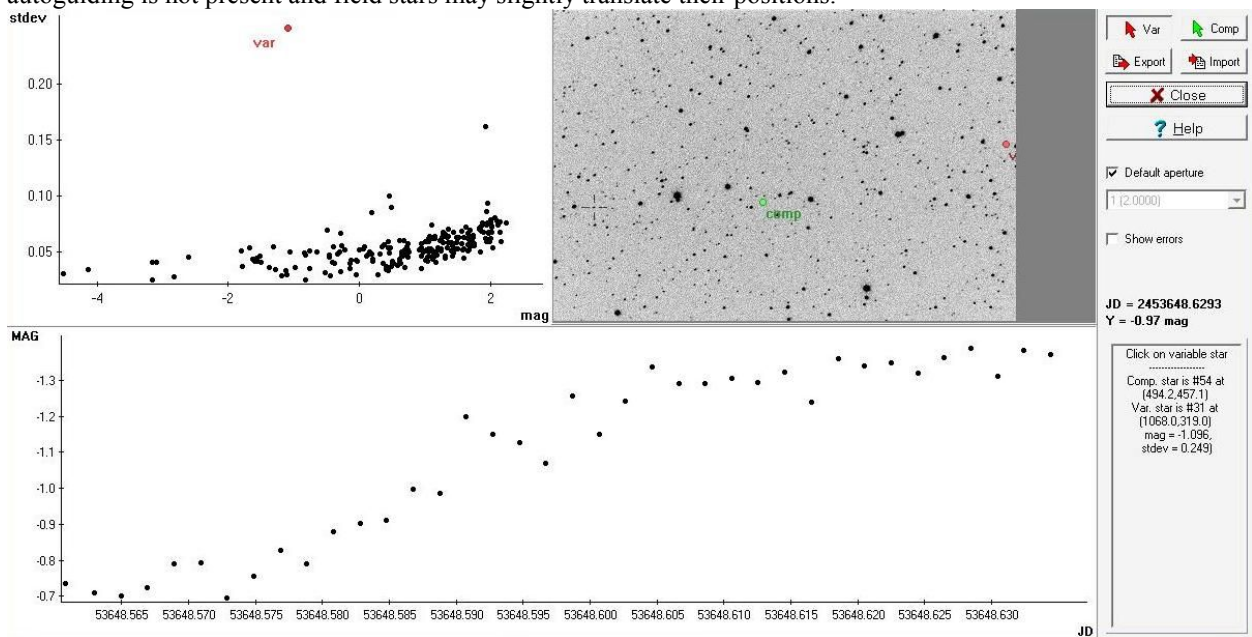


Fig. 2

A screenshot from MuniWin. Star described as “var” is a false detection caused by eclipse on frame border. The upper right field preview is provided only for the reference frame used for cross-matching procedure. One has no information of actual field transitions.

The cross-matching phase presents another small setback. Present version of MuniWin can only operate in translation mode thus having difficulties with slightly rotated fields compared to the reference frame.

To cope with the aforementioned difficulties, some sparsely covered fields (in terms of the number of images per night) had to be processed other way. Together with my supervisor we’ve used the SExtractor (Bertin, Arnouts, 1996) program to obtain photometry. Its greatest advantage is dynamical change of the best aperture for each object and ability to identify blending. Then we’ve used a custom program with incorporated method to determine rotation and translation changes to cross-match all of the images. Images were corrected for random “borderline effect” changes by cropping their size by an implicit number of pixels (mainly 30). As a result, the sigma plot improved drastically (Fig.3).

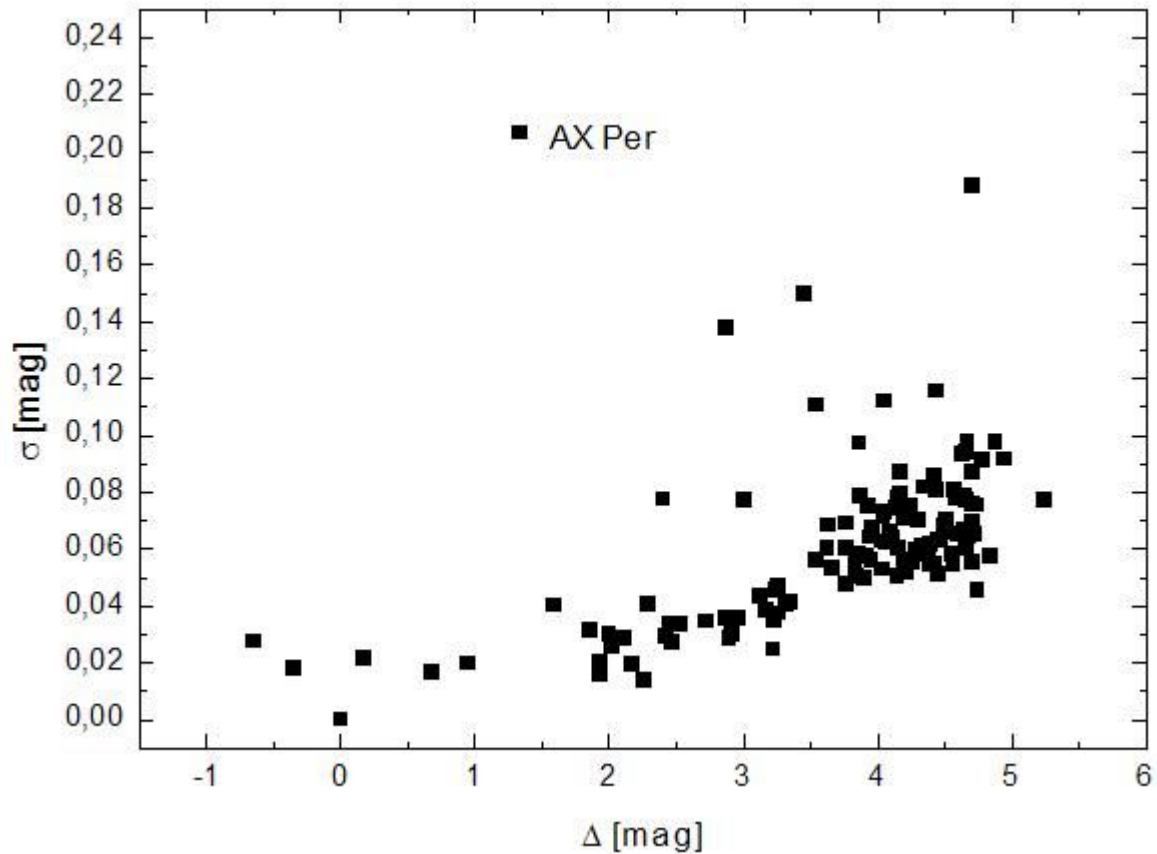


Fig. 3

*Sigma plot constructed for field around AX Per. As one could expect, the cataclysmic variable is dominant. Highest points in each magnitude bin are supposedly new variables. The true/false ratio for new variable detection was roughly around 50% in this particular case.*

Another obstacle during reduction was the need of dark frames at exposure times that weren't present in database (weren't exposed). One can assume that at constant temperature of the chip, the dark current should maintain statistically stable. Exposing longer dark frames results in gradually increasing number of dark electrons leading to a linear trend (1) with progressing time.

$$[\text{dark}]_n = \frac{[\text{dark}]_0(t_1 - t_n) + [\text{dark}]_1(t_n - t_0)}{t_1 - t_0} \quad (1)$$

The artificial dark frame inherits its characteristics from both frames used for its construction (Fig. 4).<sup>1</sup>

<sup>1</sup> Note that this technique cannot be used to match dark frames at various temperatures. The relation between temperature and dark electron allocation is definitely not linear and may vary significantly from chip to chip.

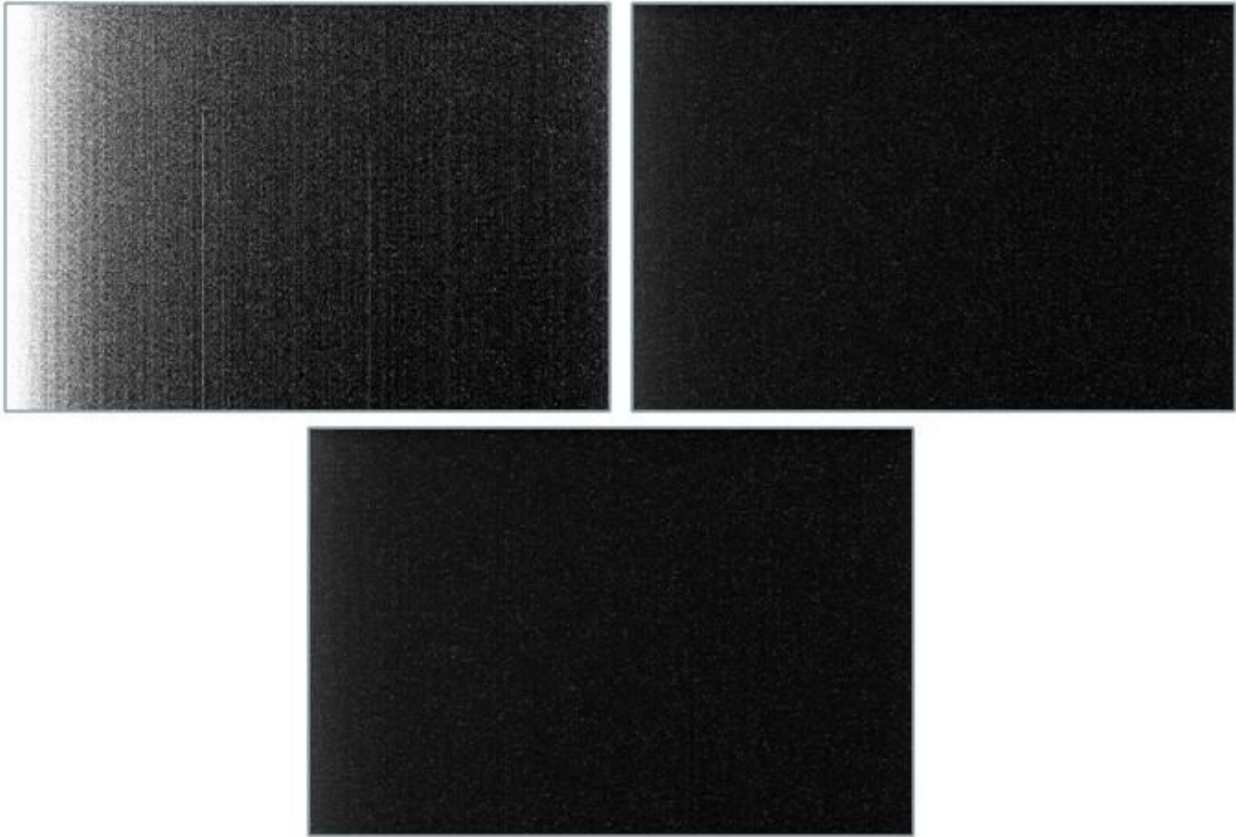


Fig. 4

An example of artificial dark construction. Upper frames were taken on June 26, 2006 at the chip temperature - 10 degrees Celsius (263.15 K) and represent bias (left) and a 10-second exposure (right). The resulting image (bottom) was computed for a 7-second-long exposure.

## Results

The differential aperture photometry was used. From all the prominent fields that underwent investigations, ten variables were flagged as newly<sup>2</sup> detected (see Table 2).

Designation	RA			Dec			Variability
	(h	m	s)	(°	'	"	
USNO-A2.0 1125-03954939	06	26	06.60	+27	55	59.0	EW
USNO-A2.0 1425-01870026	01	22	26.35	+59	12	35.6	EW
USNO-A2.0 1425-01825909	01	20	23.37	+59	17	15.1	EW
NSV 25409	20	58	01.50	+35	09	19.0	δ Sct
USNO-A2.0 1200-11760524	19	29	27.34	+30	26	04.3	EW/EB
USNO-A2.0 1200-11795087	19	30	01.21	+30	25	05.8	EW
USNO-A2.0 1650-00359348	01	42	47.36	+80	07	52.1	EW
USNO-A2.0 1575-05595838	23	22	58.75	+73	02	59.0	EW
USNO-A2.0 1425-01501019	01	04	50.21	+54	06	20.0	EA
USNO-A2.0 1425-01524030	01	05	53.38	+53	56	06.8	EW

Tab. 2

### *AH Aur field*

Three nights from February 5 and March 31, 2003 as well as February 1, 2006 showed the new variable in V(RI)<sub>C</sub> passbands<sup>3</sup>. Its peak magnitudes<sup>4</sup> are B = 15.2<sup>m</sup> and V = 15.9<sup>m</sup>, respectively. An early estimate for upper limit in period determination being less than 7 hours show that star USNO-A2.0 1125-03954939 belongs to the W UMa type of eclipsing binaries. Only three total observations of uneven length couldn't provide enough information for a successful period analysis.

<sup>2</sup> Weren't mentioned in GCVS catalogue nor Simbad

<sup>3</sup> See the addendum for all light curve plots

<sup>4</sup> Source: USNO-A2.0 catalogue

*BS Cas field*

In this field, eight nights have yielded objects with light changes. They span from August 12, 2004 to October 2, 2004. There were no observations in later years. The color information comes from  $V(RI)_C$  passbands. Star USNO-A2.0 1425-01870026 exhibits a roughly 5 hour long ascend from its minimum gaping  $\Delta V \cong \Delta R \cong 0.15^m$  and  $\Delta I \cong 0.09^m$ . After its peak at  $12.8^m$  (V) a descent occurs – a clear sign of EW variability. Star USNO-A2.0 1425-01825909 embodies similar light variations, but on significantly larger scale:  $\Delta V \cong \Delta R \cong \Delta I \cong 0.5^m$ . The descent from its peak  $12.3^m$  (V) takes approximately 3.5 hours.

*CG Cyg field*

All of the four observations that yielded a positive new variable object result occurred in August and September 2003. No newer data were accumulated. A star of  $10^m$  (V) designated NSV 25409 was considered suspected variable since 1991 (Heckert, Zeilik, 1991), there was no other systematic survey however. Our observations were in  $BV(RI)_C$  passbands and showed only very small variations, namely  $\Delta B \cong 0.07^m$ ,  $\Delta V \cong 0.05^m$ ,  $\Delta R \cong \Delta I \cong 0.04^m$ . The B-V diagram gives  $B-V = -0.14 \pm 0.01^m$  and one can estimate period to be less than 5 hours. Based on these results we can suggest that this object could be a  $\delta$  scuti type variable.

*V401 Cyg field*

A rich field set in Milky Way contains some already known variables. However, two more were detected during five or three nights, respectively. Star USNO-A2.0 1200-11760524 was observed on images from five nights in summer 2005. Fragments of the light curve show some indications of Beta Lyrae type variable. To be sure, one has to obtain a complete light curve or at least the behavior of light changes after the minimum phase. Our data didn't contain this kind of information. The magnitude changes in  $V(RI)_C$  passbands are as follows:  $\Delta V \cong 0.6^m$ ,  $\Delta R \cong \Delta I \cong 0.55^m$ . The star is of the order  $R=13.4^m$ . The other object USNO-A2.0 1200-11795087 is fainter ( $R=15.4^m$ ) and appears to be an EW variable. Our dataset magnitudes varied  $\Delta V \cong 1.15^m$ ,  $\Delta R \cong 1.0^m$ ,  $\Delta I \cong 0.95^m$ .

*GW Cep field*

The  $14.1^m$  (R) star USNO-A2.0 1650-00359348 has showed variability only during one single night on April 30, 2005. Primary minimum descended with  $\Delta V \cong 0.45^m$ ,  $\Delta R \cong 0.55^m$ ,  $\Delta I \cong 0.42^m$ . Both minima were detected during the run yielding periodicity  $P < 7$  hours. This variable belongs to the W UMa type.

*WZ Cep field*

Single new variable USNO-A2.0 1575-05595838 presented itself on November 14 and December 3, 2003. This star of red magnitude  $14.4^m$  expressed both minima with period  $P \sim 6$  hours. The light curve was affected by unfavorable seeing conditions and light changes were greatly aggravated. Their magnitudes were as follows:  $\Delta V \cong 0.3^m$ ,  $\Delta R \cong \Delta I \cong 0.25^m$ . According to the period of changes, this object is an EW type eclipsing binary.

*V723 Cas field*

A  $12.6^m$  (V) star USNO-A2.0 1425-01501019 has been monitored during August – November period in 2003. However, only on August 15, 2003 showed its primary minimum while descending  $\Delta B \cong 2.1^m$ ,  $\Delta V \cong 1.6^m$ ,  $\Delta R \cong 1.2^m$ ,  $\Delta I \cong 1.1^m$ . Its color index<sup>5</sup> points to an A-type star ( $CI = 0.0$ ) that may be present as the primary star giant. The greater blue shifts in magnitudes are caused by the hot white dwarf companion being eclipsed behind (along the radial vector) the primary component. The periodicity is unknown and its determination will take an intense observation campaign. The second newly discovered candidate USNO-A2.0 1425-01524030 express variations only during one night on March 2, 2005. This was due the rotation of the camera in its focal point by 90 degrees. Having a rectangular field (roughly  $25' \times 15'$ ) centered onto V723 Cas, this new object was beyond its reach. From the shape of light variations one cannot be total sure of its type of variability, however it could likely be an EW variable. The magnitude changes are  $\Delta B \cong 0.5^m$ ,  $\Delta V \cong \Delta R \cong 0.45^m$ ,  $\Delta I \cong 0.35^m$ .

**Conclusion**

The main advantage of CCD observation is their ability to store all possible light information in the current field at any time. The backward processing options are great and with each new method are repeatable with possible better results. Double and multiple star systems and other variables are fairly common and thus likely detectable in many CCD fields. The main disadvantage is that one has to monitor too many fields for a fair amount of time to obtain light variations. With the coming of new generation of robotic satellite observatories, this role of new variable finders will soon be taken over. However, many amateur astronomers with access to modern CCD cameras may provide longer runs of observations, especially in the field of cataclysmic variables.

As for this work, more observation would be welcomed. It should be then enough to determine periods and compute ephemeris. As for potential spectral information, these new objects are too faint for most of the spectrographs in the world.

<sup>5</sup> Source: USNO-A2.0 catalogue

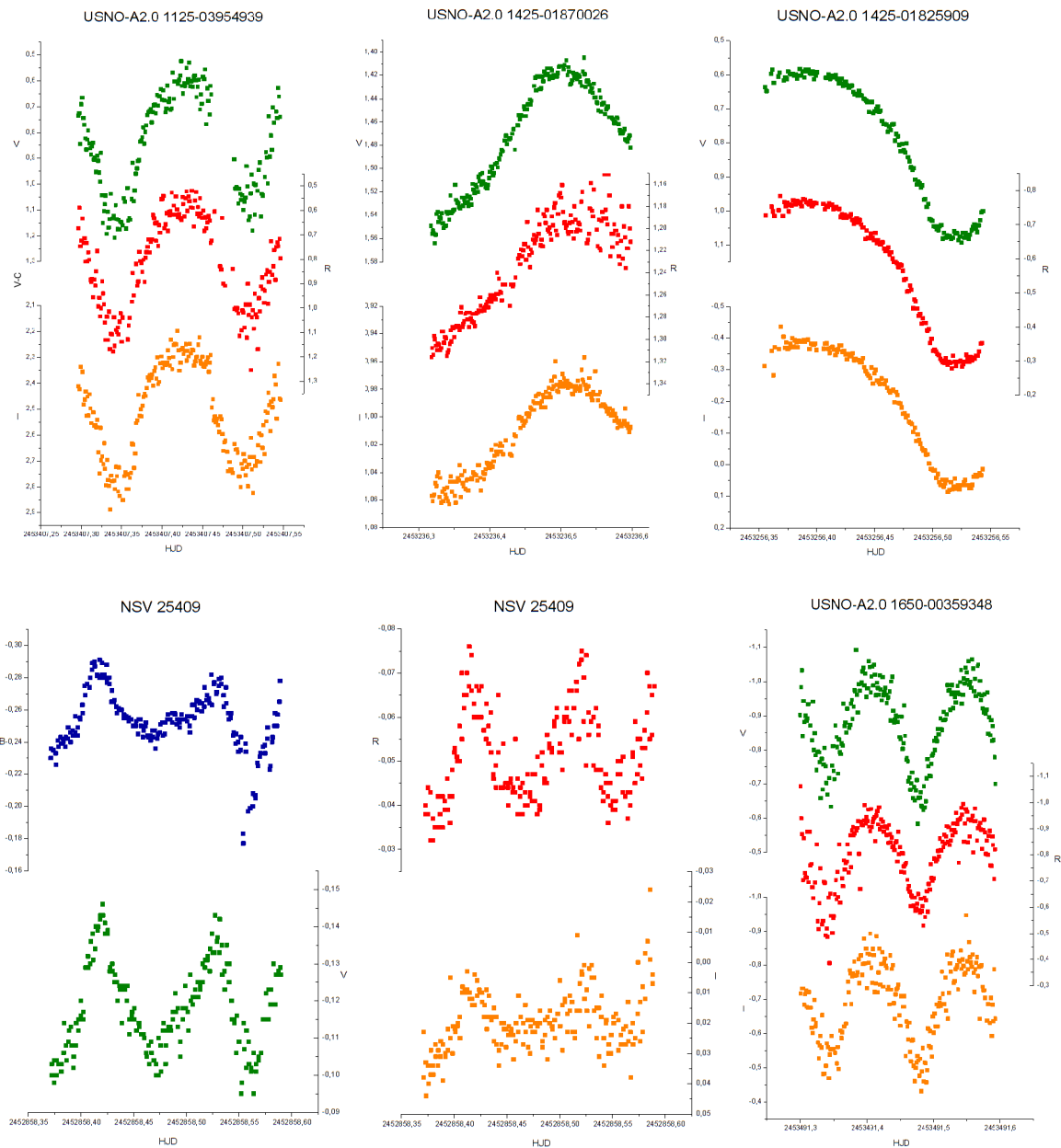
**Acknowledgements**

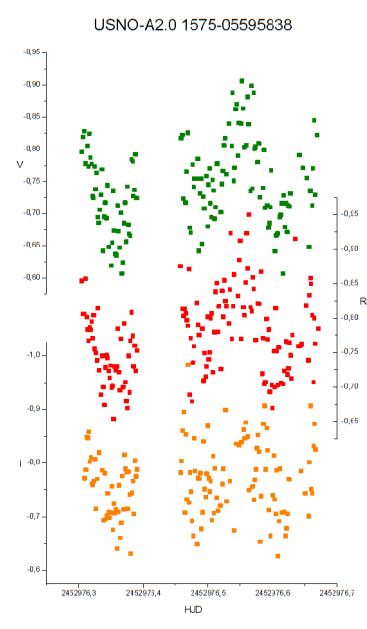
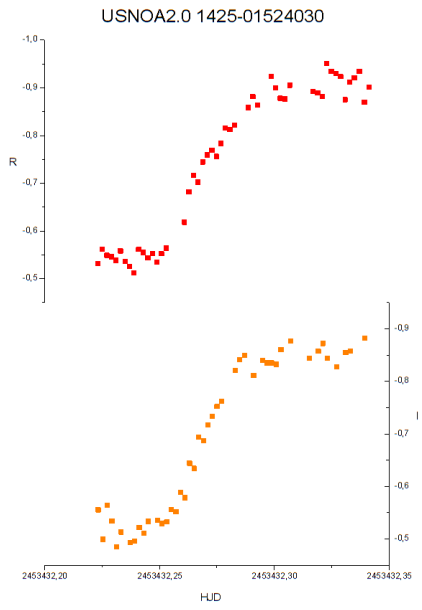
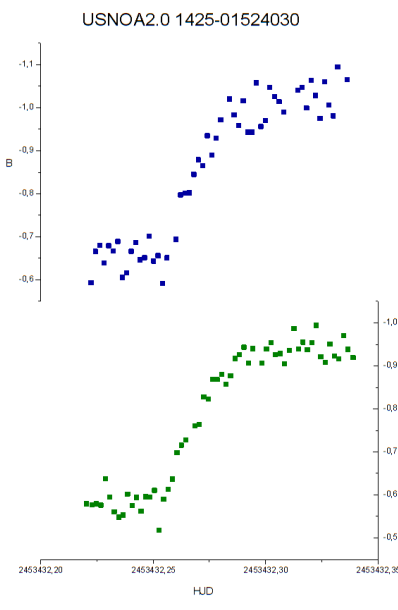
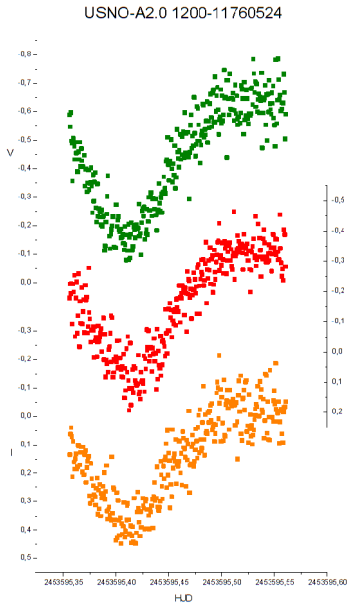
I want to thank M. Jakubik for cooperation with creating the database of archival data and D. Bozik, M. Vanko, T. Pribulla and D. Chochol, et. al. who observed the data used in this work. The dark frame correction described in this paper was performed by an IDL worksheet co-designed by E. Kundra.

**References**

Bertin, E., Arnouts, S., 1996, *A&AS*, 117, 393, [1996A&AS..117..393B](http://dx.doi.org/10.1051/aas/1996117393)  
 Heckert, P.A., Zeilik, M., 1991, *IBVS*, 3688, [1991IBVS.3688....1H](http://www.iau.org/publications/IBVS/IBVS3688-1H)  
 Hroch, F., 2007, MuniPack, <http://munipack.astronomy.cz/>  
 Motl, D., 2005, MuniWin, <http://integral.physics.muni.cz/cmuniPack/index.html>

**Addendum: Light curves of new variables**





# Objects of High Energy Astrophysics as Optically Variable Objects

RENÉ HUDEC<sup>1,2</sup>

- 1) Astronomical Institute, Academy of Sciences of the Czech Republic, 251 65 Ondřejov, Czech Republic  
2) Czech Technical University, Faculty of Electrical Engineering, Prague

## Abstract

A large fraction of objects of high-energy astrophysics emits also optical light, which is, in many cases, variable. The observation of these sources at optical wavelengths can provide valuable inputs for multispectral analyse of various categories of celestial high-energy (HE) sources. As the magnitudes of numerous objects are bright and can be hence accessed by small and amateur observatories, these observers can contribute to investigations and analyses of HE sources. We discuss in detail these possible contribution.

## CZ Abstrakt

Řada objektů astrofyziky je současně zdroji, často proměnnými, viditelného světla. Jejich výzkum ve viditelném světle je důležitý pro multispektrální analýzu a pochopení fyzikálních procesů ve zdrojích. Některé z objektů jsou opticky jasné a tedy přístupné i malým a amatérským pozorovatelům, kteří tak mohou přispět k jejich výzkumu. Tento možný příspěvek podrobně diskutujeme v tomto příspěvku.

## 1. Introduction

A large fraction of objects of high-energy astrophysics emits also optical light, which is, in many cases, variable. The observation of these sources at optical wavelengths can provide valuable inputs for multispectral analyse of various categories of celestial high-energy (HE) sources. As the magnitudes of numerous objects are bright and can be hence accessed by small and amateur observatories, these observers can contribute to investigations and analyses of HE sources.

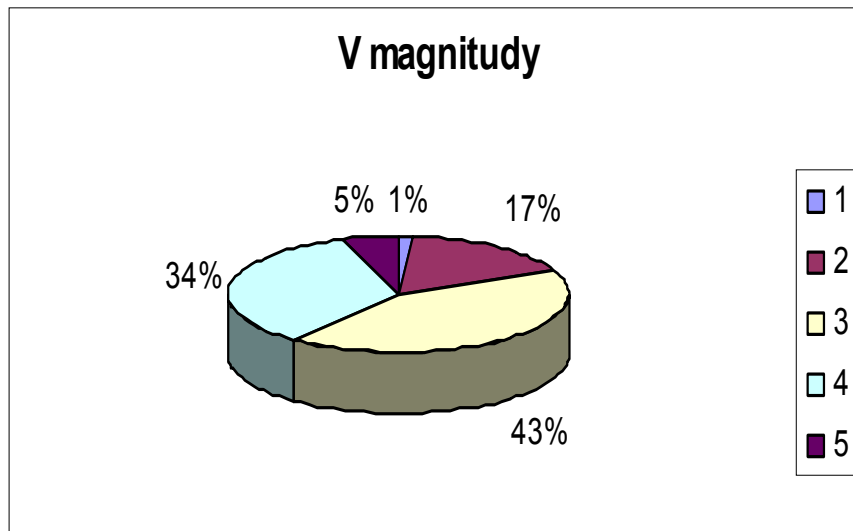


Fig.1 The distribution of optical V magnitudes of optically identified INTEGRAL gamma-ray sources. Most are brighter than mag 20, and more than half are brighter than mag 15. Legend 1 = mag 2,39 – 5, 2 = mag 5 -10, 3 = mag 10 – 15, 4 = mag 15 – 20, 5 = mag 20 – 21.

## 2. The HE sources as optical emitters

The HE sources belong to both galactic as well as extragalactic sources.

### 2. 1. Galactic HE sources

There are numerous categories of galactic HE sources, most important ones are listed below.

1. Cataclysmic Variables (CVs) and related objects. Example: GK Per
2. LMXRB. Example: HZ Her
3. HMXRB. Example: Cyg X-1

#### 4. X-ray transients

### 2. New types of sources

The fact that there are numerous CVs among the gamma-ray sources observed by the ESA INTEGRAL satellite (perhaps up to 10% of all INTEGRAL gamma-ray sources) represent one of interesting new findings over the last few years. Moreover, few symbiotic stars (SSs) were also identified with INTEGRAL gamma-ray sources.

#### 2.2. Are the optically variable galactic HE sources “variable stars”?

As many of the HE sources do have optical variable emission, a natural question arises, what is the link between these sources and variable stars.

1. Yes, some are: examples X-ray and gamma-ray loud CVs and SSs
2. Some of LMXRB, HMXRB are VS of “non-classical categories”
3. Some are newly detected VS
4. Some are not such as the new category of galactic GBSs
5. The dominant role of CVs: The contribution of CVs to galactic X-ray background may be greater than assumed before

#### 2.3. The HE sources as optical emitters II. Extragalactic

Numerous celestial HE sources belong to the category of extragalactic sources, the most important types are listed below.

1. AGN
2. Blazars
3. Optical Afterglows and Optical Transients of Gamma-Ray Bursts (GRBs)
4. SNe
5. LBV (Luminous Blue Variables in external galaxies)

Few examples of the blazars detected in gamma-rays by the INTEGRAL satellite are given and discussed later in this paper.

#### 2.4. Modes of observations

There are various modes of observations required for the HE sources. The situation is very complex, as the sources belong to various categories.

Satellite campaigns: One of the most important modes of supporting optical ground-based observations is the response to satellite observing campaigns. While the satellite observation itself usually lasts for ~days, the whole observing campaign lasts typically for weeks, as also the time before and after the satellite observation needs to be covered. Dense coverage during the satellite observation is required, with less dense coverage before and after. Magnitudes typically 12-18.

In addition to that, planned observations of optically variable sources by satellites can be supplemented by optical ground based observations, with similar requirements as described above.

Monitoring for triggering satellite (ToO – Target of Opportunity) observations belong to another important type of optical observations of HE sources. In most cases, moderate sampling of ~ 1 point/day is enough. Magnitudes typically 12-18. Example: ToO proposal on blazars within INTEGRAL project (RH co-I). Here, the blazars included in the approved list are to be optically monitored for possible brightening.

Providing optical data for non-triggered satellite observations represent another category (e.g. providing optical monitoring data for the time span of INTEGRAL operation, i.e. 2002-2012). Typically 1 point/day (or even less) is enough. Magnitudes of the objects typically 10 – 18. This type of observations allows to compare behavior of gamma-ray sources at various energies and is hence physically important as from such comparison physical conclusions may be drawn.

Alert follow-up observations represent another important type. They need fast response, better (but not necessarily) automated. However, even a site with non automated instrumentation has chance due to observational/weather constraints. Mostly Gamma-Ray Bursts (GRBs) belongs to the object observed this way, but occasionally various types of another flaring and transient targets may be added. Expected magnitudes 6 – 22. With the ESA Gaia satellite, we expect another type (Gaia project related) type of alerts, which will point on suspicious (mostly flaring) objects detected within Gaia. As the Gaia itself will have limited ability to confirm the reality of these objects, in most cases the final confirmation and further analyses of Gaia alert triggers will rely on ground based observers.

Verifying suggested identifications represent another type of job where small observatories may contribute. Typical magnitudes 10 – 20. The preferred response is within days or a week. Photometry both with good sampling as well as moderate sampling, photometry with filters, spectroscopy (including low dispersion), are required.

Optical supplementary analyses of HE sources (for complex multispectral analyses) may also add valuable optical data for understanding the physics of the sources. The typical magnitudes are 10 – 20. Again, photometry both with good sampling as well as moderate sampling, photometry with filters, and spectroscopy (including low dispersion) are required.

### 3. Need for optical monitoring

As it will be shown later, very common is the situation when we have satellite monitoring data covering extended time periods up to ~ years, but we do not have simultaneous optical data.

At the same time, the most important goal is to recognize active states of the sources (flares, high states, etc) either to trigger the satellite observations, or, alternatively, to be able to concentrate of archival satellite data for that's periods.

In this respect, small and amateur observatories can effectively contribute to these tasks.

### 4. Cataclysmic variables and related objects as seen in gamma-rays by INTEGRAL satellite

The ESA INTEGRAL satellite (Winkler et al., 2002), launched in 2002 and expected to operate at least until 2012, with its 4 onboard telescopes for analyses of gamma-ray sources simultaneously in gamma-ray, X-rays, and (for brighter objects) optical V band, is suitable for:

- (a) detection of the populations of CVs and symbiotics with the hardest X-ray spectra
- (b) simultaneous observations in the optical and hard X-ray regions
- (c) long-term observations with OMC – including a search for rapid variations in observing series during science window (OMC observations also for systems below the detection limit in hard X-rays)

In total, 21 CVs were detected (surprise, more than expected, almost 10% of INTEGRAL detections)

- 17 seen by IBIS (Barlow et al., 2006, Bird et al., 2007) – correlation of IBIS data and Downes CV catalogue
- 4 are CV candidates revealed by optical spectroscopy of IGR sources (Masetti et al., 2006) – new CVs, not in Downes catalogue

They are mainly magnetic systems: 11 confirmed or probable IPs, 3 polars, 2 dwarf novae, 4 probable magnetic CVs, 1 unknown. Periods: vast majority  $P_{orb} > 3$  hr, i.e. above the period gap (only one  $< 3$  h). 5 long period systems with  $P_{orb} > 7$  hr.

Some statistics: Intermediate polars – only ~2% of the catalogued CVs, but they dominate the group of CVs seen by IBIS. More such detections and new identifications can be hence expected. Many CVs covered remain unobservable by IBIS, but new have been discovered. IBIS tends to detect IPs and asynchronous polars: in hard X-rays, these objects seem to be more luminous (up to the factor of 10) than synchronous polars (but detection of more CVs needed for better statistics).

Some examples are listed and discussed below.

#### V834 Cen

The optical light curve of V834 Cen during the lifetime of INTEGRAL shows active and inactive states. V834 Cen is a polar of AM Her class. This polar was probably detected by IBIS since it was in high (active) state. This may explain why some CVs have been detected by IBIS and some not.

Optical monitoring of sources is important as it can indicate active intervals when the object is expected to be active also in gamma-rays. However, comparing optical and gamma-ray activity is difficult in most cases due to lack of optical (!) data. Goal for robotic telescopes.

#### V1223 Sgr

Intermediate polar. Most significantly detected CV in the IBIS survey, with a significance of 38 sigma in the 20-40 keV final mosaic. Accretion via disk, bright X-ray source (4U 1849–31). Orbital period:  $P_{orb} = 3.37$  h

(Osborne et al. 1985, Jablonski and Steiner 1987). Rotational period of the white dwarf:  $P_{rot} = 746$  sec (Osborne et al. 1985).

Beat period (combined effect of  $P_{orb}$  and  $P_{rot}$ ):  $P_{beat} = 794.3$  sec (Steiner et al. 1981). Prominent long-term brightness variations: - outburst with a duration of  $\sim 6$  hr and amplitude  $> 1$  mag (van Amerongen & van Paradijs 1989) - episodes of deep low state (decrease by several magnitudes) (Garnavich and Szkody 1988).

Indications for flaring activity: Seen by IBIS (flare lasting for  $\sim 3.5$  hrs during revolution 61 (MJD 52743), peak flux  $\sim 3$  times of average (Barlow et al., 2006). Seen in optical by ground-based instrument (duration 6-24 hrs), Amerrongen & van Paradijs (1989). Confirms the importance of OMC instrument onboard INTEGRAL: even with  $V$  lim mag 15, it can provide valuable optical simultaneous data to gamma-ray observations.

Similar flares known also for another IPs in optical, but not in soft gamma: Example TV Col (Hudec et al., 2005), where 12 optical flares have been observed so far, five of them on archival plates from the Bamberg Observatory. TV Col is an intermediate polar (IP) and the optical counterpart of the X-ray source 2A0526-328 (Cooke et al. 1978, Charles et al. 1979). This is the first cataclysmic variable (CV) discovered through its X-ray emission.

Physics of the outbursts in IPs:

- Disk instability or
- An increase in mass transfer from the secondary

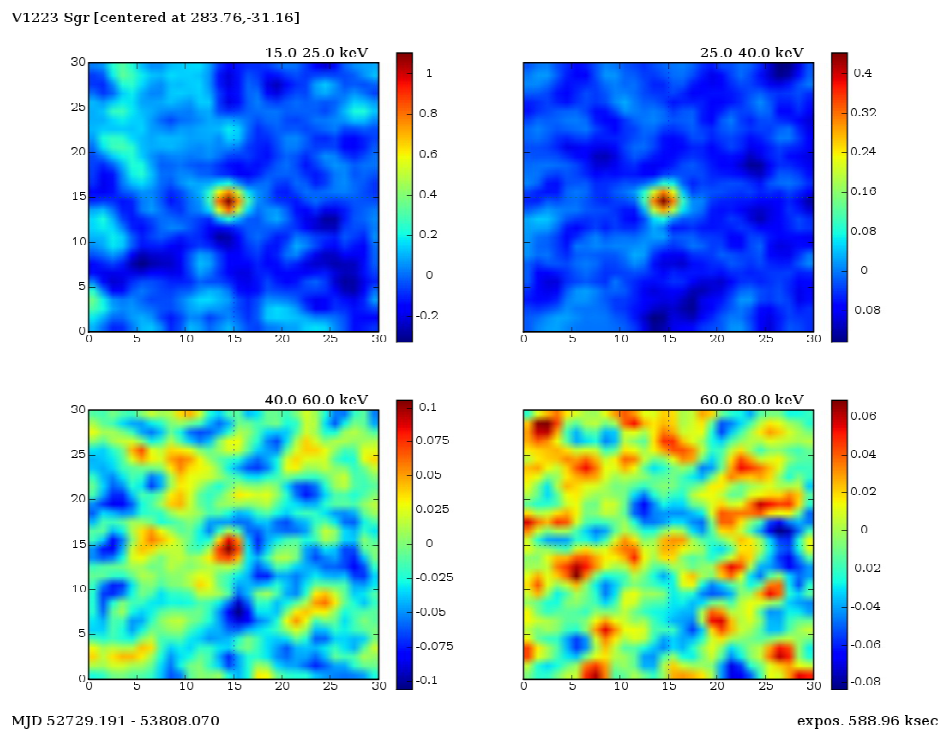


Fig. 2: V1223 Sgr recent IBIS mosaics (co-added frames) all data (589 ks) intensity maps. The object is in the centre of the images.

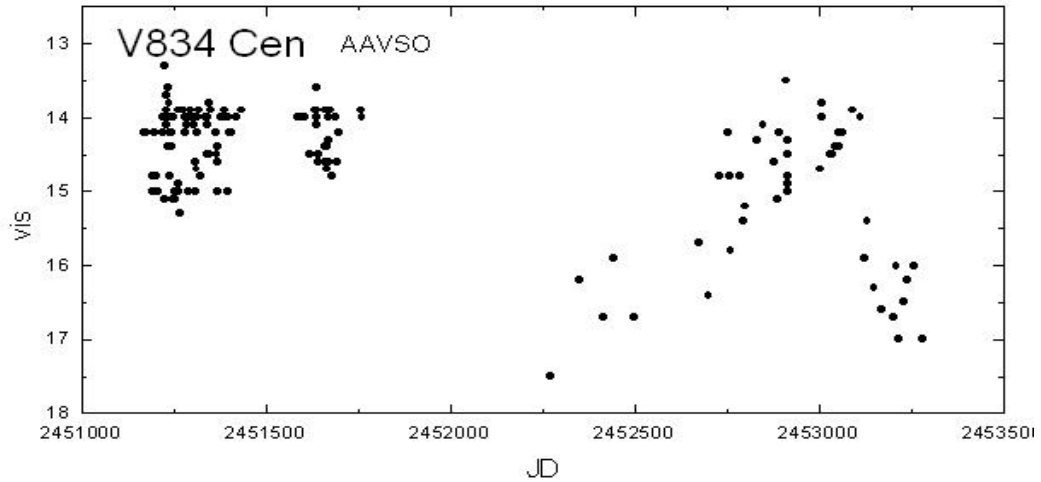


Fig. 3: The AAVSO light curve for V834, a cataclysmic gamma-ray loud variable detected by the ESA INTEGRAL satellite. The active state around JD 2453000 represents the time period when the source was detected in gamma-rays, while it remained undetected at times when the source was in the inactive state.

JD (24..)	Exp. Time	Flux (15 - 25)keV	Flux (25 - 40)keV	Flux (40 - 60)keV	Flux (60 - 80)keV
		[ $10^{-12}$ erg s $^{-1}$ cm $^{-2}$ ]	[ $10^{-12}$ erg s $^{-1}$ cm $^{-2}$ ]	[ $10^{-12}$ erg s $^{-1}$ cm $^{-2}$ ]	[ $10^{-12}$ erg s $^{-1}$ cm $^{-2}$ ]
52 710,38 - 52 752,01	109,2	161,00 ± 14,50	57,90 ± 4,88	< 4,93	< 6,26
52 917,17 - 52 926,84	151,1	112,00 ± 11,30	51,10 ± 4,19	21,30 ± 4,24	< 5,48
53 082,07 - 53 119,10	228,1	127,00 ± 8,90	50,00 ± 3,28	23,10 ± 3,48	10,00 ± 4,54
53 267,41 - 53 305,97	134,5	126,00 ± 12,50	55,40 ± 4,46	25,40 ± 4,75	27,70 ± 6,23
53 440,61 - 53 479,81	90,9	155,00 ± 15,20	61,30 ± 5,53	24,10 ± 5,85	< 7,69
53 602,80 - 53 672,88	409,6	< 7,17	31,80 ± 2,65	< 2,82	< 3,78
53 781,06 - 53 809,24	282,1	132,00 ± 10,00	48,50 ± 3,50	13,90 ± 3,56	< 4,69
52 710,38 - 53 809,25	1405,5	103,00 ± 3,90	46,40 ± 1,42	15,10 ± 1,48	12,30 ± 1,97

Tab 1: IBIS observations of V1223 Sgr.

## 5. INTEGRAL blazars

From the extragalactic HE sources, blazars belong to the most important, and also optically violently variable objects. Below we list a few examples of blazars analyzed with INTEGRAL observations.

### 1ES 1959+650

This blazar is a gamma-ray loud variable object visible in 2006 only, invisible in total mosaics and/or other periods.

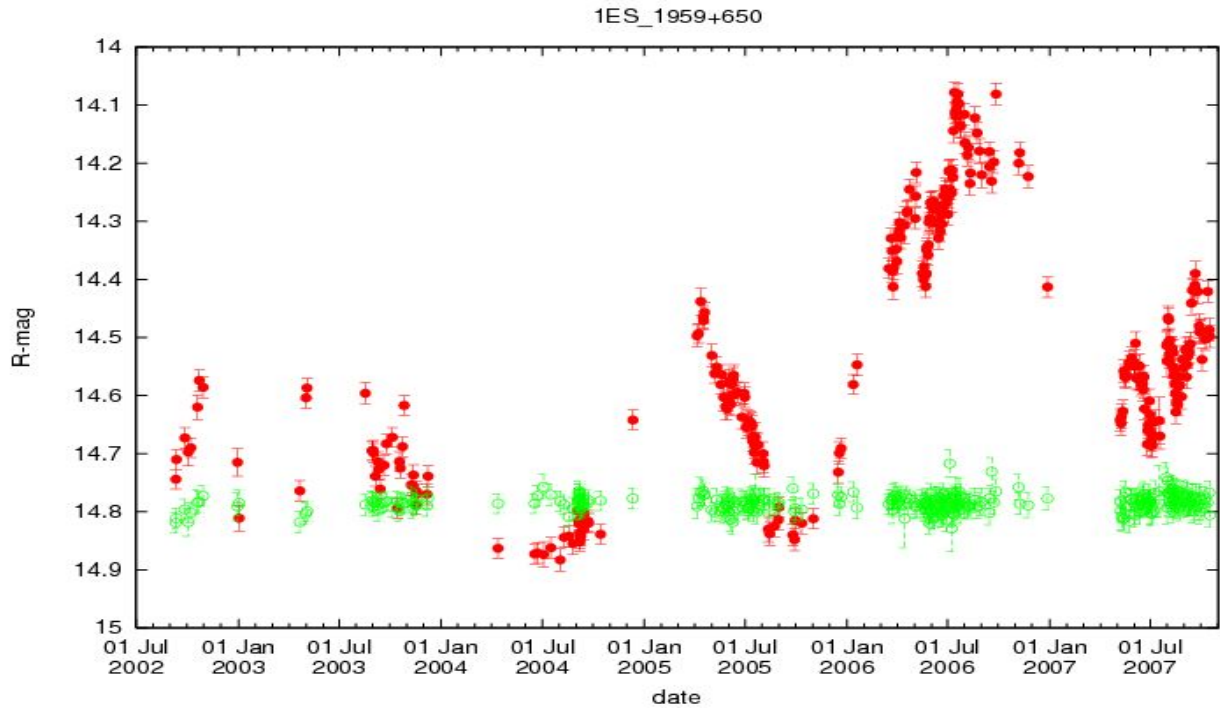


Fig. 4: Optical light curve of blazar 1ES 1959+650 (Tuorla Observatory blazar monitoring program).

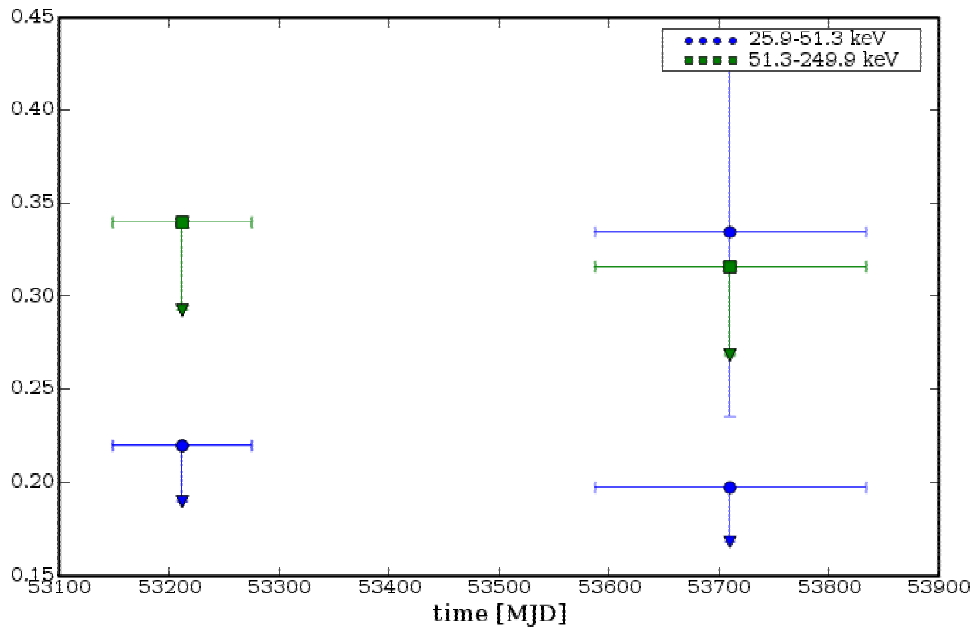


Fig. 5: IBIS gamma-ray light curve of 1ES 1959+650. Blazar is in INTEGRAL gamma-ray imager IBIS visible only in data set corresponding to optical flare.

**3C66A**

This blazar is visible by IBIS gamma-ray imager onboard INTEGRAL only during the optical flare shown below and is invisible other times.

3C 66A [centered at 35.66, 43.04]

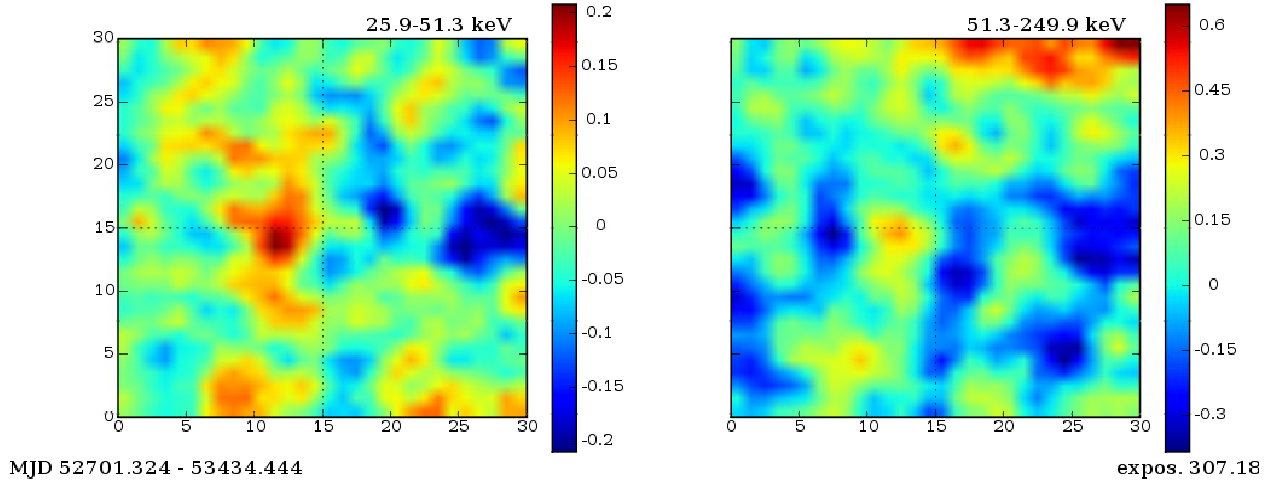


Fig. 6: IBIS gamma-ray image of blazar 3C66A. MJD interval 52701.32-52849.62 i.e. 148.30 days [Mar 2004 - Jul 2004] time mean  $1294.368 \pm 44.479$ , size  $60 \times 60$  [pixels  $-0.082 \times 0.082$ ] — exposure 128.563 ksec The flux is  $(1.66 \pm 0.285) 10^{-11} \text{ erg/cm}^2/\text{s}$ . The object is clearly variable.

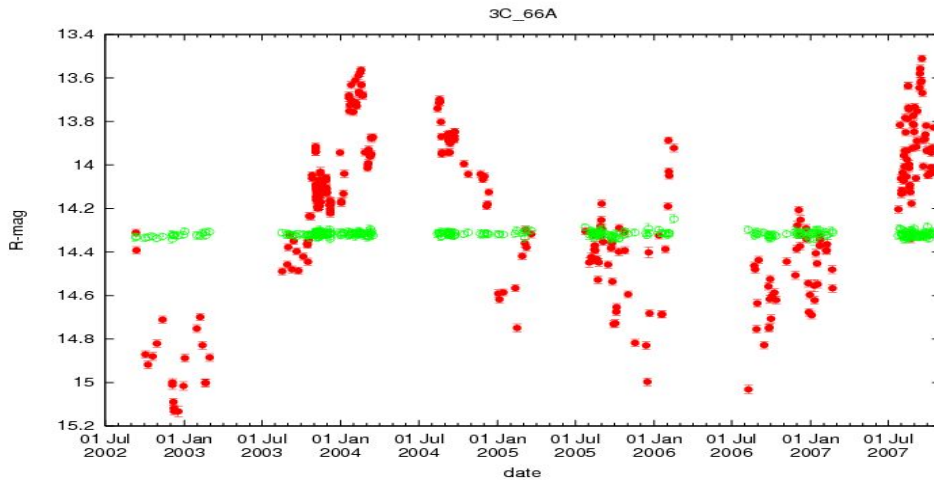


Fig. 7: Optical light curve of blazar 3C66A (Tuorla Observatory blazar monitoring program).

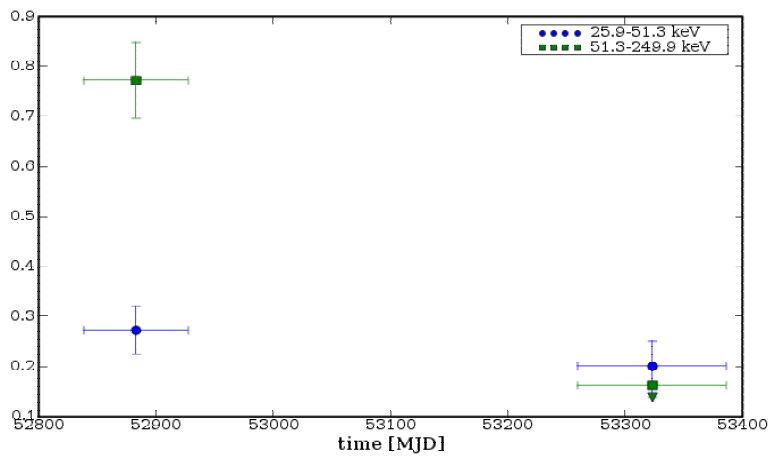


Fig. 8: IBIS gamma-ray light curve of blazar 3C66A.

## 7. Unknown Discoveries

In addition to the main types of HE objects described above, occasionally also objects worth study of another categories appear. The variable objects at positions of Ultra High-Energy (UHE) sources can serve as an example.

- Puzzling poorly investigated variable star at positions of UHE source
- the variable M6 star V347 Aql, with coordinates J2000.0 ICRS position of RA=19h08m01.3s, DEC=+06d18'27", and magnitude B= 11.5 mag
- Within the error box of the new VHE source HESS J1908+063
- T Tauri star?
- Oxygen rich irregular variable? IRAS source
- Light curve unknown ..... object at B 11 ..... good target for small observatories

## 8. New Types of Optically Variable Objects

There are also newly detected types of optically variable HE sources. The optical counterpart of GRB070610 may serve as an example (DeUgarte Postigo, 2007). The basic parameters of this GRB are given below:

- Detected on 10 June 2007 20:52:26 UT by *Swift*/BAT as a **normal burst** (GCN 6489)
- $T_{90}=4.6$ s
- Photon index  $1.76 \pm 0.25$
- Fluence  $(2.4 \pm 0.4) \cdot 10^{-7}$  erg/cm<sup>2</sup> (Tueller et al. GCN 6491)
- XRT detected an **X-ray counterpart** 3100s later (GCN 6490) with a column density consistent with the Galactic.
- Stefanescu et al. (GCN 6492) reported the detection of a variable **optical counterpart**.
- de Ugarte Postigo et al. (GCN 6501) **confirmed the detection** with observations from the 1.5m OSN.
- D.A. Kann et al. (GCN 6505) suggested a **Galactic origin**, based on unusual flaring activity and location near the galactic plane:  $l=63.3^\circ$   $b=-1^\circ$
- SWIFT J195509+261406
- The emission between flares slowly decreased until it disappeared.
- No detectable quiescent source.

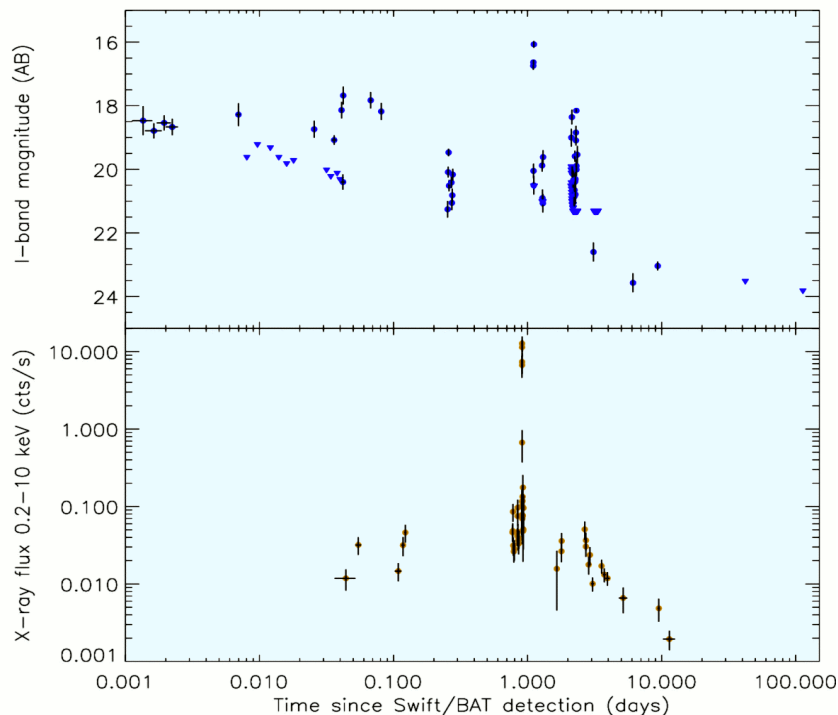


Fig. 9: Optical I-band and X-ray light curve of flaring counterpart of GRB070610.

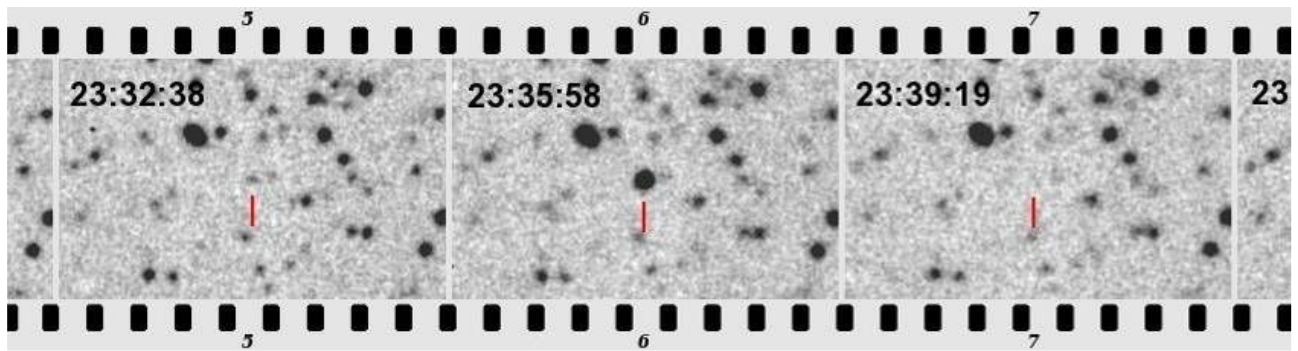


Fig.10: Flaring episodes of optical counterpart of galactic GRB070610.

What is the source?

- Gamma-ray burst event
- X-ray, optical and nIR counterpart
- No radio or millimetre counterpart
- Dramatic flaring activity
- Very faint quiescent source
- Galactic
- GRB?
- Light curve behaviour and location rule it out.
- Microquasar?
- Stronger gamma-ray and radio emission is expected
- Bursting pulsar?
- Would have shown further gamma-ray bursts
- Soft gamma-ray repeater?
- First detected at optical wavelengths

## 9. Conclusions

The HEA objects in many cases exhibit optical (and mostly variable emission) accessible in some cases even by small observatories. For many of these sources there is a lack of optical data. The optical data are important for multispectral analyses of the sources, contributing of better understanding of related physical processes.

## Acknowledgements

The analyses of HE sources by the ESA INTEGRAL satellite were supported by ESA PECS project No. 98023. The investigation of high-energy sources by the ESA Gaia satellite is supported by the ESA PECS Project No. 98058. The analyses of gamma-ray sources in optical light were supported by GA CR, grant 205/08/1207.

## References

- Winkler, C., Courvoisier, T.J.-L., Di Cocco, G., et al., *Astronomy and Astrophysics*, Vol. 411, L1, 2003.
- DeUgarte Postigio A. et al., *Proceedings of GRB Conference Santa Fe*, AIP Conf Proceedings, in press.
- Bhat C. L., et al. Possible detection of TeV gamma rays from AM Herculis, *Astrophysical Journal*, Part 1, Vol. 369, 475-478, 1991.
- Downes R., et al. *PASP*, Vol. 113, 764, 2001.
- Van Amerongen, S. and Van Paradijs J. Detection of a brief outburst from the intermediate polar V 1223 SGR, *Astronomy and Astrophysics*, Vol. 219, 195-196, 1989.
- Garnavich, P., Szkody, P., *PASP*, 100, 1522, 1988.
- Hudec, R., 1981, *BAIC*, 32, 938
- Bianchini, A. and Sabbadin, F. The Old-Nova GK Per (1901): Evidence for a Time-Delay Between its X-Ray and Optical Outbursts, *Information Bulletin on Variable Stars*, 2751, 1, 1985.
- Watson, M.G., King, A.R., Osborne, J, *MNRAS*, Vol. 212, 917, 1985.
- Warner, B., *Cataclysmic Variable Stars*, Cambridge Univ. Press, 1995.
- Dobrzycka, D., et al. The Hot Component of RS Ophiuchi, *Astronomical Journal*, Vol. 111, 2090, 1996.
- Barlow, E. J.; Knigge, C.; Bird, A. J.; J Dean, A.; Clark, D. J.; Hill, A. B.; Molina, M.; Sguera, V. *Monthly Notices of the Royal Astronomical Society*, Volume 372, Issue 1, pp. 224-232,

2006.

Bird A. et al. The Astrophysical Journal Supplement Series, Volume 170, Issue 1, pp. 175-186, 2007.

Simon, V.; Hudec, R.; Strobl, J.; Hroch, F.; Munz, F., The Astrophysics of Cataclysmic Variables and Related Objects, Proceedings of ASP Conference Vol. 330. Edited by J.-M. Hameury and J.-P. Lasota. San Francisco: Astronomical Society of the Pacific, p.477, 2005.

Masetti N. et al., Astronomy and Astrophysics, Volume 459, Issue 1, November III 2006, pp.21-30, 2006.

Hudec, R.; Simon, V.; Skalicky, J., The Astrophysics of Cataclysmic Variables and Related Objects, Proceedings of ASP Conference Vol. 330. Edited by J.-M. Hameury and J.-P. Lasota. San Francisco: Astronomical Society of the Pacific, p.405, 2005.

Cooke, B. A., et al., Royal Astronomical Society, Monthly Notices, vol. 182, Feb. 1978, p. 489-515, 1978.

Charles et al. 1979

Motch, C.; Haberl, F., Cape Workshop on Magnetic cataclysmic variables; Astronomical Society of the Pacific Conference Series, Volume 85, Proceedings of the Cape Workshop, held in Cape Town, 23-27 January 1995, San Francisco: Astronomical Society of the Pacific (ASP),—c1995, edited by D.A.H. Buckley and B. Warner, p.109, 1995.

Motch et al., Astronomy and Astrophysics, v.307, p.459-469, 1996.

de Martino, D. et al., Astronomy and Astrophysics, v.415, p.1009-1019, 2004.

Suleimanov, V.; Revnivtsev, M.; Ritter, H., Astronomy and Astrophysics, Volume 443, Issue 1, November III 2005, pp.291-291, 2005.

Ishida M. et al., MNRAS 254, 647, 2002.

Sokolski J. L. et al., BAAS 37, 1216, 2005.

Jablonski, F., Steiner, J.E., 1987, ApJ, 323, 672

Osborne, J., Rosen, R., Mason, K.O., Beuermann, K., 1985, Sp.Sc.Rev., 40, 143

# On the light curves of symbiotic stars

AUGUSTIN SKOPAL

Astronomical Institute, Slovak Academy of Sciences, 059 60 Tatransk'a Lomnica, Slovakia (e-mail: [skopal@ta3.sk](mailto:skopal@ta3.sk))

## Abstract

In this contribution I introduce a special type of long-period interacting binaries, the symbiotic stars, focusing on fundamental types of variations recorded in their light curves. In particular, I introduce the orbitally-related wave-like modulation observed during quiescent phases, eclipses indicated during active phases and apparent orbital changes measured during transitions between quiescence and activity.

## 1 Introduction

At the beginning of the 20th century, W. Fleming and A. Cannon discovered a few stars whose spectra showed characteristic features of the simultaneous presence of two extremely different temperature regimes. The cooler was that of an M-giant spectral type, and the hotter was expressed by the blue continuum and bright emission lines. They called them as the stars with combination spectra. It was easy to voice the hypothesis that they could be binary stars, but it was extremely difficult to prove it. Even in 1950, P. Merrill was not able to reveal the true nature of combination spectra of RW Hydrae, BF Cygni and CI Cygni. He concluded that these 'symbiotic' stars require systematic monitoring with fairly high dispersion to get a better knowledge of their nature. The attribute *symbiotic* was then adopted to denote this class of objects.

Currently the symbiotic stars are understood as interacting binary systems consisting of a cool giant and a hot compact star – most probably a white dwarf. Typical orbital periods are between 1 and 3 years, but can be significantly larger. The giant component loses mass via the wind, part of which is accreted by its companion. This process makes the accretor very hot ( $T_{\text{hot}} \sim 10^5$  K) and luminous ( $L_{\text{hot}} \sim 10 - 10000$  solar units), and thus to be capable of ionizing a fraction of the neutral wind from the giant giving rise to *nebular* emission. As a result the spectrum of symbiotic stars consists of three basic components of radiation – two stellar and one nebular. If the processes of the mass-loss, accretion and ionization are in a mutual equilibrium, then symbiotic system releases its energy approximately at a constant rate and energy distribution. This stage is called as the *quiescent phase*. Once this equilibrium is disturbed, symbiotic system changes its radiation significantly, brightens up in the optical by a few magnitudes and shows signatures of a mass-outflow for a few months to years. We name this stage as the *active phase*.

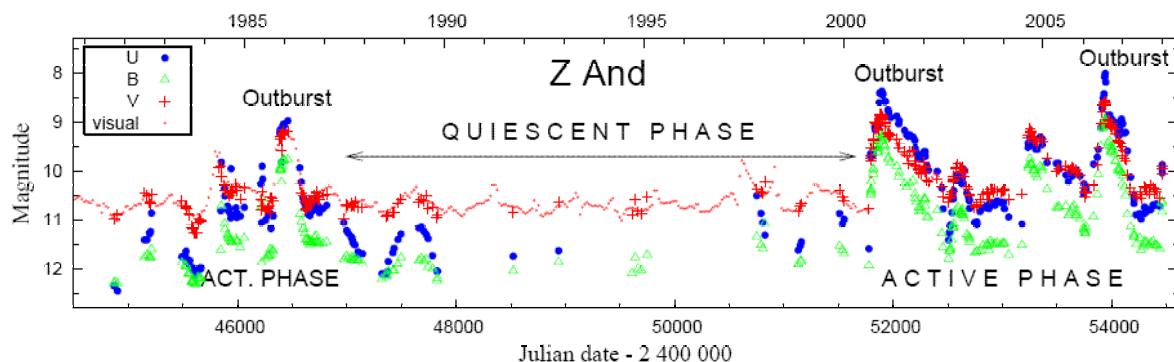


Figure 1: The *UBV* light curves of the symbiotic prototype *Z And* during the last 27 years. In the 2000 autumn *Z And* entered new active phase showing numerous eruptions in its light curve. Two major outbursts that peaked in 2000 December and 2006 July are denoted.

Figure 1 shows example of quiescent and active phases as recorded in the light curve of the symbiotic prototype *Z And* during the last 27 years. According to the spectral energy distribution (SED) in the infrared (IR), we distinguish between S-type (Stellar) and D-type (Dusty) symbiotic stars. The former is represented by a stellar type of the IR continuum from the giant, whereas the latter contains an additional emission from the dust. D-type symbiotics comprises the Mira variable and thus are called as symbiotic Miras. Figure 2 shows examples of the UV–IR SED for both these types – the symbiotic prototype *Z And* and the symbiotic Mira *V1016 Cyg*.

The circumstellar environment of symbiotic stars extends to about 100–1000 astronomical units with densities running from about  $1E+12$  particles per cubic centimeter in its inner parts, and comprising strong sources of ionizing photons (the compact hot star) and neutral particles (the red giant). Symbiotic stars thus represent an

ideal medium for studying many physical processes like the mass loss from giant stars, effects of accretion from the wind, processes of ionization and scattering, instabilities of accretion disk, outbursts, many kinds of high-velocity outflows, wind collisions, dust creation, late stages of binary star evolution, etc. From this point of view they are considered as space laboratories to investigate macroscopic processes on the long-term scales. Many particular aspects have recently been discussed and summarized with outlined problems at the conference on the symbiotic stars research held in Los Cancajos, La Palma, in 2002 May (Corradi et al. 2003).

Generally, investigation of symbiotic stars needs theoretical modeling of photometric and spectroscopic variations in both the continuum and the line spectrum. Their long orbital periods require the long-term both photometric and spectroscopic observations, and the simultaneous presence of two extremely different temperature regimes in their spectra require to analyze the multifrequency observations. Nevertheless, majority of observations have been undertaken in the optical - the most accessible wavelength domain from the ground. And the simplest way how to obtain valuable information on a symbiotic star, it is to use the method of the multicolour photometry, by means of which we can obtain time evolution of the star's brightness, i.e. the light curve. However, to explain the observed variations in different photometric passbands, we have to understand the basic physical processes, radiation of which contributes to the optical. In this respect, the process of ionization proves to be most important, because it responds most sensitively the variation of energy production by the symbiotic system.

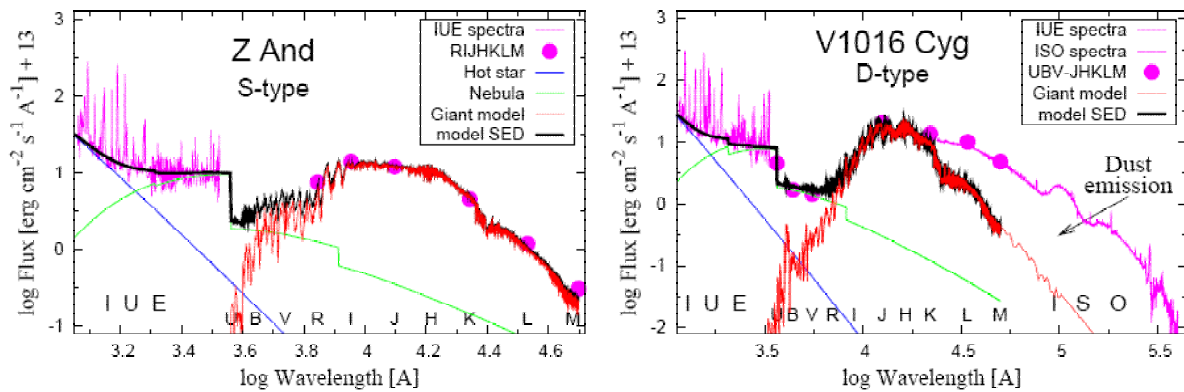


Figure 2: Examples of UV-IR SED for S-type (left) and D-type (right) symbiotic stars. Observed SED (pink) consists of IUE/ISO spectra and the multicolour photometric measurements. Model SEDs (black) for S-type objects were elaborated by using the method of Skopal (2005).

In this contribution I introduce just fundamental types of variations in the light curves of symbiotic stars, i.e. those that reflect most closely the nature of the symbiotic phenomenon. They are represented by the orbitally-related wave-like variation observed during quiescent phases, eclipses that can develop during active phases, and apparent changes of the orbital period, measured during transition periods between activity and quiescence. Nature of these types of variations can be understood with the aid of the SED of the composite spectrum of symbiotic stars and their simple ionization model.

## 2 Fundamental types of variations in the light curves

I distinguish three *fundamental* types of variations in the light curves of symbiotic stars. They represent most pronounced features in light curves and are caused by physical processes determining the presence of the symbiotic phenomenon. On the other hand, these types of the light variations can exclusively be produced only by symbiotic stars.

Figure 2 demonstrates a significant contribution of the nebular emission to the optical continuum. This suggests that the ionization process represents a very energetic interaction in symbiotic stars. In addition, the ionization process responds most sensitively variations in the temperature regime during different stages of a symbiotic system. Therefore this process is of crucial importance to understand the nature of the fundamental types of photometric variations. During quiescence the ionization process creates an extended massive nebula (emission measure around of  $10^{59} \text{ cm}^{-3}$ ), whereas during active phases the nebula changes significantly its physical properties and geometrical shaping. Figure 3 shows these limiting cases – basic ionization structure of a symbiotic star during quiescent phase as proposed by Seaquist, Taylor & Button (1984) and Nussbaumer & Vogel (1987), and active phase according to Skopal (2005).

As a result the different ionization structure during quiescent, active and also transition phases then corresponds to the three fundamental types of the light variations. They are:

1. Wave-like variation as a function of the orbital phase that represents the most characteristic feature of the light curves during quiescent phases. It is caused by the apparent variation of the amount of nebular emission observed at different positions of the binary.
2. The eclipse-like minimum that develops during active phases for systems with a high orbital inclination. During outbursts the structure of the symbiotic nebula rapidly changes, so that a significant fraction of the hot object radiation is located around the central star. As a result the broad wave-like profile changes rapidly into a narrow minimum. However, the eclipse profile differs significantly in both the depth and the width from that observed for standard eclipsing binaries.
3. Systematic variation in the minima positions during transition periods between activity and quiescence. During these periods the change in the profile of the minimum is followed also by a change in its position, which produces the effect of apparent changes in the orbital period.

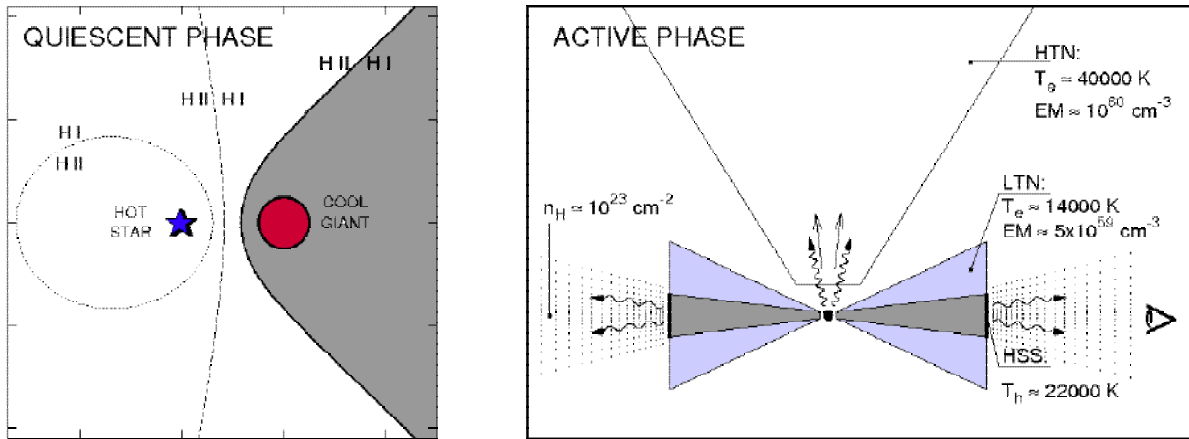


Figure 3: Left: Ionization boundaries (H II/H I) during quiescent phase calculated for three limiting cases of the Seaquist, Taylor & Button (1984) model: the cool giant loses neutral wind that is ionized by the hot star. Right: Scheme of basic structure of the hot objects during active phases (see Skopal 2005 in detail). The disk-like structure (HSS + LTN) is eclipsed at the position of the inferior conjunction of the giant, while the outside high-temperature nebula (HTN) partially fills in the light minimum (cf. Fig. 6).

In the following sections I will introduce these types of variations in more detail.

## 2.1 Wave-like orbitally-related variation

Generally, we observe a periodic wave-like profile of the light curve, whose minima and maxima occur at/around conjunctions of the binary components. The inferior conjunction of the giant (the cool component in front of the hot star) corresponds to the light minimum (orbital phase  $\phi = 0$ ), while at its superior conjunction (the hot star in front) we observe a light maximum ( $\phi = 0.5$ ). This variation is characterized with a large magnitude difference between the minimum and maximum,  $\Delta m \sim 1 - 2$  mag. This 'amplitude' is always larger in the blue part of the spectrum than in the red one, i.e.  $\Delta U > \Delta B > \Delta V$ . This relationship can be understood with the aid of the SED throughout the  $UBV$  region. Figure 4 shows examples of this type of the light variations for BF Cyg (it contains a red M5 giant with the effective temperature  $T_{\text{eff}} \sim 3400 \text{ K}$ ) and AG Dra (yellow K2 giant with  $T_{\text{eff}} \sim 4300 \text{ K}$ ) with their SEDs covering the optical domain. This spectral region is dominated by the radiation from the nebula and the giant. The latter does not depend on the orbital phase and strengthens considerably towards the longer wavelengths, while the nebular radiation has the opposite behaviour (it dominates the  $U$  passband and is fainter in  $V$ ) and it is the source of the orbitally-related variation (Sect. 2.1.1, Fig. 5). Therefore the  $\Delta m$  amplitudes are declining to longer wavelengths, where the nebular emission is superposed with the increasing light from the giant, which does not vary with the orbital motion. By other words the observed amplitude of the wave-like variation is proportional to the ratio of fluxes from the nebula and the giant, which is a function of the wavelength – flux from the giant/nebula increases/decreases with increasing lambda.

In the cases of the so-called yellow symbiotic stars (they contain a giant of the spectral type K to G), the giant's contribution into the  $V$  passband is very strong, which produces very different  $\Delta U$  and  $\Delta V$  amplitudes:  $\Delta U/\Delta V \gg 1$ . If the system contains a red giant, whose contribution in  $V$  is relatively lower to the total composite spectrum, the ratio  $\Delta U/\Delta V \sim 1$ . In our example on Fig. 4,  $\Delta U/\Delta V \sim 1.4$  for BF Cyg, whereas for the yellow symbiotic star

AG Dra  $\Delta U/\Delta V \sim 10$ . On the other hand a markedly different amplitude in  $U$  and  $V$  filters signals the presence of a yellow cool component in the symbiotic system.

**2.1.1 On the nature of the wave-like variation**

Skopal (2001) found a relationship between the wave-like variation in light curves and the radiation from the symbiotic nebula. Both dependencies are of the same type. We observe a maximum/minimum of the nebular emission around the conjunctions of the binary components, similarly as for the periodic wave-like variation of the photometric magnitudes. Figure 5 demonstrates this case for V1329 Cyg. Maximum/minimum of the nebular emission at  $\phi = 0.57/0.95$  (bottom panels) corresponds to the maximum/minimum in the light curve (top). Thus the orbitally related variation of the nebular component of radiation causes that observed in light curves.

It is simple to imagine that the orbitally-related variation in the nebular emission are only apparent. This implies that a fraction of the nebular medium has to be partially optically thick to produce different contributions of its total emission into the line of sight at different orbital phases.

**2.2 Eclipses**

During active phases of systems with high orbital inclination a significant change in the minima profile is observed – the very broad profile becomes to be narrow. As the minima coincide with the inferior conjunction of the cool component, it is believed that they are caused by eclipses of the hot object by the cool giant. Examples of this effect are shown in Figs. 4 and 6 for eclipsing symbiotic binaries BF Cyg, AX Per and CI Cyg.

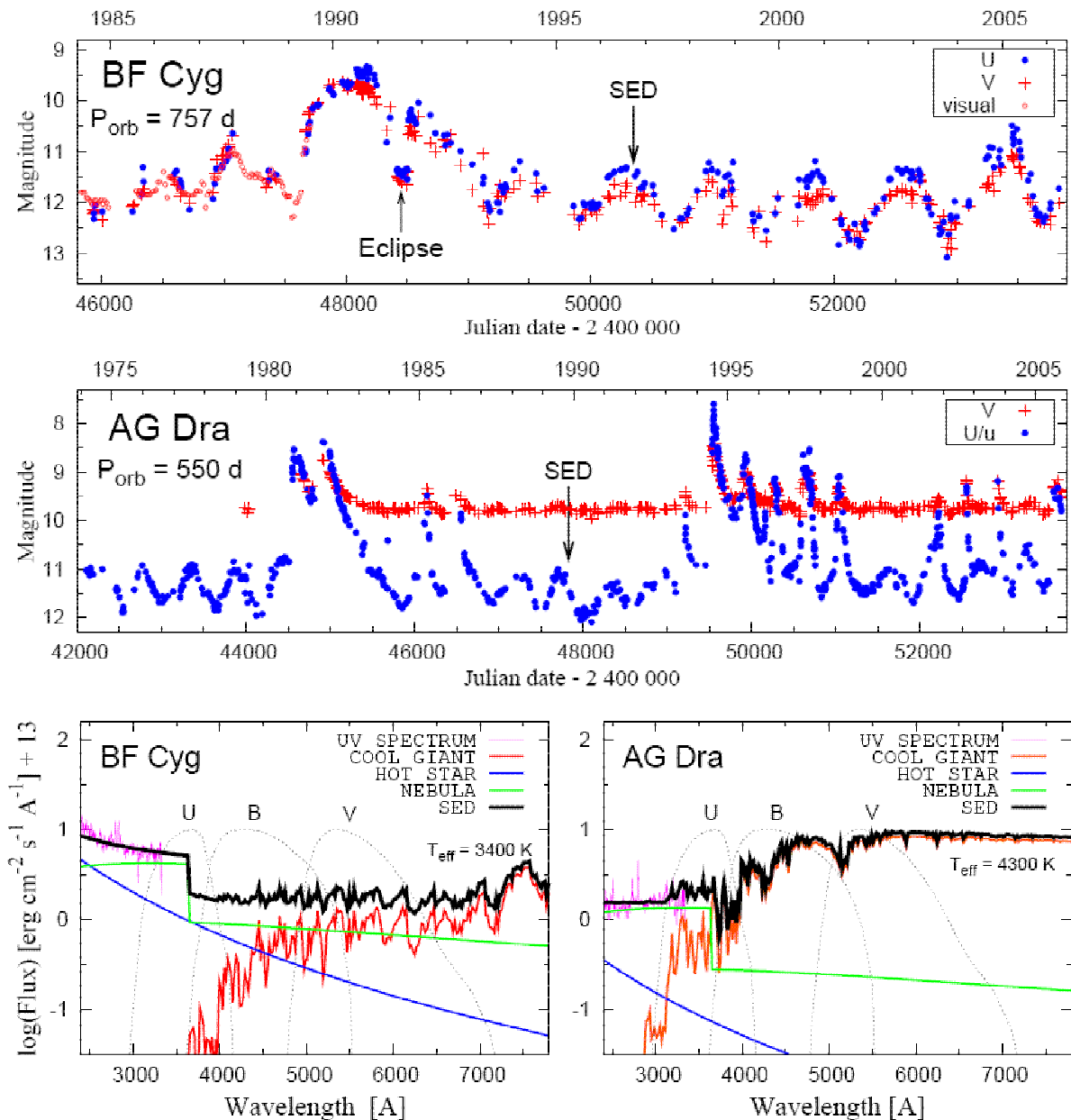


Figure 4: Top panels show the light curves of BF Cyg and AG Dra in U and V filters. During active phase the eclipsing system BF Cyg displays a relatively narrow minimum at the inferior conjunction of the giant, while during quiescent phase its light curve shows pronounced wavelike variation, characterized with amplitudes  $\Delta U = \Delta V \sim 1.5$  mag. The yellow symbiotic star AG Dra is not eclipsing. Amplitudes of its wave-like variations are smaller and depend considerably on the wavelength:  $\Delta U \sim 1$  mag,  $\Delta V \sim 0.1$  mag. The bottom panels show the SEDs of these objects throughout the UBVR passbands, which explain the observed differences in the wave-like variation (Sect. 2.1).

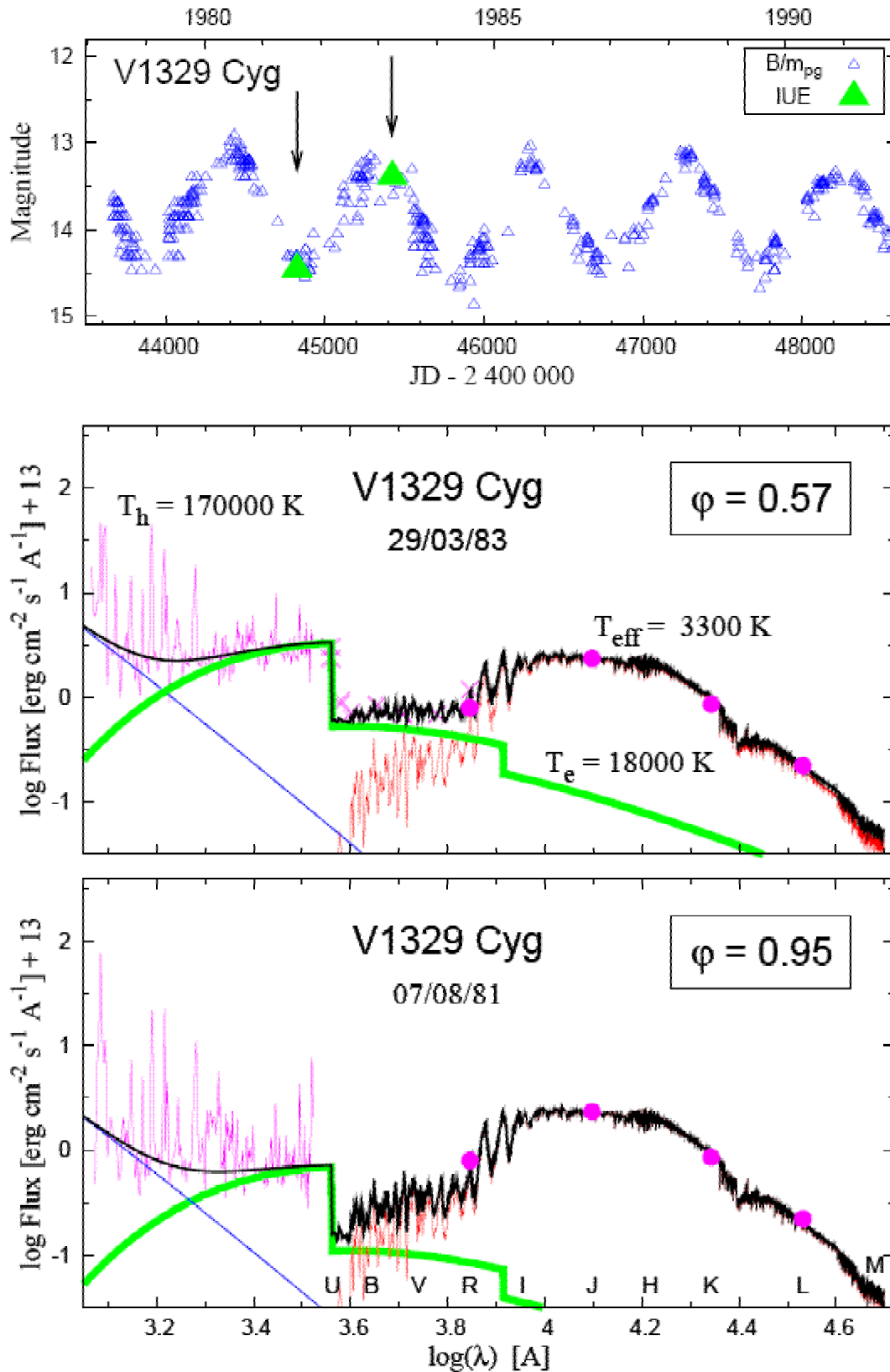


Figure 5: Example of the wave-like orbitally-related variation in the light curve of V1329 Cyg (top). It is caused by variation in the quantity of the nebular radiation observed at different orbital phases (bottom panels). Magnitudes derived from the IUE spectra agree perfectly with those obtained photometrically (green triangles in the top panel). This result thus demonstrates that the periodic variation in the nebular radiation is responsible for that observed in the light curves.

According to spectroscopic observations an optically thick shell – a false photosphere – is created around the hot active star, which redistributes a significant fraction of its radiation. As the temperature of the false photosphere (around 22000 K, Skopal 2005) is considerably lower than that of the hot star during the quiescence ( $\sim 10^5$  K) its light contribution will be shifted to longer wavelengths according to the Wien's displacement law, and thus make the visual region to be brighter. Usually, the radius of the false photosphere is of a few solar radii, so the cool giant can eclipse it easily for a time of about one tenth of the orbital period (i.e. 2 – 3 months).

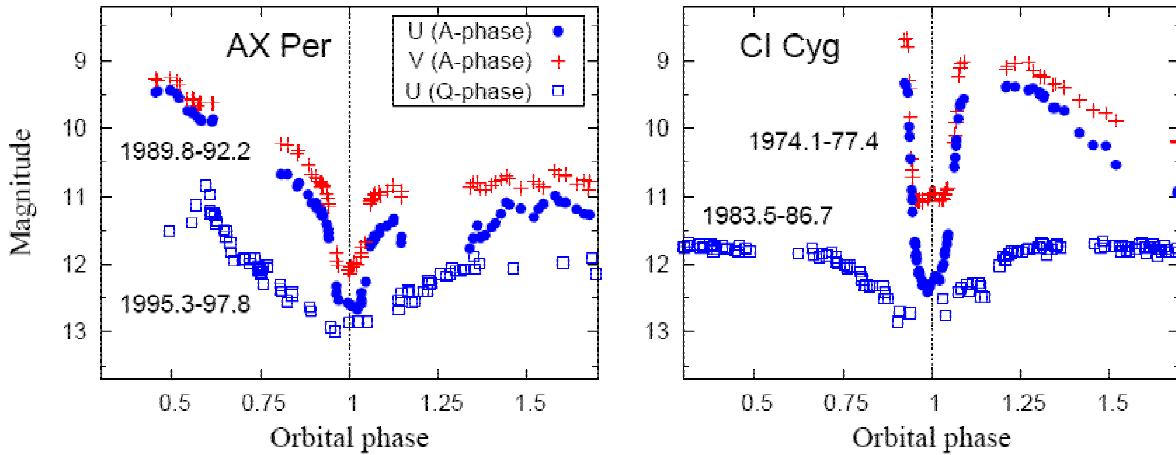


Figure 6: Eclipses and wave variation for eclipsing symbiotic stars AX Per and CI Cyg. During activity the contribution from a warm false photosphere around the hot star is relatively strong in the visual region. As a result narrow minima – eclipses – are observed in the light curve at the inferior conjunction of the giant. The minima are in part filled in with a strong residual light from the HTN nebula, which is not subject to eclipse (Fig. 3 right). During quiescence the radiation from extended nebula dominates the optical region, which causes the minima to be very broad (Fig. 3 left).

The depths of eclipses usually obeys the relation:  $\Delta U > \Delta B > \Delta V$ , because the light from the hot star decreases towards the red part of the spectrum, while that from the giant increases here. However, the resulting eclipse depth and colour indices are modulated by the presence of rather strong nebula in the system, which is not subject to eclipses (right panel of Fig. 3). Thus during the totality the nebula partially fills in the minima and, in combination with the radiation from the giant, produces colour indices that differ significantly from those of a normal red giant.

### 2.3 Apparent changes in the orbital period

This effect is connected with transitions between active and quiescent phases of a symbiotic system. Aside from the significant change of the minima profile during these periods (Sect. 2.2, Fig. 6), a systematic variation in the minima position, i.e. the effect of apparent orbital changes, was revealed (Skopal, 1998).

Here I will demonstrate this effect on the historical light curve of the eclipsing symbiotic system BF Cyg (Fig. 7). First, we determine positions of the observed ('O') minima in its light curve and calculate those ('C') using a reference ephemeris. Then we construct the so-called *O – C* diagram (i.e. the residuals between the observed and calculated timing of the minima). In our example of BF Cyg the *O – C* diagram was constructed using the reference ephemeris given by the primary minima measured in the historical light curve (Skopal, 1998):

$$JD_{\text{Min}} = 2\,411\,268.6 + 757.3(\pm 0.6) \times E, \quad (1)$$

which is identical (within uncertainties) with the spectroscopic ephemeris of Fekel et al. (2001).

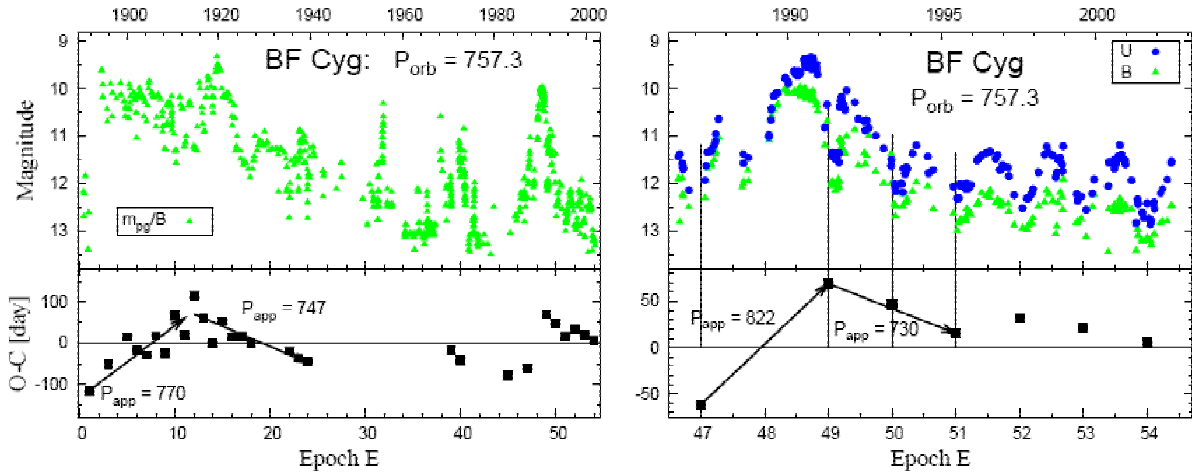


Figure 7: Historical and recent light curves of BF Cyg with the  $O - C$  diagrams. During transition from quiescent to active phases and vice versa, the main source of radiation contributing to the optical continuum changes significantly its location and geometry in the symbiotic system. As a result the observed minima change their profile and position, what we indicate in the  $O - C$  diagram as the apparent orbital changes.

A systematic variation in the  $O - C$  residuals is clearly seen. This behaviour was already noted by Jacchia (1941). The gradual increase of the  $O - C$  values before the 1920 bright stage ( $E = 1$  to 11) corresponds to an apparent period of 770 days, larger than the orbital one, while their subsequent decrease ( $E = 12$  to 24) indicates a shorter period of 747 days. The same type of variability appeared again during the recent, 1989 active phase. Observed changes in both the position and the shape of the minima are illustrated in Figs. 7 and 6. During the transition from the active phase to quiescence ( $A \rightarrow Q$  transitions), a systematic change in the minima positions at  $E = 49$  to 51 corresponded to the apparent period of only 730 days. During the transition from the quiescent to the active phase ( $Q \rightarrow A$  transitions) a significant change in the  $O - C$  values by jump of +130 days was observed. The minima positions at  $E = 47$  and  $E = 49$  indicated an apparent period of 822 days.

### 2.3.1 Principle of apparent orbital changes

During the  $A \rightarrow Q$  transitions the optically thick shell is gradually diluting, which leads to the increase of the hot star temperature and thus the increase of the ionizing photons. As a result the optical continuum declines and changes significantly its nature – from blackbody to nebular radiation. This process causes an *expansion* of the H II zone and thus the change of the minimum profile from the narrow one to the broad wave throughout the orbital cycle. As the nebula is asymmetrical with respect to the binary axis (cf. Skopal 2001) the light minima occur prior to the time of spectroscopic conjunction. This behaviour is also illustrated by Fig. 7. Thus during the  $A \rightarrow Q$  transitions we indicate an apparent period, which is *shorter* than the orbital one.

During  $Q \rightarrow A$  transitions a sudden decrease in the luminosity of the ionizing photons results from rather rapid creation of the false relatively cool photosphere. This implies a disruption of the H II zone. Optical region is then (usually) dominated by the stellar radiation from the pseudophotosphere and a narrow minimum (eclipse) is observed at the inferior conjunction of the giant. In such the case the time difference between the preceding broad minimum ( $\varphi \sim 0.9$ ) and the eclipse ( $\varphi \sim 0$ ) is  $P_{app} \approx P_{orb} + 0.1 \times P_{orb}$ . This apparent change in the period happens suddenly and in the  $O - C$  diagram is indicated by a jump in the residuals. In our illustrative case of BF Cyg (Fig. 7, minima just prior to the 1989 outburst), the timing of the broad minimum at the epoch  $E = 47$  and the following eclipse at  $E = 49$  corresponds to the apparent period  $P_{app} \approx 822$  days. More details about this effect can be found in Skopal (1998).

## 3 Concluding remarks

The presence of physically different sources of radiation in the symbiotic system, diversing extremely in temperatures and also the nature (stellar and nebular component), produce a complex composite spectrum. Its resulting flux thus depends on the wavelength, activity of the star and also the projection of these regions into the line of sight, i.e. on the orbital phase of the binary. Throughout the optical the light contributions from these sources rival each other, which produces the spectrum, whose colour indices differ significantly from those of standard stars. For example, during quiescence the wave-like variation is not a simple sinusoid, but alters its profile from cycle to cycle in both scales – the time and the brightness (e.g. EG And, AG Peg, AX Per, Skopal et al. 2007). During active phases the light curve profiles are very heterogeneous. Eruptions arise unexpectedly with a rapid (e.g. RS Oph and most of AG Dra events) or more frequently with a gradual increase to the maximum within a few months (e.g. recent outbursts of Z And and AG Dra, Skopal et al. 2006, 2007). Also the recurrence time is unpredictable phenomenon. For some objects no active phase has been yet recorded (e.g. SY Mus, RW Hya, EG And). For others, eruptions are scattered in historical light curves irregularly. For example,

during 1994-98 period the AG Dra light curve showed eruptions with a strict recurrence of  $\sim 1$  year (Viotti et al. 2007, Fig. 4 here). Previously, Iijima (1987) suggested that since 1930 AG Dra periodically entered active stages with an interval of about 15 years. However, from the beginning of its historical records of the brightness, in 1890 to about 1927, it was quiet with a first strong outburst indicated around 1932 (Robinson 1969).

In this contribution I have discussed just fundamental variations in the light curves of symbiotic stars, i.e. those that can be explained with the aid of their basic model. However, light curves of symbiotic stars record much larger variety of light changes that are unexpectable and never repeat again. At present they remain far beyond our full understanding. Investigation of interactions between the cool giant and its hot luminous compact companion in a symbiotic binary requires simultaneous, multi-frequency observations from X-rays to radio wavelengths.

This is extremely challenging task, addressed mainly to large ground-based telescopes and those on the boards of satellites. In spite of this, photometric monitoring of symbiotic stars, usually carried out with small telescopes, plays an important role in their research.

### *Acknowledgments*

This work was in part supported by the Slovak Academy of Sciences grant No. 2/7010/7. The author thanks the conference organizers for facilitating his attendance at the meeting.

### **References**

- Corradi, R. L. M., Mikolajewska, J., & Mahoney, T. J. 2003, *Symbiotic Stars Probing Stellar Evolution*, ASP Conf. Ser. 303 (San Francisco: ASP)
- Fekel, F. C., Hinkle, K. H., Joyce, R. R., Skrutskie, M. F. 2001, *AJ* 121, 2219
- Iijima, T., Vittone, A., Chochol, D. 1987, *A&A*, 178, 203
- Jacchia, L. 1941, *Bull. Harv. Coll. Obs.* No. 915
- Merrill, P.W. 1950, *ApJ*, 111, 484
- Nussbaumer, H., & Vogel, M. 1987, *A&A*, 182, 51
- Robinson, L. 1969, *Peremenye zvezdy*, 16, 507
- Seaquist, E. R., Taylor, A. R., & Button, S. 1984, *ApJ*, 284, 202
- Skopal, A. 1998, *A&A* 338, 599
- Skopal, A. 2001, *A&A*, 366, 157
- Skopal, A. 2005, *A&A*, 440, 995
- Skopal, A., Vittone, A. A., Errico, L., et al. 2006, *A&A*, 453, 279
- Skopal, A., Vaňko, M., Pribulla, T. et al. 2007, *Astron. Nachrichten*, 328, 909 [arXiv:0708.1578]
- Viotti, R. F., Friedjung, M., Gonzalez-Riestra, R., Iijima, T., Montagni, F., Rossi, C. 2007, *Baltic Astronomy*, 16, 20

## On the Possibility of the Amateur Detection of GRBs by Ionospheric Response

Rudolf Slošiar<sup>1</sup> and René Hudec<sup>2,3</sup>

- 1) Astronomical Union of Amateur Astronomers, Bojnice, Slovak Republic
- 2) Astronomical Institute, Academy of Sciences of the Czech Republic, CZ 251 65 Ondřejov, Czech Republic
- 3) Czech Technical University, Faculty of Electrical Engineering, Prague

### Abstract

We report on the amateur independent and indirect detection of GRBs by their ionospheric response (SID-Sudden Ionospheric Disturbance) observed at VLF (Very Low Frequency). Although few such detections have been already reported in the past, the capability of such alternative and indirect investigations of GRBs still remains to be investigated in more details. We present and discuss an example of such VLF/SID detection of the GRB 060124A.

### CZ Abstrakt

Referujeme o amatérské nezávislé a nepřímé detekci kosmických gama záblesků (GRB) na základě jejich ionosférické odezvy pozorované na velmi nízkých (VLF) frekvencích. Příkladem je detekce GRB 060124A, o níž pojednáváme. Jen několik takových detekcí je známo v minulosti a vědecký význam, možnosti i limitace této metody bude ještě třeba podrobněji analyzovat.

### Introduction

The amateur and inexpensive instrumentation allows the alternative detections of Gamma Ray Bursts (GRBs). Only few such detections were reported before. Previous reported VHL detections of GRBs were as follows. (i) SGR1806: detection of a Sudden Ionospheric Disturbance [1], (ii) GRB030329 observed as a Sudden Ionospheric Disturbance (SID) [2]. Although there were numerous efforts to detect GRBs by VHL and despite the fact that the necessary instrumentation is inexpensive, this field still remains little exploited. We note that the direct physical meaning and importance of such detections to GRB and/or ionosphere science is difficult to evaluate at the moment, but are expected to evolve in more details later.

### Ionospheric detections

This type of GRB detections is very closely related to ionosphere science and behavior. The solar particle stream, solar wind, shapes and controls the Earth's magnetic envelope—the magnetosphere—and increases heat in the aurora zones. But not all ionospheric variability is caused by solar or geomagnetic disturbances. The ionosphere is not a constant 'mirror in the sky'. The E layer (100-200 km above ground) and the F1 layer (170-200 km) usually behave in regular, solar-controlled way, but the F2 layer (250-350 km) does not. It is the F2 layer, which has the greatest density of free electrons, and is potentially the most effective reflector of radio waves ([3]). The ionospheric D layer plays in the GRB detections an important role, as the detection of X-ray and gamma-ray triggers is based on the measurement (monitoring) of reflected radio waves from this layer. The ionospheric D layer is not transparent for radio VLF waves (frequencies 3kHz to 30 kHz) and behaves like a mirror. If the transmitter is at large distance (800 to 2000 km) then the radio waves are guided like in a waveguide consisting of the D layer and the earth surface. Any change in the quality of this waveguide results then in the signal change in the SID monitor. The change can be positive but in some cases such as the sudden phase anomaly also negative.

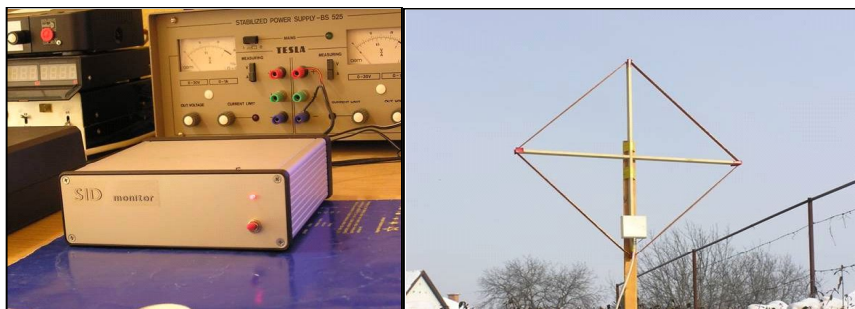


FIGURE 1. Instrumentation used for the indirect detection of GRB 060124A: the receiver (left) and a loop antenna (right). The antenna size is 75 x 75 cm.

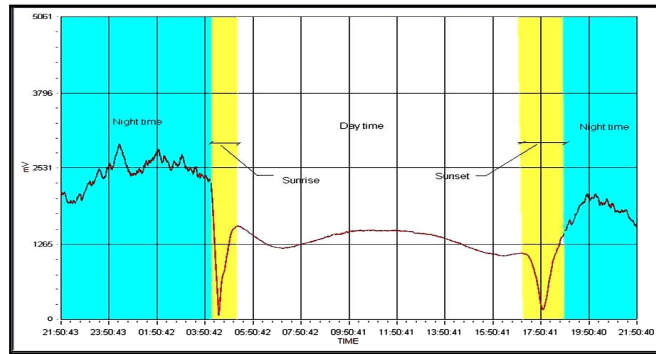


FIGURE 2. This picture shows the typical behaviour of the ionosphere during one day. Note the different behavior at night with absence of the D layer.

**Discussion**

The conditions to detect GRB with SID monitor in VLF can be briefly listed as follows.

- (i) The presence of the D layer of the ionosphere,
- (ii) The suitable combination of the GRB position (RA, DEC) and
- (iii) Time and hence direction and angle of the incoming gamma-ray radiation in relation to the D layer, and
- (iv) The fluence and duration of the GRB.

The detection statistics can be briefly discussed as follows. The recent detection rate of GRBs is about 130 in a year. For one observing station, the number of GRBs occurring during the presence of a D layer and in the field of view is about 20. This is ideal number,

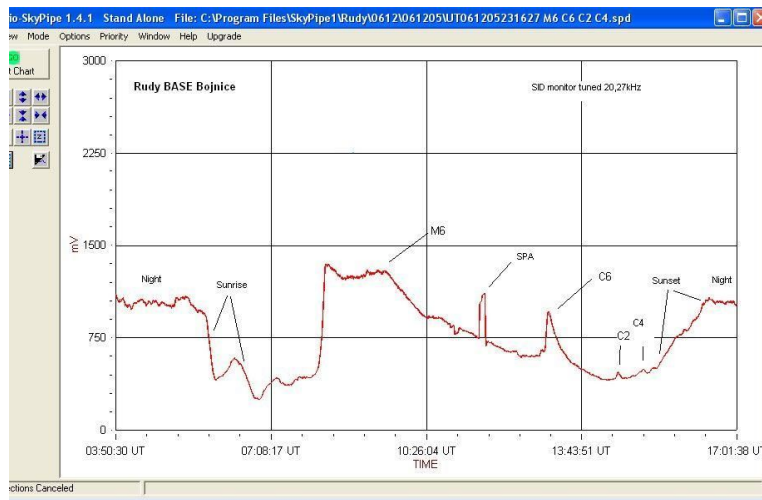


FIGURE 3. Demonstration of the possibility and sensitivity of the method. Four Solar Flares (SF) are visible with intensities M6, C6, C2, C4, exactly corresponding to the measurements by the GOES satellite. The peak related to the SF C4 occurs around 15:03UT, which is nearly the detection time of GRB060124A, on Jan 24, 2006, confirming that even at the time of the decay of the D ionospheric layer reliable measurements are feasible.

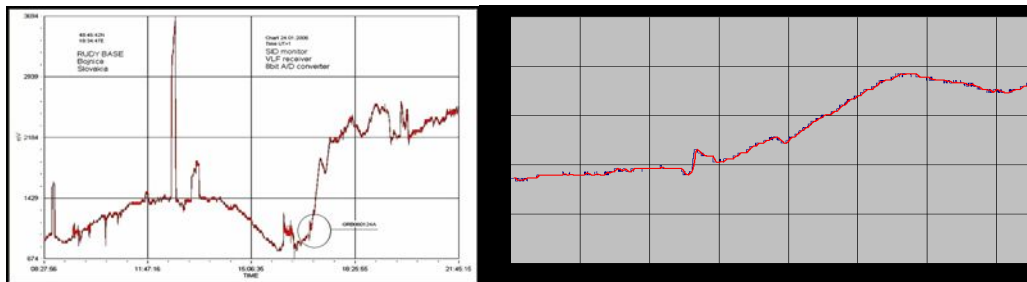


FIGURE 4. The detection of GRB 060124A

the real one is less than 10 due to occasional non-availability of transmitters and other technical and observational issues.

## Conclusions

The independent and indirect detection of GRBs by their ionospheric response (SID, Sudden Ionospheric Disturbance) observed at VLF (Very Low Frequency) is feasible. We present and discuss an example of such VLF/SID detection of the GRB 060124A. Although few such detections have been already reported in the past, the capability of such alternative and indirect investigations of GRBs, as well as the possible contribution to analyses of GRBs still remains to be investigated in more details.

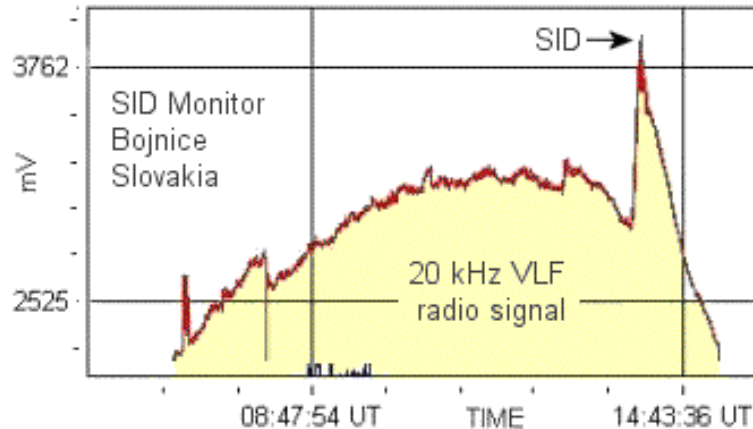


FIGURE 5. This picture shows (for comparison) the SID from C2-class solar flare (represented by the peak at around 14:40 UT) erupted from sunspot 958 .

## Acknowledgements

We acknowledge grant GA CR 205/08/1207. Some parts of the study are related to project PECS 98023.

## REFERENCES

1. P. Campbell et al., GCN, 2932, (2003).
2. P. W. Schnoor et al., GCN, 2176, (2003).
3. Rishbeth, H.; Müller-Wodarg, I. C. F.; Zou, L.; Fuller-Rowell, T. J.; Millward, G. H.; Moffett, R. J.; Idenden, D. W.; Aylward, A. D., Annales Geophysicae, 18, Issue 8, 945-956, (2000).

# Optical Photometry of Be/X-ray Binary V 615 Cas = LS I +61°303

LUBOŠ BRÁT

ALTAN.Observatory, Velká Úpa 193, Pec pod Sněžkou, [brat@pod.snezkou.cz](mailto:brat@pod.snezkou.cz)

**Abstract:** Two years of intensive CCD+R photometry of V 615 Cas = LS I +61°303 at ALTAN.Observatory are presented. New optical observation fits well to known orbital period modulation  $P = 26,496$ d. The usability of optical observation in research of currently not-understant behavior of the object is discussed.

**CZ Abstrakt:** Jsou představeny výsledky dvou let intenzivní fotometrické kampaně v R filtru této supermasivní dvojhvězdy vyzařující v rentgenovém oboru, známé jako V 615 Cas = LS I +61°303. Optická pozorování potvrzují orbitální modulaci s periodou  $P = 26,496$  dní. Diskutován je přínos pozorování tohoto zdroje vysokoenergetického záření v optickém oboru při objasnění dosud neznámých příčin optické proměnnosti v závislosti na orbitální fázi.

## INTRODUCTION

V 615 Cas = LS I +61°303 is well studied object – it is issued 16-17 papers per year. Total 326 papers shows ADS / Simbad bibliography. V615 Cas was discovered as highly variable radio source (1-10 GHz) and gamma-ray source (0,1 – 1 GeV) by satellite COS-B. Discovered / observed as variable x-ray source (2 – 10 keV) by satellites Einstein, ROSAT, ASCA, RXTE, BeppoSAX, XMM-Newton, INTEGRAL, Chandra. Following this, the object was found to be a variable star (named V615 Cas) in optical and infrared. In 2005, found as source of high energy TeV gamma-rays by 17m MAGIC telescope. Behavior in every spectrum band confirms clearly modulation with orbital period 26,496 days. And what is important – in each spectral band the outburst / emission / maximum occurs in different orbital phase.

These findings leads us to describe V615 Cas = LS I +61°303 as High Mass X-Ray Binary, subclass Be / X-ray binary with transient nature of x-ray, radio, gamma emmissions. The primary component is highly rotating B0Ve star,  $M = 12M_{\odot}$  with circumstellar depression disc. The secondary – compact component is probably neutron star or a black hole with  $M = 2.5 M_{\odot}$ . Bipolar radio jets found by Massi et al. (2004) in distance 10 – 50 mas arrange this object among Galactic micro-quasars. Distance of the object is about 2.3 kpc far from Earth.

## Be/X-RAY BINARIES VERSUS OTHER MASSIVE X-RAY BINARIES

V615 Cas belongs to subclass of massive x-ray binaries Be/X-ray binary. These objects are transient x-ray / gamma-ray sources with primary component hot B star on main sequence with circumstellar matter – BeV spectral type. Secondary component is compact star – neutron star or black hole. High energy emissions are produced by interaction between circumstellar matter around primary star and compact object. This usually happens when orbit is close or in periastron phase in case of excentric orbit. Known Be/X-ray binaries have orbital periods between  $P > 17$  days and  $P < 250$  days.

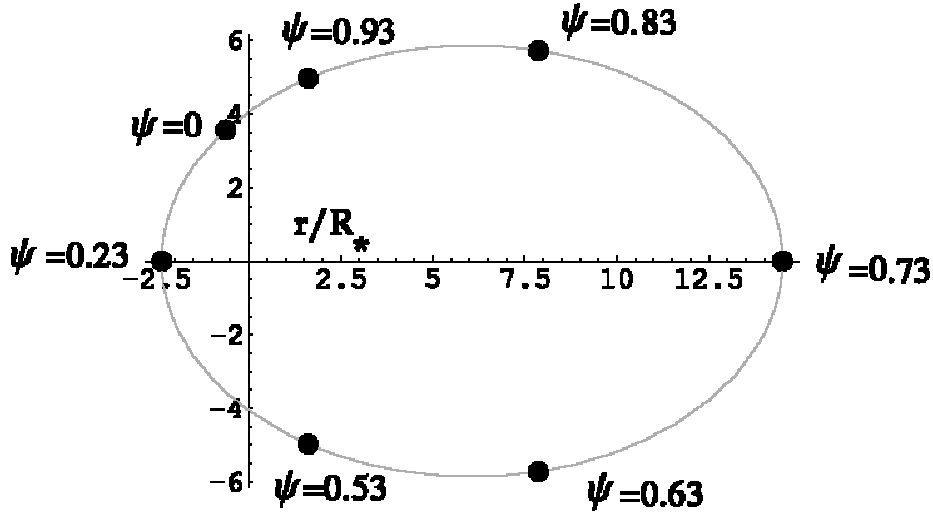
On the other hand, other HMXRBs (High Mass X-Ray Binaries), which irregular x-ray / gamma-ray emmissions are objects with highly evolved primary component (giants, supergiants) and compact secondary component on very close orbit ( $P < 10$  days). There are continuous variable HE emissions, which correspond with interaction between primary and secondary (compact) component through lagrange L1 point (mass transfer).

	<i>Be/X-ray binaries</i>	<b>Other masive X-ray binaries</b>
Primary component	Be V	O-Be I
Secondary component	NS	NS / BH
Orbital Excentricity	0,3 – 0,9	any
$P_{\text{orb}}$	17 – 250 d	Less than 10 d
Fill-factor	Less than 1	1 and more
Mass transfer	Circumstellar disc, star wind	Transfer through Lagrange point L1
X-ray emmission	Transient nature - <b>type I</b> repeating outburst every $P_{\text{orb}}$ , could dissapear when circ. disc is smaller, stronger outburst at objects with smaller $P_{\text{orb}}$ - <b>type II</b> longer duration, irregular, relating with variability of	Strong permanent emissions

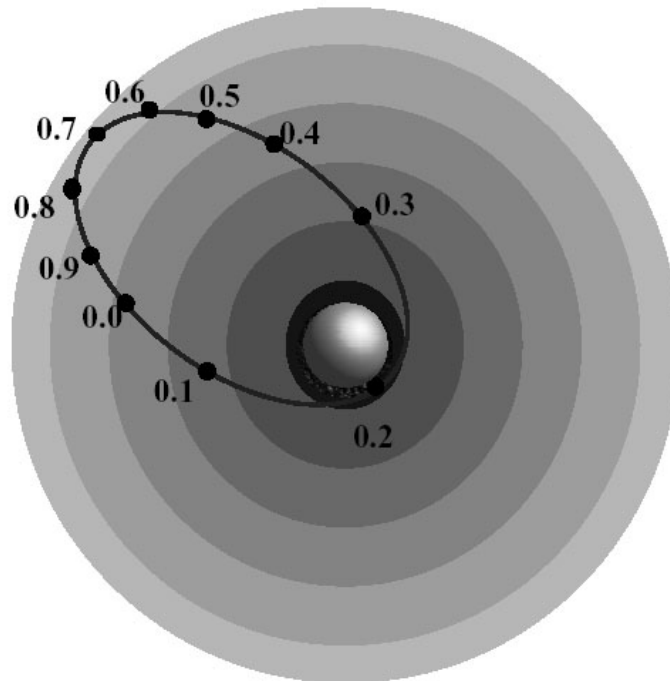
	circumstellar disc around primary	
Energy bands	15 keV and more, hard X-ray	15 keV and more, hard X-ray
Notes	X-ray transients	massive X-ray systems with evolved primary component

Table adopted from Ziolkowski (2002)

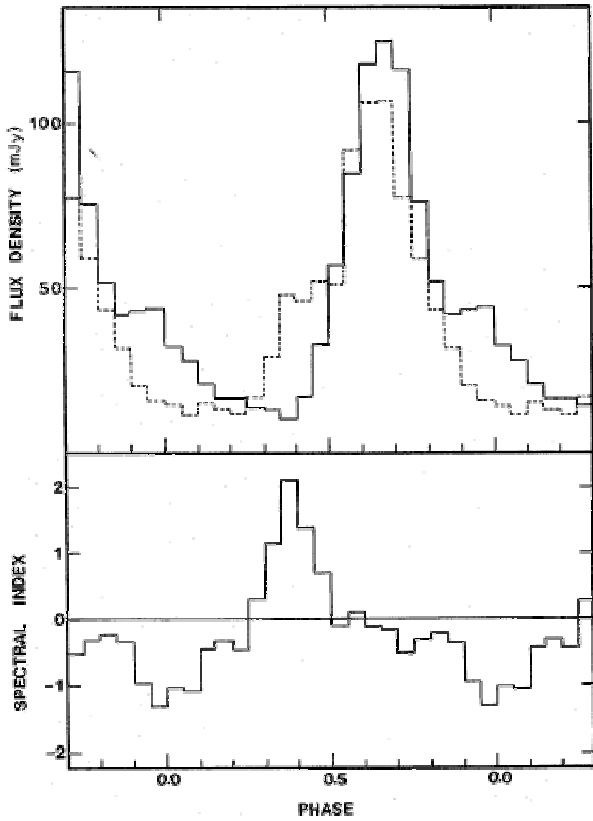
V615 CAS = LS I +61°303 – A Be/X-RAY BINARY



Picture 1: Orbit of LS I +61°303 drawn to scale, illustrating the geometry of the system. Periastron passage occurs at phase 0,23 (elements found from radio observations). (Romero et al. 2005)



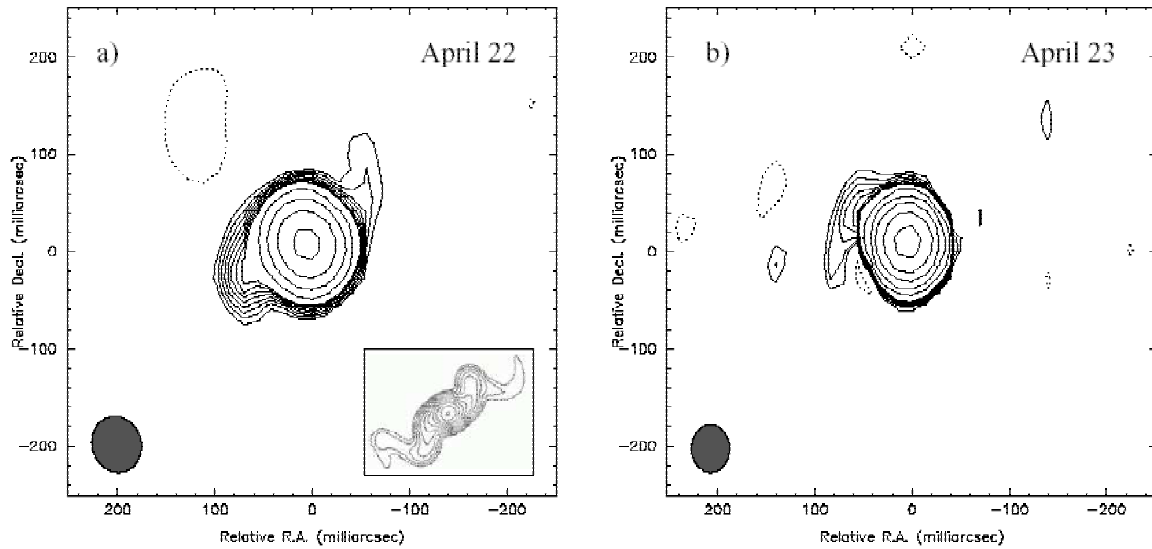
Picture 2: Sketch of the binary system LS I +61 303: Orbital phase of compact object travelling through the envelope around Be companion. Dark color = most dense interstellar matter, light gray = sparse matter and absorption of synchrotron radiation is the smallest => radio outburst. (Massi 2004b)



**Picture 3:** Mean radio light curves at 5GHz (solid line) and 10.5GHz (dashed line). Also shown (bottom) is the two frequency spectral index derived from mean curves. Radio outburst occurs around phase 0.7, when system is in apastron. (Gregory and Taylor 1982)

**JET DETECTION**

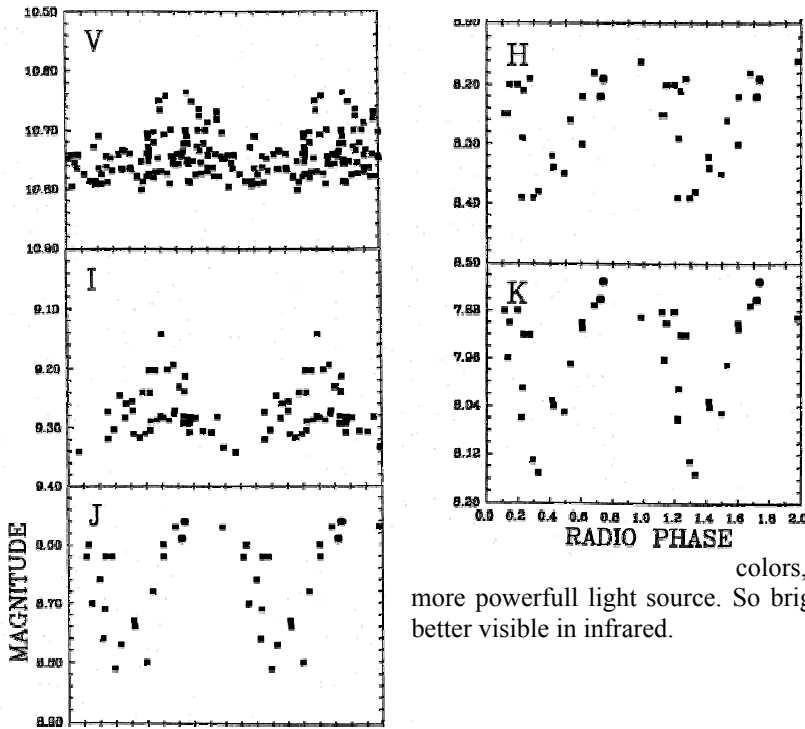
Massi et al. (2004) has reported discovery of precessing radio jets around the source at 5 GHz. MERLIN image from 22<sup>nd</sup> April 2001 and 23<sup>rd</sup> April 2001 clearly shows presence of S-shape morphology known from precessing jets – e.g from SS 433. The situation is shown at picture 4.



**Picture 4 :** a) MERLIN image of LS I +61 303 at 5 GHz obtained on 2001 Apr 22. b) The same picture from 2001 Apr 23. S-shape morphology strongly recalls the precessing jet of SS 433, whose simulated emission is given in small box. (Massi 2004b)

**INFRARED OBSERVATION**

Paredes et al. (1994) has published IJHK observation, that shows variations corresponding to orbital motion. Phased light curves shows wave with increasing amplitude from optical to far infrared band. Amplitude is about 0,2 – 0,3 magnitude in IR.

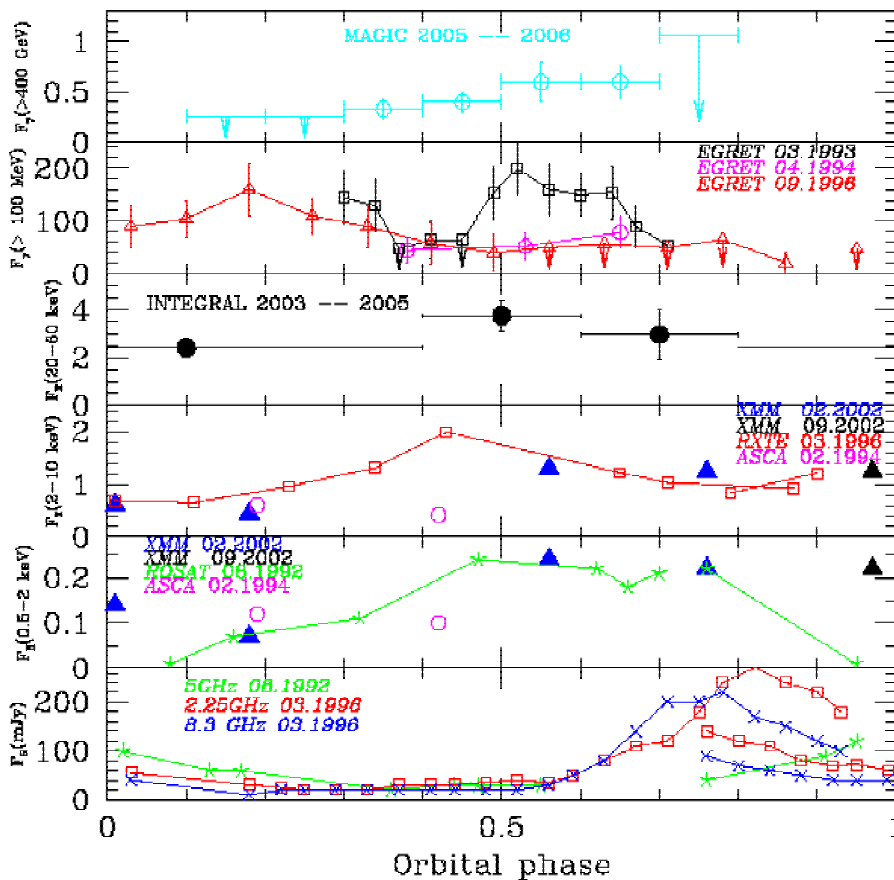


**Picture 5:** Optical and infrared observations (bands VIJHK) folded on the 26,496 d radio period. Phase zero has been set at JD 2443366.775 (Paredes et al. 1994).

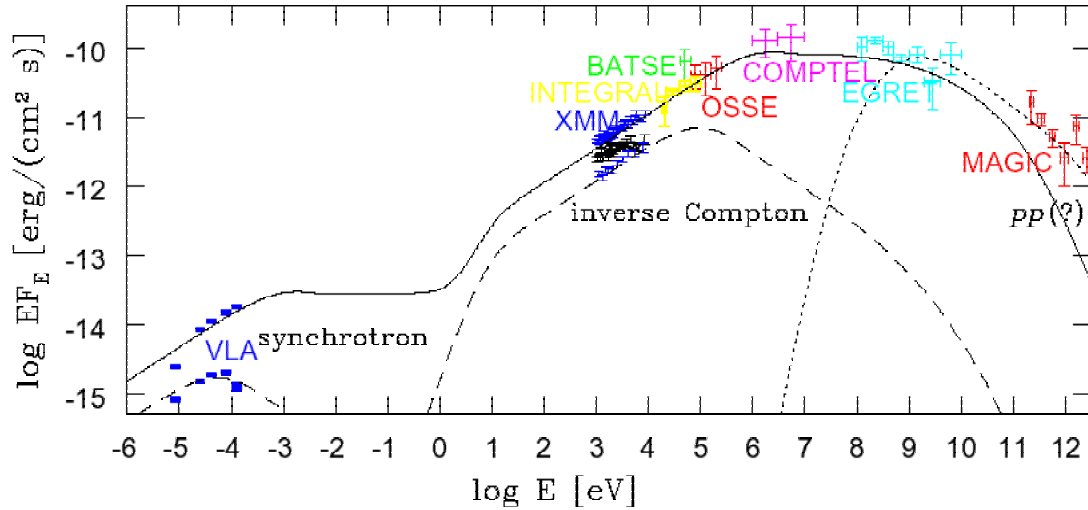
Amplitude increases with rising wavelength (from V up to K). We can suppose, that such optical behavior corresponds with situation, when optical variations comes up from cooler circumstellar envelope. In blue spectral band, there is dominant light source a hot B component, while in red and infrared

colors, cooler circumstellar matter become more powerfull light source. So brightness variations from an envelope are better visible in infrared.

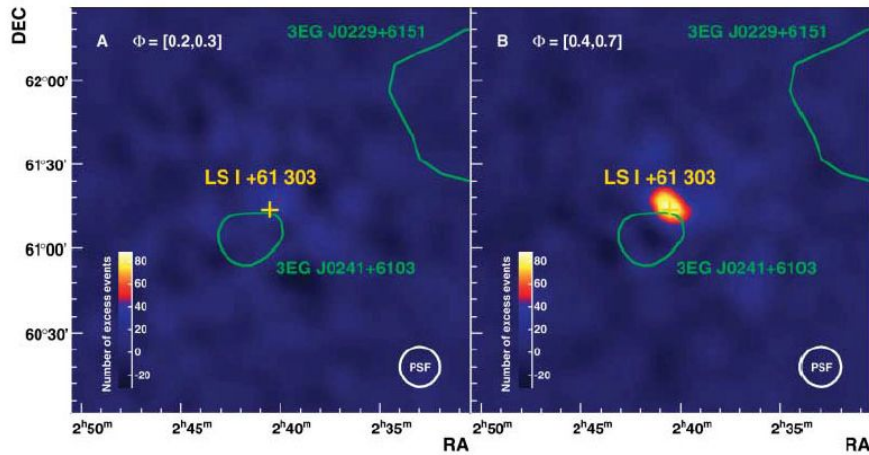
**X-RAY AND GAMMA-RAY OBSERVATION**



**Picture 6:** Comparison between the TeV (top), GeV gamma-ray orbital lightcurves with the hard X-ray (20-60 keV), X-ray (2-10 keV), soft X-ray (0,5 - 2 keV) and radio (bottom) orbital lightcurves. (Chernyakova et al. 2006)



**Picture 7:** Broad band spectrum. The solid (dashed) line shows the model fit of collected data within the synchrotron-invers Compton model for the high (low) flux state of the source. The dotted line shows possible contribution from the proton-proton interactions. (Chernyakova et al. 2006)



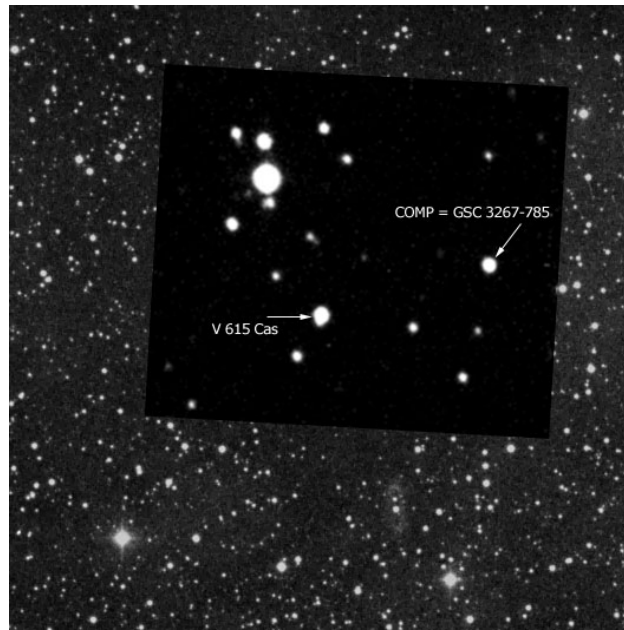
**Picture 8:** Smoothed maps of gamma-ray excess events above 400 GeV around V615 Cas. Left: 15,5 hours long MAGIC observation around phases 0,2 – 0,3 (in periastron). Right: 10,7 hours long MAGIC observation at orbital phase between 0,4 – 0,7. Significant gamma-ray emission was recorded in the second case. (Albert et al, 2007)

## NEW OPTICAL OBSERVATION

I have obtained 260 CCD+R<sub>C</sub> observations in period from October 2006 till November 2007 at my private ALTAN.Observatory in Giant mountains, Czech republic. Equipment used was Vixen catadioptric cassegrain telescope, 0.2 m aperture, 2m focal length attached with CCD camera SBIG ST-8.

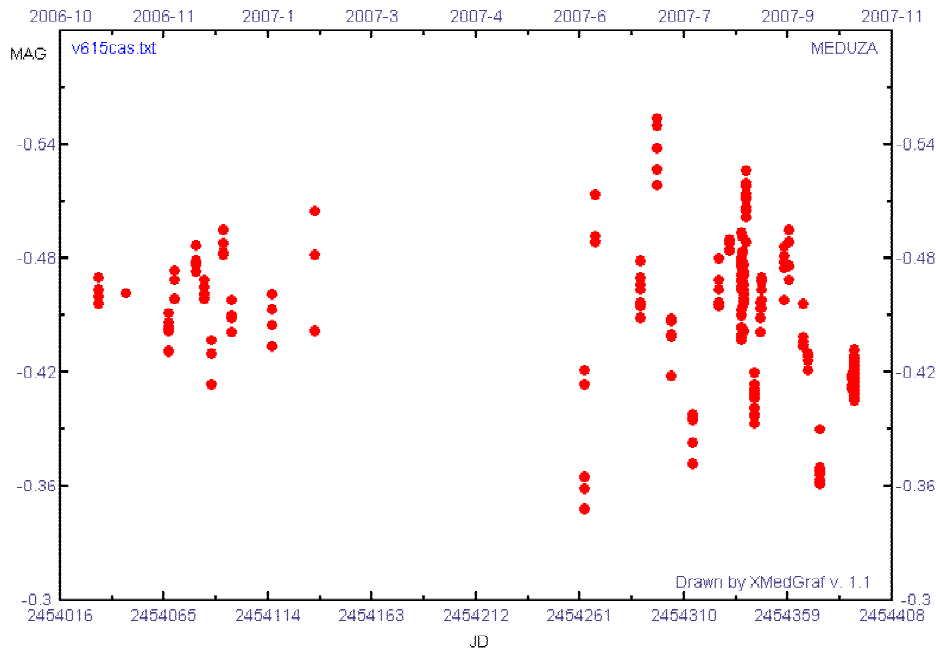
**Picture 9:** ALTAN.Observatory in Giant mountains (in czech “Krkonose”). There is roll-off roof lodge with the robotic telescope in front, control room in background on the picture.



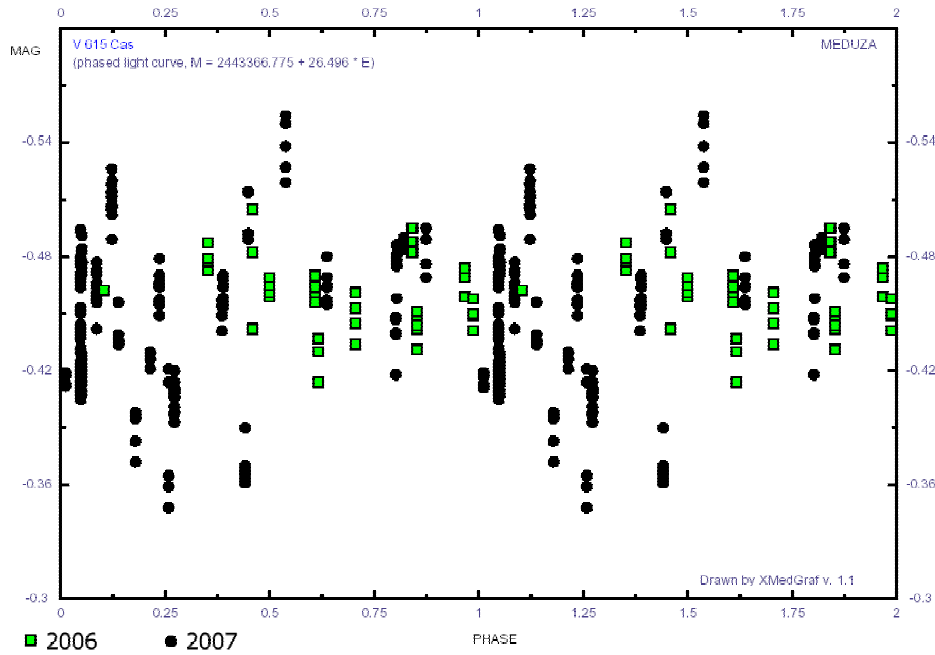


**Picture 10:** DSS image of close vicinity of V615 Cas with typical photometri CCD frame in front of the picture. As comparison star was used nearby GSC 3267-785 in all cases.

Picture 11 shows all results of two observing seasons. In July 2007, light curve began to show significantly higher (2 times) amplitude than in previous season (from 10-2006 till 2-2007). So more intensive observing has started. At end of year 2007, I have constructed phase light curve according to orbital elements given in literature  $M = 2443366.775 + 26.496 * E$  (Romero et al. 2005).

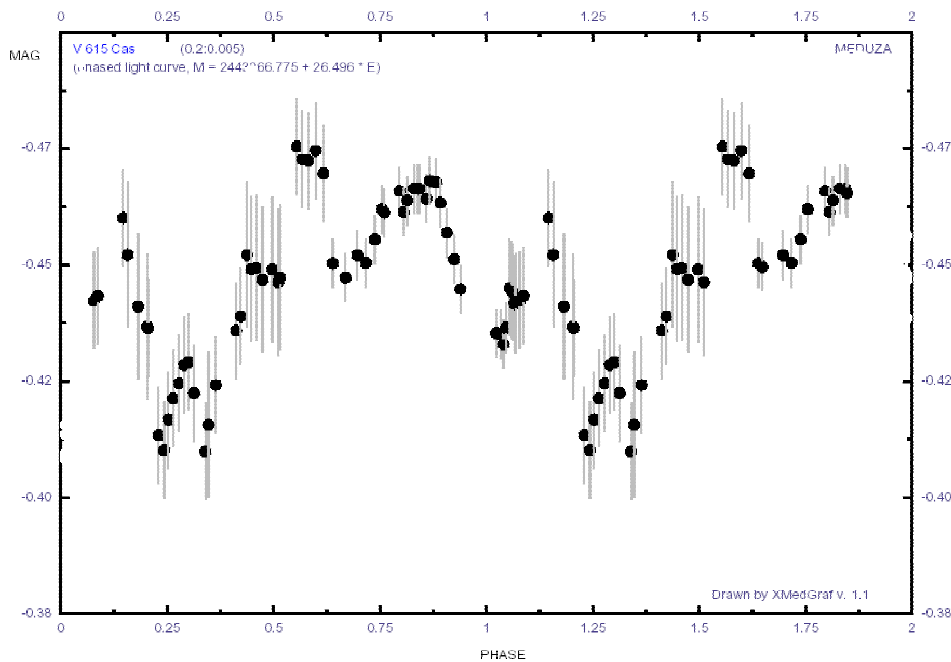


**Picture 11:** Two year light curve of V 615 Cas in  $R_C$  obtained by author. Comparison star's magnitude value was set to zero.



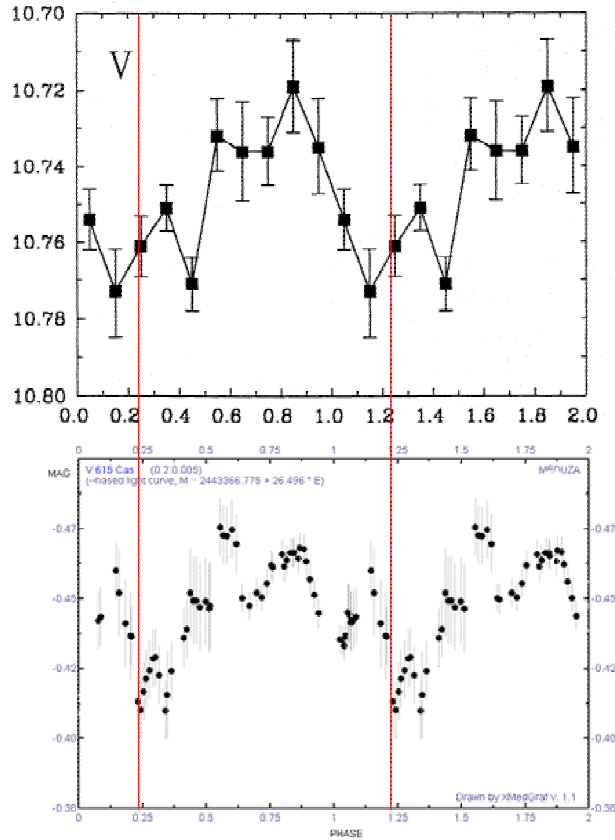
**Picture 12:** Phased light curve with highlighted observations made in 2006 (green squares) and in 2007 (black points). Orbital elements used:  $M = 2443366.775 + 26.496 * E$ .

The phase light curve shows picture 12. To solve the question, if amplitude of optical variability has increases in 2007, the season 2006 data was plotted using different symbols. It is clearly seen, that data obtained in 2006 miss the main brightness minimum and maximum and that's why amplitude of light curve in 2006 was smaller than in year 2007, when maximum and minimum were caught out.

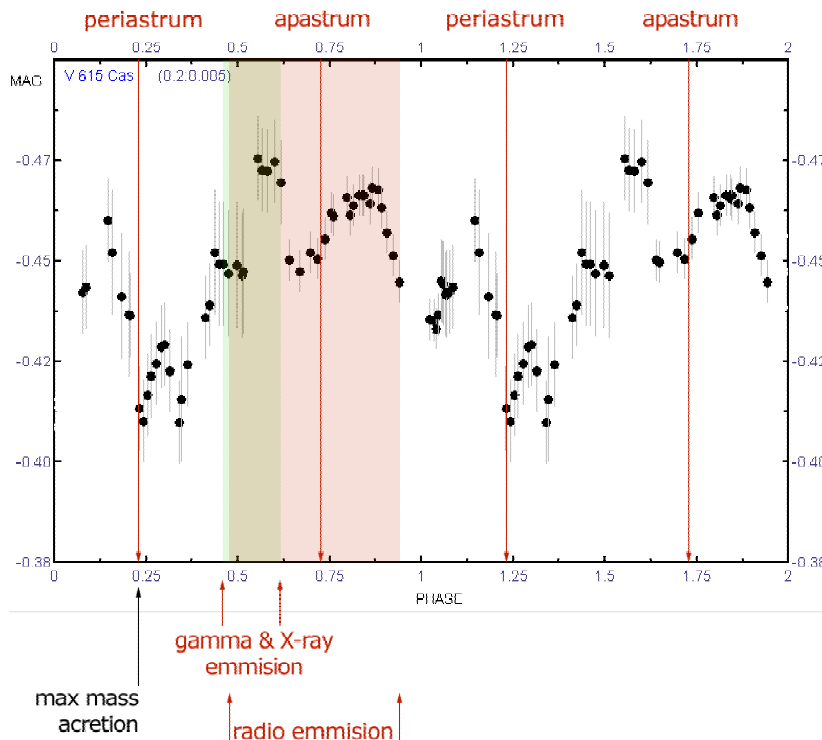


**Picture 13:** Phased light curve smoothed using running averages procedure. Width of averaged section 0,2 (of orbital phase), step 0.005.

To remove data scatter in phase light curve, algorithm of running averages was applied. The result shows picture 13. There is minimum around phase 0,25 and maximum between phases 0,5 and 0,9. Amplitude of phase light curve is only 0,05 mag. In such small light variations, applying of running averages procedure could produce non trustfulness result. So I have compared the light curve with data published by Paredes et al., 1994. Picture 14 shows both phased light curves in the same scale. Periastrum is marked by red line at phase 0,23. The amplitude and shape of light curve is very similar.



**Picture 14:** Comparing of phased light curve published by Paredes et al. 1994 obtained using 1,5m telescope with photoelectric photometer in V band (top) and authors observation obtained using 0,2m RL with CCD camera SBIG ST-8 in R band (bottom).



**Picture 15:** Phased light curve in R band with highlighted periastrum / apastrum points (red lines) and phases, when gamma and X-ray emissions are observed. Maximum of radio emissions is highlighted too.

There is double peaked maximum visible in the light curve between phases 0.5 and 0.9. Using data from Chernyakova et al. 2006 (see picture 6) and Albert et al, 2007 (see picture 8) I have compared new optical light curve in R with phase “light curve” in gamma, X-rays and radio observation.

Most high energy emissions became between phases 0,5 and 0,7, while radio signal is strongest between phases 0,5 and 0,9. As shows picture 15, the connection between optical and high energy and radio behaviour is evident. First optical maximum becomes when high energy emissions appears. The second maximum peak become when radio emission is the strongest.

### **DISCUSSION AND CONCLUSION**

V615 Cas = LS I +61°303 is unique astrophysical laboratory, where we can study both very high energy gamma ray and X-ray exhibitions, optical variability and radio outbursts. This happens in a very short time period – orbital period – 26,5 days.

Spinning relativistic jets were directly observed at 5 GHz using MERLIN radio telescope, so the object was classified as Galactic microquasar.

New optical light curve in R band obtained by author is presented. Even the amplitude is only 0.05 mag, phased light curve confirms the regular light changes connected with orbital period. Minimum of brightness becomes in phase 0.25, which corresponds to periastron phase at 0.23, while flat, double peaked maximum appears between phases 0.5 and 0.9.

First maximum peak around phase 0.6 is connected with high energy emission and the second peak around phase 0.8 – 0.9 corresponds to radio outburst.

As found by Paredes et al. (1994), the amplitude of optical variability increases with increasing wavelength. Very small amplitude in V band, higher amplitude in red and infrared colors. This optical behaviour corresponds with situation, when optical variability comes from cool, circumstellar matter surroundings the binary system. In blue color, there is dominant light source primary component BeV, which does not show any light variations. On the other hand, in red and infrared spectral bands, primary component is fainter and cooler circumstellar matter is more dominant light source. So amplitude is higher in IR.

Adopting this theory, we can identify the origin of optical variations as cooler – outer parts of accretion disc around secondary component - neutron star. While travelling around the primary on excentric orbit, neutron star with accretion disc is hidden in inner – dense parts of circumstellar envelope in periastrum and objects displays minimum of brightness. On the other hand, in apostrum, the accretion disc is well visible and system displays maximum of brightness.

Narrow optical maximum around phase 0.6 connected with HE emissions can be described as accretion disc instability when matter obtained in periastrum is transported to neutron star.

Optical observation, especially multicolor BVRI data, can contribute significantly to understanding of processes in V615 Cas system. Even more than 300 papers were published about the system, less than 10% is concerning of optical behaviour. Optical observation with high time-resolution, which could document possible cycle – to – cycle differences is completely missing. It is strongly encouraged to make very intensive multicolor observation, which helps us to resolve some questions about this unique and interesting binary object.

### **REFERENCES**

- Gregory, P.C., & Taylor, A.R. 1982, *Astrophysical Journal*, Part 1, vol. 255, Apr. 1, 1982, p. 210-216  
 Bosch-Ramon, V. & col., 2006, *A&A* 459, 25  
 Gregory, P.C., & Taylor, A.R. 1978, *Nature*, 272, 70  
 Hermsen, W., Swanenburg, B.N., & Bignami, G.F., et al. 1977, *Nature*, 269, 494  
 Massi, M., Ribó, M., Paredes, J. M., Garrington, S. T., Peracaula, M., & Martí, J. 2004a, *A&A*, 414, L1  
 Paredes, J.M. et al., 1994, *Astronomy and Astrophysics* 288, 519-528, 1994 *A&A*...288..519P  
 Paredes, J.M. et al., 2007, *The Astrophysical Journal*, 664: L39–L42, 2007 July 20  
 J. Albert, et al., 2006, *Science* 312, 1771  
 ZIOLKOWSKI J., 2002, *Mem. Soc. Astron. Ital.*, 73, 1038-1038, 2002 *MmSAI*..73.1038Z  
 Zamanov, R.K., et al., 2007, *IBVS* 5776

## Recommended tips for variable stars observers

PETR ZASCHE

The Astronomical Institute of Charles University in Prague, Czech Republic,  
[zasche@sirrah.troja.mff.cuni.cz](mailto:zasche@sirrah.troja.mff.cuni.cz)

**Abstract:** The minimum light observations of eclipsing binaries could be very useful, especially in one small group of eclipsing binaries, which are also the members of the astrometric doubles. With the combined analysis one is even able to find the parallax to this system by analyzing the times of minima behavior.

The observations of the eclipsing binaries and their times of minimum light could provide us an unique insight into the basic physical parameters of stars. The eclipsing binaries (hereafter EBs) could be also used for studying the physical parameters of their orbits and also for discovering the additional component(s) in these systems.

The combined analysis of astrometry together with times of minima and the possible explanation of the long-term period changes due to the light-time effect (hereafter LITE) was introduced in Zasche & Wolf (2007). The method presented in this paper could be used only on the basis of the assumption that the third body detectable via LITE is the same as detected via astrometry. From this presumption, there are some limitations of the method, but generally it could be used in a few dozens of systems. Some of these systems were presented in Chambliss (1992).

Such systems are of big importance, because the presented method could be potentially used for an independent derivation of their distance. Generally, such a combined approach is very powerful, especially in upcoming astrometric and photometric space missions.

The main problem is the data non-availability. In the most of the systems only very small part of the orbit is covered. In some of the systems there is satisfactorily covered the orbit in astrometry, while the LITE orbit is only poorly covered (see the case HT Vir in Zasche & Wolf). On the other hand there are the systems, where the orbit in LITE is sufficiently covered by the data, but the astrometry is only very poor (for example V505 Sgr). The former cases could be very useful to observe photometrically also by amateur astronomers.

The catalogue of the potential systems for the variable stars observers was carried out and from this set of binaries there were selected a few for the recommended observation (see Table 1). The most important systems for the observation are the following:

- V348 And: The star supposed to be an eclipsing variable. The minima were observed by the Hipparcos satellite, but since then no other confirmation of the eclipses and of the period was carried out. The period is about 5.5 days and the depth of the minima about 0.15 mag.
- V773 Cas: The star was also observed by the Hipparcos satellite. These measurements indicate the orbital period of the eclipsing pair of about 1.3 days, but with the depth of minima about 0.8 mag.
- V592 Per: The  $\gamma$  Lyrae star with 3 times of minima found in the literature and one minimum recently measured in 2007. The depth of minima (both primary and secondary) is about 0.3 mag, it is easily observable.
- V1031 Ori: The star with a few times of minima, which is really desperately needed to be observed. The predicted LITE variation is only about 92 years, while the interval covered by the times of minima is about 30 years. The orbital period is about 3.4 days, while the depth of minima is about 0.4 mag.
- DN UMa: The eclipsing binary with the orbital period of about 1.73 days, the depth of both minima about 0.1 mag. The astrometric orbit was computed with the period of about 137 years, but the times of minima covers about 30 years.
- V819 Her: The system was precisely analyzed in Muterspaugh et al. (2006) on the basis of the astrometry and radial velocities, but the combined solution using the times of minima plus astrometry was not used. Due to its relatively short third-body period it could be also a suitable system for the combined analysis. Its orbital period is about 2.2 days and the depth of the primary minimum is about 0.1 mag, while the secondary about 0.05 mag.
- V2388 Oph: The very interesting EB with the short orbital period of the eclipsing pair, but also with the short period of the third body. This body is detectable astrometrically, but it could not be detected via the LITE variation in times of minima. This is only due to a small data set, and the third body hypothesis could be confirmed by observing the star at least few times a year.
- V2083 Cyg: This Algol-type EB has its apparent brightness about 6.88 mag in V filter and orbital period about 1.9 days. The depth of both minima is about 0.3 mag. There are only the times of minima measured by the Hipparcos satellite. The astrometry covers about 70° during the last century, and the analysis resulting in an orbit with period about 372 yr.

*Table 1: The table with recommended systems to be observed by amateur astronomers. All of them has the astrometric orbits.  $P$  denotes the period of the eclipsing pair,  $p_3$  denotes the period of the astrometric (and supposed also the LITE) orbit, while  $N$  and  $M$  denote the number of times of minima and astrometric measurements, respectively. "Last Meas." indicates the year of the most recent time of minimum observation.*

HD	Star Designation	Spectrum	V [mag]	P [days]	$p_3$ [years]	N Min.	M Astr.	Last. Meas.
1082	V348 And	B9V	6.76	5.54	138	1	61	1991
10543	V773 Cas	A3V	6.21	1.29	304	1	79	1991
29911	V592 Per	F2	8.37	0.72	117	3	18	2007
38735	V1031 Ori	A4V	6.06	3.41	92	9	20	2005
—	AC UMa	A2	10.3	6.85	$\approx 1200$	77	10	2006
103483	DN UMa	A3Vn	6.54	1.73	136.5	13	34	2007
—	ET Boo	F8	9.09	0.65	113	26	20	2007
157482	V819 Her	F9Vn	5.57	2.23	5.5	90	34	1992
163151	V2388 Oph	F5Vn	6.26	0.80	9.0	23	47	2007
184242	V2083 Cyg	A3	6.88	1.87	372	1	58	1991

#### References:

- Chambliss, C.R., 1992, PASP, 104, 663, [1992PASP..104..663C](#)  
 Muterspaugh, M.W. et al., 2006, A&A, 446, 723, [2006A&A...446..723M](#)  
 Zasche, P., Wolf, M., 2007, AN, 328, 928, [2007AN....328..928Z](#)

# Transiting Exoplanet Light Curve Solution by Phoebe Code

STANISLAV PODDANÝ<sup>1,2</sup>

- 1) Astronomical Institute, Charles University, V Holešovičkách 2, Prague, Czech Republic
- 2) Štefánik observatory, Petřín 205, Prague 1, Czech Republic,  
email: [poddany@observatory.cz](mailto:poddany@observatory.cz)

## Abstract:

We present a brief demonstration of photometric light curves solution of transiting exoplanets using the code Phoebe 0.29c. We determined a new radius, mass and inclination for exoplanet Wasp-2b ( $R_p=1.068 R_J$ ,  $M_p=0.874 M_J$ ,  $i=84.83 \pm 0.14$ ) and for exoplanet TrES-1 ( $R_p=1.050 R_J$ ,  $M_p=0.809 M_J$ ,  $i=88.8 \pm 0.2$ ). Except these parameters we derived the time of the transits for exoplanet Wasp-2b ( $54357.3894 \pm 0.0006$  HJD) and TrES-1 ( $53186.8044 \pm 0.0004$  HJD). All our results are in good agreement (inside error bars) with the last results published in other papers.

**CZ Abstrakt:** Ukázka řešení světelných křivek transitujících exoplanet programem Phoebe 0.29c. Pomocí programu Phoebe jsme určili nový poloměr, hmotnost a sklon oběžné exoplanet Wasp-2b ( $R_p=1.068 R_J$ ,  $M_p=0.874 M_J$ ,  $i=84.83 \pm 0.14$ ) a TrES-1 ( $R_p=1.050 R_J$ ,  $M_p=0.809 M_J$ ,  $i=88.8 \pm 0.2$ ). Kromě těchto parametrů jsme spočetli okamžiky středů transitů exoplanet Wasp-2b ( $2454357.3894 \pm 0.0006$  HJD) a TrES-1 ( $53186.8044 \pm 0.0004$  HJD). Všechny prezentované výsledky jsou v dobré shodě (v rámci chyb měření) s výsledky publikovanými v posledních odborných článcích o těchto exoplanetách.

---

## 1. Introduction

The first exoplanet was discovered already in 1995 at a star 51 Pegasi similar to our Sun by Mayor and Queloz (1995). Since then the count of known exoplanets grows quickly. Currently there are 270 such bodies known (January 2008, see the list<sup>1</sup>).

51 Pegasi was similarly to the most known exoplanets discovered by a method based on the changes of radial velocity curve of the parent star. From these variations it is possible to determine the orbital period, semi-major axis of the orbit and the  $M \sin i$  quantity (where  $M$  represents the mass of the planet and  $i$  is the unknown inclination of the planet's orbit around the star). Only in special cases where the orbital inclination is close to  $90^\circ$  and the main semi-major axis of the orbit is small, it is possible to observe the transit of the exoplanet in front of the star itself. Charbonneau and Henry detected the first transit independently in 2000 at the star HD 209458 (Charbonneau, 2000; Henry, 2000).

In past years the observation of transiting exoplanets has not longer been the domain of large telescopes. As proved by Alonso (2004), a large telescope is not a necessary tool for observation of an exoplanet's transit. Amateur astronomers currently provide a large amount of data of selected transits.

## 2. Observation

We observed one transit of the exoplanet Wasp-2b with the 0.65-m telescope at the Ondřejov observatory during the night of 13 August 2007. The observations were carried out in the R and V filter, without auto-guiding using the G2 CCD camera with Kodak KAF-3200ME CCD chip. Exposure time was 60 seconds in R filter and 90 seconds in V filter (figure 1). The weather conditions were very good. The transit of the exoplanet TrES-1 was observed during the night of 1 April 2005 at the Nicolas Copernicus Observatory and Planetarium in Brno. These observations of exoplanet TrES-1 were carried out by Miloslav Zejda using SBIG ST7 CCD camera and the R filter. The weather conditions were excellent and the exposure time in the R filter was 60 seconds as in our case.

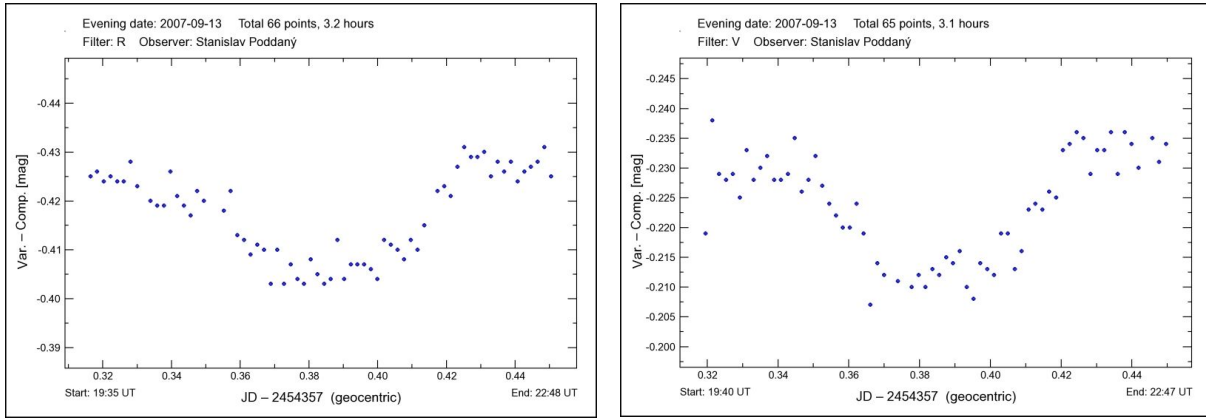


Figure 1 – occultation exoplanet Wasp-2b in R filter on the left and V filter on the right.

### 3. Data analysis

The data from observations were reduced using the program C-Munipack<sup>2)</sup>. Reduced data were used as input for the program Phoebe 0.29c (Prša and Zwitter, 2005). This well-known photometric program is based on the Wilson-Devinney code (Wilson, 1971) which is ordinarily used to simulate the light curves of eclipsing binaries and to determine parameters of systems based on these models.

With light curve alone (without radial velocity measurement) it is not possible to determine all system parameters as Kallrath and Milone showed in their work (table 1; Kallrath, 1999). Hence we used semi-major axes, mass ratio (primary over secondary – 0.00100 for Wasp-2b and 0.00058 for TrES-1) and orbital period as published in the Extrasolar Planets Encyclopedia<sup>1)</sup>.

	Only LC	Only RV SB1	Only RV SB2	LC RV SB1	LC RV SB2
$a_1 \sin i$ or $a_2 \sin i$		✓	✓	✓	✓
$a \sin i, a_1 \sin i, a_2 \sin i, M_1 \sin^3 i, M_2 \sin^3 i$			✓		✓
$a, a_1, a_2, M_1, M_2, R_1, R_2, L_1, L_2, d$				(✓)	✓
$P, e, \omega, (\dot{\omega})$	✓	✓	✓	✓	✓
$\gamma$		✓	✓	✓	✓
$q$	(✓)		✓	(✓)	✓
$i, \frac{R_1}{a}, \frac{R_2}{a}, L_1/L_2, g_1, g_2, A_1, A_2, F_1, F_2, x_1, x_2, l_3$	✓			✓	✓
$T_2$	✓	?	?	✓	✓

Table 1 - The table shows which entities can be derived when the measurements of a particular type are available. Column LC (light curve only) is our case. We can see what is possible and what is impossible to be derive. In the table  $a_1$  and  $a_2$  denote for the semi-major axis,  $i$  for inclination,  $M_1$  and  $M_2$  masses of the primary and secondary,  $R_1$  and  $R_2$  radii of components in eclipsing binaries,  $L_1$  and  $L_2$  for bolometric luminosities,  $d$  for the separation between the components,  $e$  for eccentricity,  $\omega$  for the argument of periastron,  $\gamma$  is the systematic velocity of the eclipsing binary pair,  $q$  is the photometric or spectroscopic mass ratio (the brackets are not only for contact systems),  $L_1$  and  $L_2$  monochromatic luminosities,  $g_1$  and  $g_2$  gravity darkening coefficients,  $A_1$  and  $A_2$  albedo coefficients,  $F_1$  and  $F_2$  rotation parameters,  $x_1$  and  $x_2$  limb darkening coefficients,  $l_3$  the third light and finally  $T_2$  temperature of the secondary body ( $T_1$  is fixed). (Kallrath, 1999)

Other parameters like primary star’s temperature were obtained from a spectral model (Harmanec, 1988). The primary and secondary albedo coefficients we assumed to be 0.5 (Rucinski, 1969) because the temperature of the both observed stars is lower than 7200 K and gravity darkening coefficients we assumed to be 0.32 (Lucy, 1968).

The limb darkening law is a very important parameter in the modeling of the light curves of transiting exoplanets. In this work the square root limb darkening law was used. Coefficients for fitting were taken from the Van Hamme limb darkening tables that are calculated down to 3500 K temperature and are included in the Phoebe code. Hence we assumed the exoplanet’s temperature to be 3500 K.

Fitting script, the most powerful part of the Phoebe code for finding parameters of eclipsing binaries, cannot be used in this case. Because of the extremely small mass ratio and the low luminosity of the exoplanet fitting script often failed. We had to increase “Stellar surface fine grid raster” and “Stellar surface coarse grid raster” from 20 (fine grid) and 5 (coarse grid), to 60 and 15 points. After that it is still necessary to fit manually and the iteration step has to be carefully chosen.

For the first time we fit primary and secondary star luminosities (HLA), after that combination HLA with surface potentials (PHSV and PCSV) and then we derived other parameters (orbital inclination (INCL), heliocentric julian date (HJD0)). In each fit we tried to obtain the lowest  $\chi^2$  which represents accuracy between our synthetic light curve and the real light curve. After several fitting steps a good agreement between the observed light curve and a synthetic light curve was obtained (figure 2 and 3). In the Phoebe 0.29c code only three decimal places are used for results of the star masses and radii (the solar units are used). For the higher accuracy it is necessary to increase the semi-major axis (10 times) and later compensate it in the derived values.

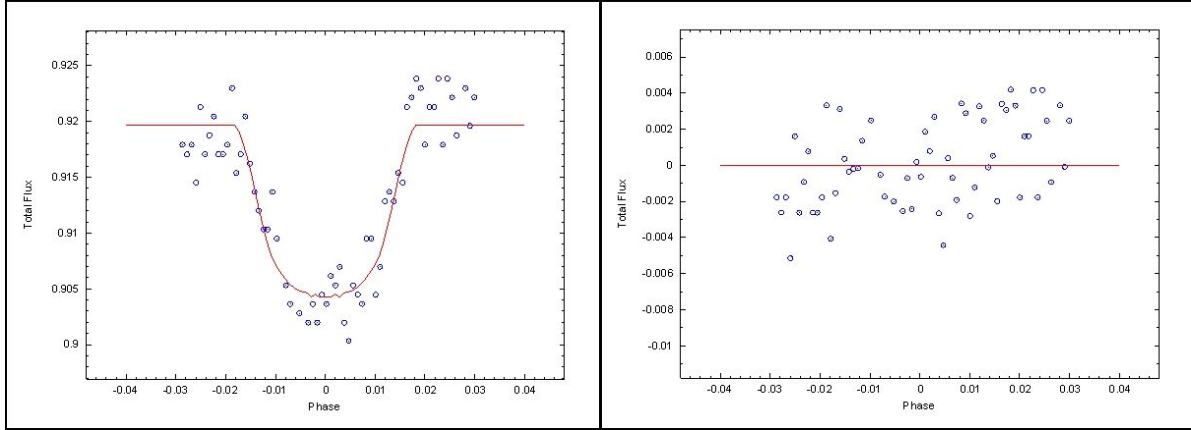


**Figure 2** - Transit light curve of the exoplanet Wasp-2b, observed at the Ondřejov observatory during the night of 13 August 2007. Relative flux is plotted against the orbital phase and the best-fitting model is plotted (on the left) -  $\chi^2$  of the synthetic light curve is 0.002980. Residuals, derived by the subtraction of the model from the measurements, are plotted on the right.

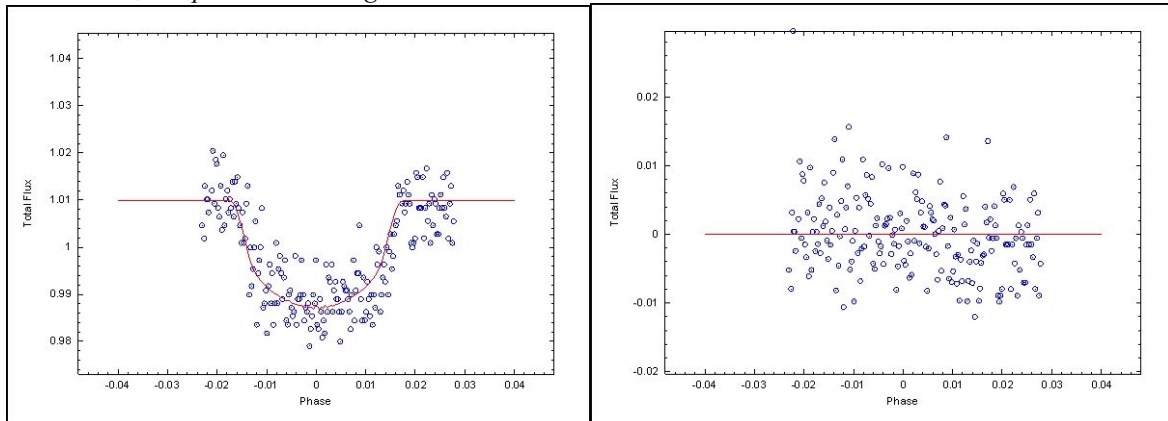


**Figure 3** - Transit light curve of the exoplanet TrES-1, at the Nicolas Copernicus Observatory and Planetarium in Brno during the night of 1 March 2005. Relative flux is plotted against the orbital phase and the best-fitting model is plotted (on the left) -  $\chi^2$  of the synthetic light curve is 0.005838. Residuals, derived by the subtraction of the model from the measurements, are plotted on the right.

#### 4. Discussion

We derived a new planetary radius  $R_p=1.068 R_J$ , new mass  $M_p=0.874 M_J$  and inclination  $84.83 \pm 0.14$  for exoplanet Wasp-2b and radius  $R_p=1.050 R_J$ , new mass  $M_p=0.809 M_J$  and inclination  $88.8 \pm 0.2$  for exoplanet TrES-1. Except these parameters we derived the central time of the transits -  $T_c$ . We fix orbital period  $P=2.152226$  days for Wasp-2b, as assumed Charbonneau (2007) and  $P=3.0300737$  days for TrES-1 (Winn, 2006). After that we obtained  $T_c=2454357.3894 \pm 0.0006$  HJD for Wasp-2b and  $T_c=53186.8044 \pm 0.0004$  HJD for the exoplanet TrES-1. Finally we computed O-C values for the central time of each transit. All our results (table 2 and 3) are in good agreement (inside error bars) with the last results published in other papers (Charbonneau, 2007; Burrows, 2007).

**Table 2** - Our results compared with last results published in other papers for Wasp-2b.

Wasp-2b			
Radius [ $R_{\text{Jupiter}}$ ]	1.068	1.04 (0.06)	1.038 (0.032)
Mass [ $M_{\text{Jupiter}}$ ]	0.874	0.88 (0.11)	X
Inclination [deg.]	84.83 (0.14)	x	84.74 (0.39)
Source	this paper ( $\chi^2 = 0.002980$ )	Burrows, 2007	Charbonneau, 2007

<b>T<sub>c</sub> [HJD]</b>	54357.3894 (0.0006)
<b>O-C [day]</b>	0.00298 (ephemeris taken from <sup>1</sup> )

**Table 3** - Our results compared with last results published in other papers for TrES-1.

TrES-1		
<b>Radius [R<sub>Jupiter</sub>]</b>	1.050	1.08 (0.03)
<b>Mass [M<sub>Jupiter</sub>]</b>	0.809	0.75 (0.07)
<b>Inclination [deg.]</b>	88.8 (0.2)	X
<b>Source</b>	this paper ( $\chi^2 = 0.005838$ )	Burrows, 2007
<b>T<sub>c</sub> [HJD]</b>	53186.8044 (0.0004)	
<b>O-C [day]</b>	0.001551 (ephemeris taken from <sup>1</sup> )	

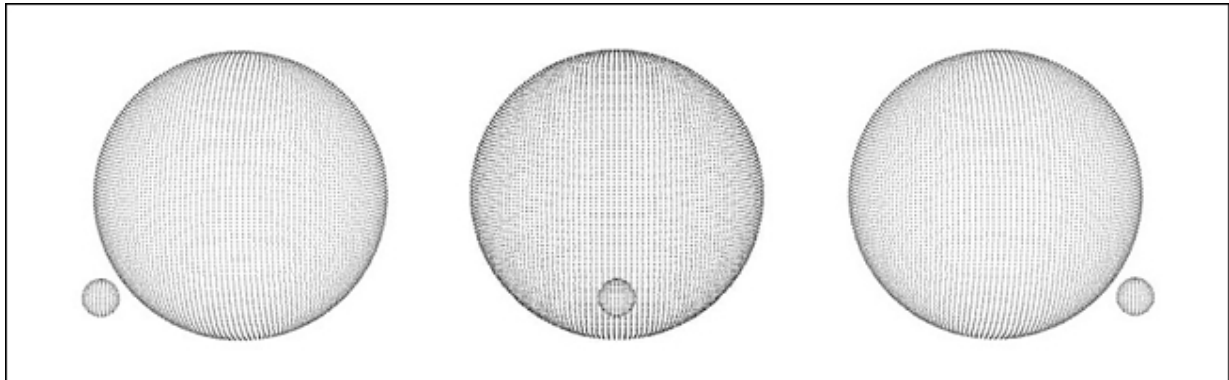


**Figure 4** - transit Wasp-2b visualization by Phoebe 0.29c (orbital phases 0.98, 0.0 and 0.02)

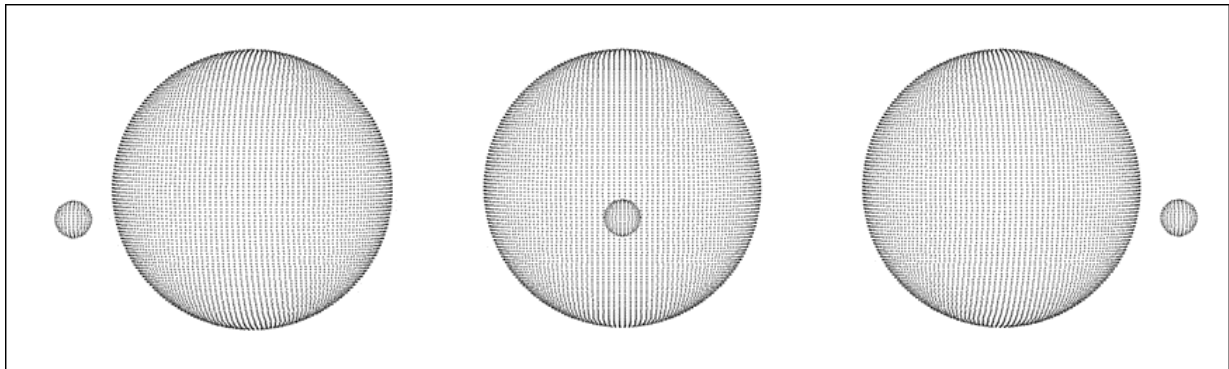


**Figure 5** - transit TrES-1 visualization by Phoebe 0.29c. (orbital phases 0.98, 0.0 and 0.02)

## 5. Acknowledgements

We thank Kamil Hornoch for his help with observation of exoplanet Wasp-2b during the night of 13 August 2007, Marek Wolf for his helpful advices, Miloslav Zejda for his agreement to use his data and Petr Zasche for his help with the Phoebe code.

This investigation was supported by the Grant Agency of the Czech Republic, grant no. 205/06/0217.

## 6. References

- Alonso R., et al., 2004, TrES-1: The Transiting Planet of a Bright K0 V Star <http://adsabs.harvard.edu/abs/2004ApJ...613L.153A>
- Burrows A., et al. 2007, Possible solutions to the radius anomalies of transiting giant planets, APJ 661: 502-514
- Charbonneau D., et al., 2000, Detection of Planetary Transits Across a Sun-like Star <http://adsabs.harvard.edu/abs/2000ApJ...529L..45C>
- Charbonneau D., et al., 2007, Precise radius estimates for the exoplanets Wasp-1b and Wasp-2b, APJ 658:1322-1327 <http://adsabs.harvard.edu/abs/2007ApJ...658.1322C>
- Harmanec P., 1988, Stellar masses and radii based on modern binary data <http://adsabs.harvard.edu/abs/1988BAICz...39..329H>

- Henry G. W., et al., 2000, A Transiting ``51 Peg-like" Planet  
<http://adsabs.harvard.edu/abs/2000ApJ...529L..41H>
- Kallrath J., Milone E. F., 1999, Eclipsing binary stars: modeling and analysis  
<http://adsabs.harvard.edu/abs/1999ebs.conf....K>
- Lucy L. B., 1968, The Structure of Contact Binaries,  
<http://adsabs.harvard.edu/abs/1968ApJ...151.1123L>
- Mayor, M., Queloz, D., 1995, A Jupiter-Mass Companion to a Solar-Type Star  
<http://adsabs.harvard.edu/abs/1995Natur.378..355M>
- Prša A., Zwitter T., 2005, A computing guide to physics of eclipsing binaries. I. Demonstrations and perspectives <http://adsabs.harvard.edu/abs/2005ApJ...628..426P>
- Rucinski S. M., 1969, The Proximity Effects in Close Binary Systems. II. The Bolometric Reflection Effect for Stars with Deep Convective Envelopes <http://adsabs.harvard.edu/abs/1969AcA....19..245R>
- Wilson R. E., Devinney E. J., 1971, Realization of Accurate Close-Binary Light Curves: Application to MR Cygni <http://adsabs.harvard.edu/abs/1971ApJ...166..605W>
- Winn, Joshua N.; Holman M. J.; Roussanova A., The Transit Light Curve Project. III. Tres Transits of TrES-1 [http://adsabs.harvard.edu/cgi-bin/bib\\_query?2007ApJ...657.1098W](http://adsabs.harvard.edu/cgi-bin/bib_query?2007ApJ...657.1098W)

<sup>1)</sup> <http://www.exoplanet.eu>

<sup>2)</sup> <http://integral.sci.muni.cz/cmunicipack/index.html>